RDECOM TR 10-D-109

U.S. ARMY RESEARCH, DEVELOPMENT AND ENGINEERING COMMAND

TITLE: Design and Experimental Results for the S407 Airfoil

AUTHOR: Dan M. Somers and Mark D. Maughmer

COMPANY NAME: Airfoils, Incorporated

COMPANY ADDRESS: 122 Rose Drive
Port Matilda PA 16870-7535

DATE: August 2010

FINAL REPORT: Contract Number W911W6-07-C-0047, SBIR Phase II, Topic Number A06-006, Proposal Number A2-2972

Prepared for:

U.S. ARMY RESEARCH, DEVELOPMENT AND ENGINEERING COMMAND, AVIATION APPLIED TECHNOLOGY DIRECTORATE, FORT EUSTIS, VA 23604-5577

AIRFOILS, INCORPORATED
122 ROSE DRIVE
PORT MATILDA, PA 16870-7535 USA
WEBSITE WWW.AIRFOILS.COM
TELEPHONE (814) 357-0500
FACSIMILE (814) 357-0357

DESIGN AND EXPERIMENTAL RESULTS FOR THE S407 AIRFOIL

DAN M. SOMERS
AIRFOILS, INCORPORATED

MARK D. MAUGHMER
THE PENNSYLVANIA STATE UNIVERSITY

AUGUST 2010

ABSTRACT

An 11.43-percent-thick airfoil, the S407, intended for rotorcraft applications has been designed and analyzed theoretically and verified experimentally in The Pennsylvania State University Low-Speed, Low-Turbulence Wind Tunnel. The two primary objectives of high maximum lift and low profile drag have been achieved. The constraints on the pitching moment and the airfoil thickness have been satisfied. The airfoil exhibits a sharp stall, which does not meet the design objective. Comparisons of the theoretical and experimental results generally show good agreement.

INTRODUCTION

Almost all airfoils in use on rotorcraft today were developed under the assumption that extensive laminar flow is not likely on a rotor. (See ref. 1, for example.) For the present application, however, given the low Reynolds numbers, the achievement of laminar flow warrants exploration.

The airfoil designed under the present effort is intended for the rotor of a high-altitude, tandem-rotor helicopter. To complement the design effort, an investigation was conducted in The Pennsylvania State University Low-Speed, Low-Turbulence Wind Tunnel (ref. 2) to obtain the basic, low-speed, two-dimensional aerodynamic characteristics of the airfoil. The results have been compared with predictions from the method of references 3 and 4 and from the method of reference 5.

SYMBOLS

Values are given in both SI and U.S. Customary Units. Measurements and calculations were made in U.S. Customary Units.

C_p	pressure coefficient, $\frac{p_l - p_\infty}{q_\infty}$
c	airfoil chord, mm (in.)
c_c	section chord-force coefficient, $\oint C_p d\left(\frac{z}{c}\right)$
c_d	section profile-drag coefficient, $\int_{Wake} c_d' d\left(\frac{h}{c}\right)$, except post stall, $c_n \sin\alpha + c_c \cos\alpha$
c_d'	point drag coefficient (ref. 6)
c_l	section lift coefficient, $c_n / \cos\alpha - c_d \tan\alpha$

c_m	section pitching-moment coefficient about quarter-chord point, $-\oint C_p\left(\frac{x}{c}-0.25\right)d\left(\frac{x}{c}\right)+\oint C_p\left(\frac{z}{c}\right)d\left(\frac{z}{c}\right)$
c_n	section normal-force coefficient, $-\oint C_p d\left(\frac{x}{c}\right)$
h	horizontal width in wake profile, mm (in.)
M	free-stream Mach number
p	static pressure, Pa (lbf/ft^2)
q	dynamic pressure, Pa (lbf/ft^2)
R	Reynolds number based on free-stream conditions and airfoil chord
t	airfoil thickness, mm (in.)
x	airfoil abscissa, mm (in.)
y	model span station, $y = 0$ at midspan, mm (in.)
z	airfoil ordinate, mm (in.)
α	angle of attack relative to x-axis, deg

Subscripts:

l	local point on airfoil
ll	lower limit of low-drag range
max	maximum
min	minimum
S	separation
T	transition
ul	upper limit of low-drag range
0	zero lift
∞	free-stream conditions

Abbreviations:

L. lower surface

S. boundary-layer separation location, x_S/c

T. boundary-layer transition location, x_T/c

U. upper surface

AIRFOIL DESIGN

OBJECTIVES AND CONSTRAINTS

The airfoil design specifications are contained in table I. Two primary objectives are evident. The first objective is to achieve a maximum lift coefficient of 1.20 at a Mach number of 0.20 and a Reynolds number of 147,000. A requirement related to this objective is that the maximum lift coefficient not decrease significantly with transition fixed near the leading edge on both surfaces. In addition, the airfoil should exhibit docile stall characteristics. The second objective is to obtain low profile-drag coefficients from a lift coefficient of 0.20 at a Mach number of 0.70 and a Reynolds number of 552,000 to a lift coefficient of 1.00 at a Mach number of 0.50 and a Reynolds number of 368,000.

Two major constraints were placed on the design of the airfoil. First, the zero-lift pitching-moment coefficient must be no more negative than −0.15 at a Mach number of 0.70 and a Reynolds number of 552,000. Second, the airfoil thickness must be greater than 6-percent chord.

PHILOSOPHY

Given the above objectives and constraints, certain characteristics of the design are apparent. The following sketch illustrates a drag polar that meets the goals for this design.

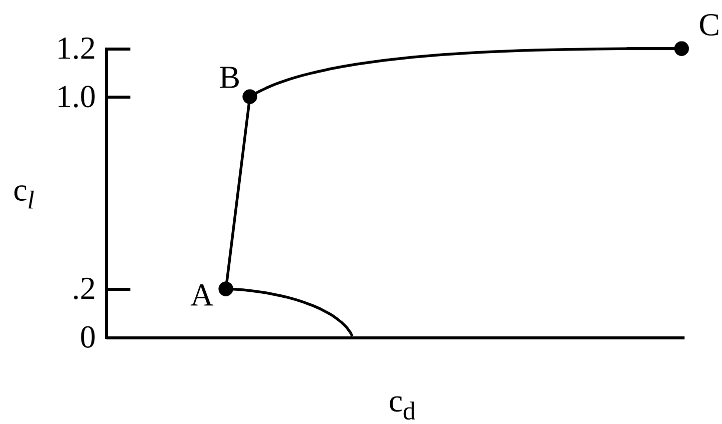

Sketch 1

The desired airfoil shape can be traced to the pressure distributions that occur at the various points in sketch 1. Point A is the lower limit of the low-drag range of lift coefficients; point B, the upper limit. The profile-drag coefficient at point B is not as low as at point A, unlike the polars of many laminar-flow airfoils where the drag coefficient within the laminar bucket is nearly constant. (See, for example, ref. 7.) This characteristic is related to the elimination of significant (i.e., drag-producing) laminar separation bubbles on the upper surface for the design range of Reynolds numbers. (See ref. 8.) The drag coefficient increases rapidly outside the low-drag, lift-coefficient range because boundary-layer transition moves quickly toward the leading edge with increasing (or decreasing) lift coefficient. This feature results in a leading edge that produces a suction peak at higher lift coefficients, which ensures that transition on the upper surface will occur very near the leading edge. Thus, the maximum lift coefficient, point C, occurs with turbulent flow along the entire upper surface and, therefore, should be relatively insensitive to roughness at the leading edge.

From the preceding discussion, the pressure distributions along the polar can be deduced. The pressure distribution at point A should look something like sketch 2.

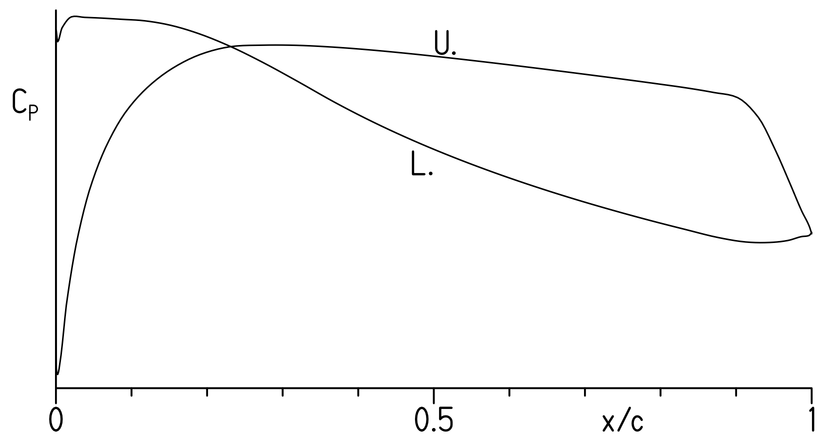

Sketch 2

To achieve low drag, a favorable pressure gradient is desirable along the upper surface to about 30-percent chord. This region is followed by a very slightly convex pressure recovery. The specific pressure recovery employed represents a compromise between maximum lift, drag, pitching moment, stall characteristics, and drag divergence. The steep, adverse pressure gradient aft of about 90-percent chord is a "separation ramp," originally proposed by F. X. Wortmann,[1] which confines turbulent separation to a small region near the trailing edge. By constraining the movement of the separation point at high angles of attack, higher lift coefficients can be achieved with little drag penalty. This feature has the added benefit of promoting docile stall characteristics. (See ref. 9.)

Along the lower surface, the pressure gradient is briefly favorable and then slightly adverse to about 10-percent chord. Aft of this point, a short region having a shallow, adverse pressure gradient (i.e., a "transition ramp") promotes the efficient transition from laminar to turbulent flow (ref. 10). The curved transition ramp (ref. 8) is followed a concave pressure recovery, which exhibits lower drag and has less tendency to separate than the corresponding linear or convex pressure recovery (ref. 10). The pressure recovery must begin much farther forward than optimum for low drag to alleviate separation at lower lift coefficients, especially with transition fixed near the leading edge.

The amounts of pressure recovery on the upper and lower surfaces are determined by the width of the low-drag range and the pitching-moment constraint.

---

[1]Director, Institute for Aerodynamics and Gas Dynamics, University of Stuttgart, Germany, 1974–1985.

At point B, the pressure distribution should look like sketch 3.

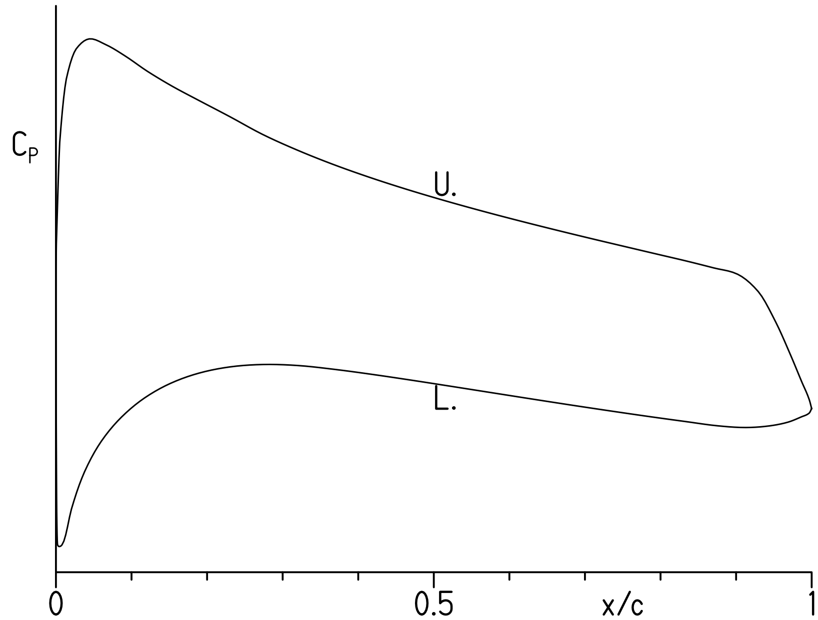

Sketch 3

No suction spike exists at the leading edge. Instead, a rounded peak occurs aft of the leading edge, which allows some laminar flow, although not to the extent of point A. Because the pressure gradient along the lower surface is favorable farther aft, the extent of laminar flow is greater than at point A.

EXECUTION

Given the pressure distributions previously discussed, the design of the airfoil is reduced to the inverse problem of transforming the pressure distributions into an airfoil shape. The Eppler Airfoil Design and Analysis Code (refs. 3 and 4) was used because of its unique capability for multipoint design and because of confidence gained during the design, analysis, and experimental verification of many other airfoils. (See ref. 11, for example.)

The airfoil is designated the S407. The airfoil shape and coordinates are available from Airfoils, Incorporated. The airfoil thickness is 11.43-percent chord, which satisfies the design constraint.

THEORETICAL PROCEDURE

The theoretical results are predicted using the method of references 3 and 4 (PROFIL07), commonly known as the Eppler code, and the method of reference 5 (MSES 3.0). Critical amplification factors of 11 and 9 were specified for the computations using the method of references 3 and 4 and the method of reference 5, respectively. It should be noted that the compressibility correction (ref. 12) incorporated in the method of references 3 and 4 is invalid if the local flow is supersonic.

Because the free-stream Mach number for all wind-tunnel test conditions did not exceed 0.20, the flow can be considered essentially incompressible for the purpose of comparing the theoretical and experimental results. This allows the (incompressible) conformal-mapping (design) method of references 3 and 4 and the fast, subcritical flow solver of the method of reference 5 to be used.

EXPERIMENTAL PROCEDURE

WIND TUNNEL

The Pennsylvania State University Low-Speed, Low-Turbulence Wind Tunnel (ref. 2) is a closed-throat, single-return, atmospheric tunnel (fig. 1). The test section is 101.3 cm (39.9 in.) high by 147.6 cm (58.1 in.) wide (fig. 2). Electrically actuated turntables provide positioning and attachment for the two-dimensional model. The turntables are flush with the top and bottom tunnel walls and rotate with the model. The axis of rotation coincided approximately with the quarter chord of the model, which was mounted vertically between the turntables. The gaps between the model and the turntables were sealed. The turbulence intensity in the test section is approximately 0.05 percent at 46 m/s (150 ft/s).

MODEL

The aluminum, wind-tunnel model was fabricated by Skytop Aerospace, Bellefonte, Pennsylvania, using a numerically controlled milling machine. The model had a chord of 160.0 mm (6.30 in.) and a span of 107.95 cm (42.50 in.) and, thus, extended through both turntables. Upper- and lower-surface orifices were located to one side of midspan at the staggered positions listed in table II. All the orifices were 0.51 mm (0.020 in.) in diameter with their axes perpendicular to the surface. The surfaces of the model were sanded to ensure an aerodynamically smooth finish. The measured model contour was within 0.13 mm (0.005 in.) of the prescribed shape.

WAKE-SURVEY PROBE

A total- and static-pressure, wake-survey probe (fig. 3) was mounted from the top tunnel wall (fig. 2). The probe was positioned 61.0 cm (24.0 in.) from the ceiling and automatically aligned with the wake-centerline streamline. A traverse mechanism incrementally positioned the probe to survey the wake. The increment was 1.27 mm (0.050 in.) for traverses less than 254.0 mm (10.00 in.) and 2.54 mm (0.100 in.) for longer traverses, which were occasionally required near the maximum lift coefficient. The tip of the probe was located 3.0 chords downstream of the trailing edge of the model.

INSTRUMENTATION

Basic tunnel pressures and the wake pressures were measured with precision transducers. Measurements of the pressures on the model were made by an automatic pressure-scanning system utilizing precision transducers. Data were obtained and recorded by an electronic data-acquisition system.

METHODS

The pressures measured on the model were reduced to standard pressure coefficients and numerically integrated to obtain section normal-force and chord-force coefficients and section pitching-moment coefficients about the quarter-chord point. Section profile-drag coefficients were computed from the wake total and static pressures by the method of reference 6. Wake surveys were not performed, however, at most post-stall angles of attack, in which case, the profile-drag coefficients were computed from the normal- and chord-force coefficients.

Standard, low-speed, wind-tunnel boundary corrections (ref. 13) have been applied to the data. The wake-survey-probe total-pressure-tube displacement correction (ref. 6) has been taken into account.

TESTS

The model was tested at Reynolds numbers based on airfoil chord of 70,000, 100,000, 150,000, 200,000, 300,000, and 600,000 with transition free (smooth) and with transition forced by serrated tape (ref. 14) near the leading edge, 5-percent chord on the upper surface and 10-percent chord on the lower surface, to simulate full-chord, turbulent flow. The thickness of the tape was determined empirically on each surface for each Reynolds number by increasing the thickness until transition moved forward to the vicinity of the tape at an angle of attack of 4°, as verified by stethoscope measurements (ref. 15). The resulting thicknesses, listed in table III, are generally at least three times those determined using the method of reference 16. The Mach number did not exceed 0.20 for any test condition.

It should be noted that the test Mach numbers are much lower than most of the operational values of the intended application.

Starting from 4°, the angle of attack was increased to post-stall values. The angle of attack was then decreased from 4° to below that for zero lift.

DISCUSSION OF RESULTS

THEORETICAL RESULTS

Pressure Distributions

The inviscid pressure distributions at various angles of attack at Mach numbers of 0.20, 0.50, and 0.70 predicted using the method of references 3 and 4 are shown in figure 4.

Section Characteristics

The section characteristics at the three design conditions with transition free and transition fixed are shown in figures 5 through 7. Based on the predictions, all the design objectives and constraints have essentially been met.

EXPERIMENTAL RESULTS

Traditionally, aerodynamic results are presented in order of increasing Reynolds number. For low Reynolds numbers, however, the results are more easily understood in reverse order. Accordingly, the results are presented in order of decreasing Reynolds number.

Pressure Distributions

The pressure distributions at various angles of attack for a Reynolds number of 300,000 and a Mach number of 0.09 with transition free are shown in figure 8. At an angle of attack of −4.01° (fig. 8(a)), laminar separation, without turbulent reattachment, occurs just forward of the trailing edge on the upper surface and a short laminar separation bubble is barely evident on the lower surface around 35-percent chord. At an angle of attack of −1.00° (fig. 8(a)), a short laminar separation bubble is evident on the upper surface just forward of the trailing edge (i.e., turbulent reattachment has occurred). As the angle of attack is increased, the bubble on the upper surface moves forward, whereas the bubble on the lower surface moves aft, eventually disappearing by an angle of attack of 6.01° (figs. 8(b)–8(c)). At an angle of attack of 10.02° (fig. 8(d)), turbulent, trailing-edge separation is evident on the upper surface. The amount of separation increases with increasing angle of attack (figs. 8(d) and 8(e)). The maximum lift coefficient occurs between the angles of attack of 12° and 13° (fig. 8(e)). As the angle of attack is increased further, the separation point continues to move forward until the leading-edge peak collapses and essentially the entire upper surface is separated at an angle of attack of 17.00° (fig. 8(f)).

The pressure distributions at various angles of attack for a Reynolds number of 150,000 and a Mach number of 0.04 with transition free are shown in figure 9. At an angle of attack of −3.01° (fig. 9(a)), laminar separation, without turbulent reattachment, occurs forward of the trailing edge on the upper surface and a short laminar separation bubble is evident on the lower surface around 45-percent chord. As the angle of attack is increased, the bubble moves aft (figs. 9(a) and 9(b)). At an angle of attack of 1.00° (fig. 9(b)), a short laminar separation bubble is evident on the upper surface just forward of the trailing edge. As the angle of attack is increased, the bubble on the upper surface moves forward, whereas the bubble on the lower surface continues to move aft, eventually disappearing by an angle of attack of 4.01° (figs. 9(b) and 9(c)). At an angle of attack of 11.02° (fig. 9(d)), turbulent, trailing-edge separation is evident on the upper surface. The amount of separation increases with increasing angle of attack (figs. 9(d) and 9(e)). The maximum lift coefficient occurs between the angles of attack of 11° and 12° (figs. 9(d) and 9(e)). As the angle of attack is increased further, the separation point continues to move forward until the leading-edge peak collapses and essentially the entire upper surface is separated at an angle of attack of 14.00° (fig. 9(e)).

The pressure distributions at various angles of attack for a Reynolds number of 70,000 and a Mach number of 0.02 with transition free are shown in figure 10. At an angle of attack of −2.00° (fig. 10(a)), laminar separation, without turbulent reattachment, occurs forward of the trailing edge on the upper surface and a short laminar separation bubble is evident on the lower surface around 70-percent chord. As the angle of attack is increased, the bubble moves aft, eventually disappearing by an angle of attack of 2.00° (figs. 10(a) and 10(b)). At an angle of attack of 3.00° (fig. 10(b)), a short laminar separation bubble is evident on the upper surface just forward of the trailing edge. As the angle of attack is increased, the bubble moves forward (figs. 10(b)–10(d)). Turbulent, trailing-edge separation is barely evident on the upper surface at an angle of attack of 10.52° (not shown), which corresponds to the maximum lift coefficient. At an angle of attack of 11.01° (fig. 10(d)), the leading-edge peak has collapsed and essentially the entire upper surface is separated, suggesting that stall, for this Reynolds number, may be caused by bursting of the bubble.

Section Characteristics

The section characteristics with transition free and transition fixed are shown in figure 11 and tabulated in the appendix. For a Reynolds number of 150,000 and a Mach number of 0.04 with transition free (fig. 11(d)), the maximum lift coefficient is 1.25, which exceeds the design objective. The stall characteristics are sharp, which does not meet the design objective. For a Reynolds number of 598,000 and a Mach number of 0.19 with transition free (fig. 11(a)), the lower limit of the low-drag range of lift coefficients is approximately 0.29 and the zero-lift pitching-moment coefficient is −0.124. For a Reynolds number of 300,000 and a Mach number of 0.09 with transition free (fig. 11(b)), the maximum lift-to-drag ratio occurs at a lift coefficient of about 0.90. (Because the upper limit of the low-drag, lift-coefficient range is not sharply defined, a precise value for the upper limit cannot be given.)

The effects of Reynolds number on the section characteristics are summarized in figures 12 and 13. In general, with transition free, the lift-curve slope, the maximum lift coefficient, the upper limit of the low-drag range, and the magnitudes of the zero-lift angle of attack and the pitching-moment coefficients, including the zero-lift value, decrease with decreasing Reynolds number. The profile-drag coefficients and the lower limit of the low-drag range generally increase with decreasing Reynolds number. The stall characteristics become sharper with decreasing Reynolds number.

The effect of fixing transition on the section characteristics is shown in figure 11. In general, the zero-lift angle of attack and pitching-moment coefficient and the maximum lift coefficient are relatively unaffected by fixing transition, whereas the lift-curve slope and the magnitude of the pitching-moment coefficients decrease with transition fixed. The latter results are primarily a consequence of the boundary-layer displacement effect, which decambers the airfoil because the displacement thickness is greater with transition fixed than with transition free. For some Reynolds numbers, the maximum lift coefficient actually increases with transition fixed, which is an atypical result for high Reynolds numbers, but not uncommon for low Reynolds numbers. This result is probably caused by the alleviation of the upper-surface laminar separation bubble by the trip or by vortices generated by the serrated tape. The drag coefficients are, of course, generally affected adversely by the trips. The stall characteristics are generally sharper with transition fixed.

It should be noted that, for almost all test conditions, the Reynolds number based on local velocity and boundary-layer displacement thickness at the trip locations is too low to support turbulent flow. (See ref. 17.) Accordingly, to force transition, the serrated tape must be so thick that it increases the displacement thickness, which abnormally decreases the lift coefficient and the magnitude of the pitching-moment coefficient and increases the drag coefficient. Conversely, at low lift coefficients and Reynolds numbers, the serrated tape eliminates the laminar separation bubble on the lower surface, resulting in higher lift coefficients and, for a Reynolds number of 70,000 particularly, lower drag coefficients.

The variations of maximum lift coefficient and profile-drag coefficient with Reynolds number are shown in figures 14 and 15, respectively. The maximum lift coefficient decreases with decreasing Reynolds number, whereas the profile-drag coefficient increases, which are typical trends for most airfoils.

COMPARISON OF THEORETICAL AND EXPERIMENTAL RESULTS

Pressure Distributions

The comparison of the theoretical and experimental pressure distributions at various angles of attack is shown in figure 16. It should be noted that the pressure distributions predicted using the method of references 3 and 4 (PROFIL07) are inviscid and incompressible, whereas the pressure distributions predicted using the method of reference 5 (MSES 3.0) as well as the experimental pressure distributions were obtained for a Reynolds number of 150,000 and a Mach number of 0.04 with transition free. It should also be noted that the theoretical lift coefficient from the method of references 3 and 4 is calculated from the lift-curve slope and the angle of attack relative to the zero-lift line, whereas the lift coefficient from the method of reference 5 and from the experiment is derived from the integrated pressure distribution. (See refs. 3–6.) Thus, at a given lift coefficient, the pressure distribution predicted using the method of references 3 and 4 does not necessarily have the same area as the measured pressure distribution. It should be noticed that the angle of attack shown in figure 16 is the value from the method of references 3 and 4, not the experimental value.

With respect to the method of references 3 and 4, at a lift coefficient of 0.25 (fig. 16(a)), neither the pressure coefficients nor the pressure gradients agree well, especially in the vicinity of the laminar separation bubble on the lower surface and toward the trailing edge on both surfaces. The latter disparity probably occurs because the method does not model the effect of the upper-surface laminar separation on the pressure distribution. At a lift coefficient of 0.79 (fig. 16(b)), the pressure coefficients and the pressure gradients agree reasonably well, again except toward the trailing edge. This disparity is probably due to the decambering viscous effects, which are not modeled in the inviscid pressure distribution. At a lift coefficient of 1.22 (fig. 16(c)), which is near the experimental maximum lift coefficient, the agreement is poor, again because of the displacement effect.

With respect to the method of reference 5, at a lift coefficient of 0.25 (fig. 16(a)), the pressure coefficients and the pressure gradients agree well. The predicted location of the lower-surface laminar separation bubble is aft of the measured location and transition is predicted forward of the trailing edge on the upper surface, causing some pressure recovery not evident in the experiment. At a lift coefficient of 0.79 (fig. 16(b)), the pressure distributions again agree well, although the predicted location of the upper-surface bubble is aft of the measured location. At a lift coefficient of 1.22 (fig. 16(c)), the agreement is less exact probably because the predicted location of the upper-surface bubble is again too far aft.

Section Characteristics

The comparison of the theoretical and experimental section characteristics with transition free is shown in figure 17. The agreement between the lift curves worsens with decreasing Reynolds number, particularly for the method of references 3 and 4 (PROFIL07). The method of references 3 and 4 underpredicts the maximum lift coefficient by an average of 1 percent for Reynolds numbers greater than 100,000 and by an average of 6 percent for Reynolds numbers of 100,000 and 70,000. The method of reference 5 (MSES 3.0) overpredicts the maximum lift coefficient by an average of 5 percent for the intermediate Reynolds numbers and by an average of 10 percent for Reynolds numbers of 600,000 and 70,000. Both methods predict the profile-drag coefficients relatively well, considering the low Reynolds numbers. The method of references 3 and 4 underpredicts the drag coefficients at low lift coefficients probably because it does not account for the effect of the upper-surface laminar separation. The method of references 3 and 4 overpredicts the magnitude of the pitching-moment coefficients.

The comparison of the theoretical and experimental section characteristics with transition fixed is shown in figure 18. In general, the predicted characteristics show similar tendencies as with transition free, although the general agreement is poorer, probably because of the abnormalities introduced by the serrated tape, as discussed previously.

CONCLUDING REMARKS

An 11.43-percent-thick airfoil, the S407, intended for rotorcraft applications has been designed and analyzed theoretically and verified experimentally in The Pennsylvania State University Low-Speed, Low-Turbulence Wind Tunnel. The two primary objectives of a high maximum lift coefficient and low profile-drag coefficients have been achieved. The constraints on the zero-lift pitching-moment coefficient and the airfoil thickness have been satisfied. The airfoil exhibits sharp stall characteristics that become sharper with decreasing Reynolds number, which does not meet the design objective. Comparisons of the theoretical and experimental results generally show good agreement.

ACKNOWLEDGMENTS

This effort was sponsored by the U.S. Army. Preston B. Martin served as the technical monitor.

REFERENCES

1. Noonan, Kevin W.: Aerodynamic Characteristics of Two Rotorcraft Airfoils Designed for Application to the Inboard Region of a Main Rotor Blade. NASA TP-3009, 1990.

2. Brophy, Christopher M.: Turbulence Management and Flow Qualification of The Pennsylvania State University Low Turbulence, Low Speed, Closed Circuit Wind Tunnel. M. S. Thesis, Pennsylvania State Univ., 1993.

3. Eppler, Richard: Airfoil Design and Data. Springer-Verlag (Berlin), 1990.

4. Eppler, Richard: Airfoil Program System "PROFIL07." User's Guide. Richard Eppler, c.2007.

5. Drela, M.: Design and Optimization Method for Multi-Element Airfoils. AIAA Paper 93-0969, Feb. 1993.

6. Pankhurst, R. C.; and Holder, D. W.: Wind-Tunnel Technique. Sir Isaac Pitman & Sons, Ltd. (London), 1965.

7. Abbott, Ira H.; Von Doenhoff, Albert E.; and Stivers, Louis S., Jr.: Summary of Airfoil Data. NACA Rep. 824, 1945. (Supersedes NACA WR L-560.)

8. Eppler, Richard; and Somers, Dan M.: Airfoil Design for Reynolds Numbers Between 50,000 and 500,000. Proceedings of the Conference on Low Reynolds Number Airfoil Aerodynamics, UNDAS-CP-77B123, Univ. of Notre Dame, June 1985, pp. 1–14.

9. Maughmer, Mark D.; and Somers, Dan M.: Design and Experimental Results for a High-Altitude, Long-Endurance Airfoil. J. Aircr., vol. 26, no. 2, Feb. 1989, pp. 148–153.

10. Wortmann, F. X.: Experimental Investigations on New Laminar Profiles for Gliders and Helicopters. TIL/T.4906, British Minist. Aviat., Mar. 1960. (Translated from Z. Flugwissenschaften, Bd. 5, Heft 8, Aug. 1957, S. 228–243.)

11. Somers, Dan M.: Subsonic Natural-Laminar-Flow Airfoils. Natural Laminar Flow and Laminar Flow Control, R. W. Barnwell and M. Y. Hussaini, eds., Springer-Verlag New York, Inc., 1992, pp. 143–176.

12. Labrujere, Th. E.; Loeve, W.; and Sloof, J. W.: An Approximate Method for the Determination of the Pressure Distribution on Wings in the Lower Critical Speed Range. Transonic Aerodynamics. AGARD CP No. 35, Sept. 1968, pp. 17-1–17-10.

13. Allen, H. Julian; and Vincenti, Walter G.: Wall Interference in a Two-Dimensional-Flow Wind Tunnel, With Consideration of the Effect of Compressibility. NACA Rep. 782, 1944. (Supersedes NACA WR A-63.)

14. Hama, Francis R.: An Efficient Tripping Device. J. Aeronaut. Sci., vol. 24, no. 3, Mar. 1957, pp. 236–237.

15. Pfenninger, Werner: Investigations on Reductions of Friction on Wings, in Particular by Means of Boundary Layer Suction. NACA TM 1181, 1947. (Translated from Mitteilungen aus dem Institut für Aerodynamik an der Eidgenössischen Technischen Hochschule Zürich, Nr. 13, 1946.)

16. Braslow, Albert L.; and Knox, Eugene C.: Simplified Method for Determination of Critical Height of Distributed Roughness Particles for Boundary-Layer Transition at Mach Numbers From 0 to 5. NACA TN 4363, 1958.

17. Schubauer, G. B.; and Klebanoff, P. S.: Contributions on the Mechanics of Boundary-Layer Transition. NACA Rep. 1289, 1956.

TABLE I.- AIRFOIL DESIGN SPECIFICATIONS

Parameter	Objective/ Constraint	Mach Number M	Reynolds Number R	Priority
Minimum lift coefficient $c_{l,min}$	0.15	0.70	552,000	Low
Maximum lift coefficient $c_{l,max}$	1.20	0.20	147,000	High
Lower limit of low-drag, lift-coefficient range $c_{l,ll}$	0.20	0.70	552,000	High
Upper limit of low-drag, lift-coefficient range $c_{l,ul}$	1.00	0.50	368,000	Medium
Zero-lift pitching-moment coefficient $c_{m,0}$	≥ -0.15	0.70	552,000	Low
Thickness t/c	> 0.06			Low
Other requirements: Maximum lift coefficient $c_{l,max}$ independent of leading-edge roughness Docile stall characteristics				

TABLE II.- MODEL ORIFICE LOCATIONS

[c = 160.0 mm (6.30 in.)]

Upper Surface		Lower Surface	
x/c	y, mm (in.)	x/c	y, mm (in.)
0.0000	–117.9 (–4.64)	0.0010	–140.0 (–5.51)
.0006	–115.8 (–4.56)	.0080	–137.9 (–5.43)
.0050	–113.8 (–4.48)	.0204	–135.9 (–5.35)
.0137	–111.8 (–4.40)	.0379	–133.9 (–5.27)
.0267	–110.7 (–4.36)	.0601	–132.8 (–5.23)
.0440	–109.7 (–4.32)	.0866	–131.8 (–5.19)
.0655	–108.7 (–4.28)	.1172	–103.8 (–5.15)
.0911	–107.7 (–4.24)	.1515	–129.8 (–5.11)
.1207	–106.7 (–4.20)	.1892	–128.5 (–5.06)
.1539	–105.7 (–4.16)	.2301	–127.3 (–5.01)
.1906	–104.4 (–4.11)	.2738	–126.0 (–4.96)
.2303	–103.1 (–4.06)	.3202	–124.5 (–4.90)
.2729	–101.9 (–4.01)	.3689	–122.9 (–4.84)
.3179	–100.3 (–3.95)	.4197	–121.4 (–4.78)
.3650	–98.8 (–3.89)	.4721	–119.9 (–4.72)
.4136	–97.3 (–3.83)	.5256	–118.4 (–4.66)
.4632	–95.8 (–3.77)	.5796	–116.8 (–4.60)
.5133	–94.2 (–3.71)	.6335	–115.3 (–4.54)
.5635	–92.7 (–3.65)	.6866	–113.8 (–4.48)
.6131	–91.2 (–3.59)	.7381	–112.3 (–4.42)
.6617	–89.7 (–3.53)	.7874	–110.7 (–4.36)
.7087	–88.1 (–3.47)	.8335	–109.2 (–4.30)
.7536	–86.9 (–3.42)	.8757	–108.0 (–4.25)
.7958	–85.6 (–3.37)	.9129	–106.7 (–4.20)
.8349	–84.3 (–3.32)	.9442	–105.7 (–4.16)
.8705	–83.3 (–3.28)	.9687	–103.6 (–4.08)
.9021	–82.3 (–3.24)	.9861	–101.6 (–4.00)
.9294	–81.3 (–3.20)	.9966	–99.6 (–3.92)
.9527	–80.3 (–3.16)		
.9720	–78.2 (–3.08)		
.9870	–76.2 (–3.00)		
.9966	–74.2 (–2.92)		
1.0000	–71.4 (–2.81)		

TABLE III.- TRIP LOCATIONS AND SIZES

R	Upper surface		Lower surface	
	x/c	Serrated-tape thickness, mm (in.)	x/c	Serrated-tape thickness, mm (in.)
70,000	0.05	0.396 (0.0156)	0.10	0.853 (0.0336)
100,000		0.351 (0.0138)		0.648 (0.0255)
150,000		0.282 (0.0111)		
200,000		0.218 (0.0086)		
300,000		0.135 (0.0053)		
600,000		0.043 (0.0017)		0.432 (0.0170)

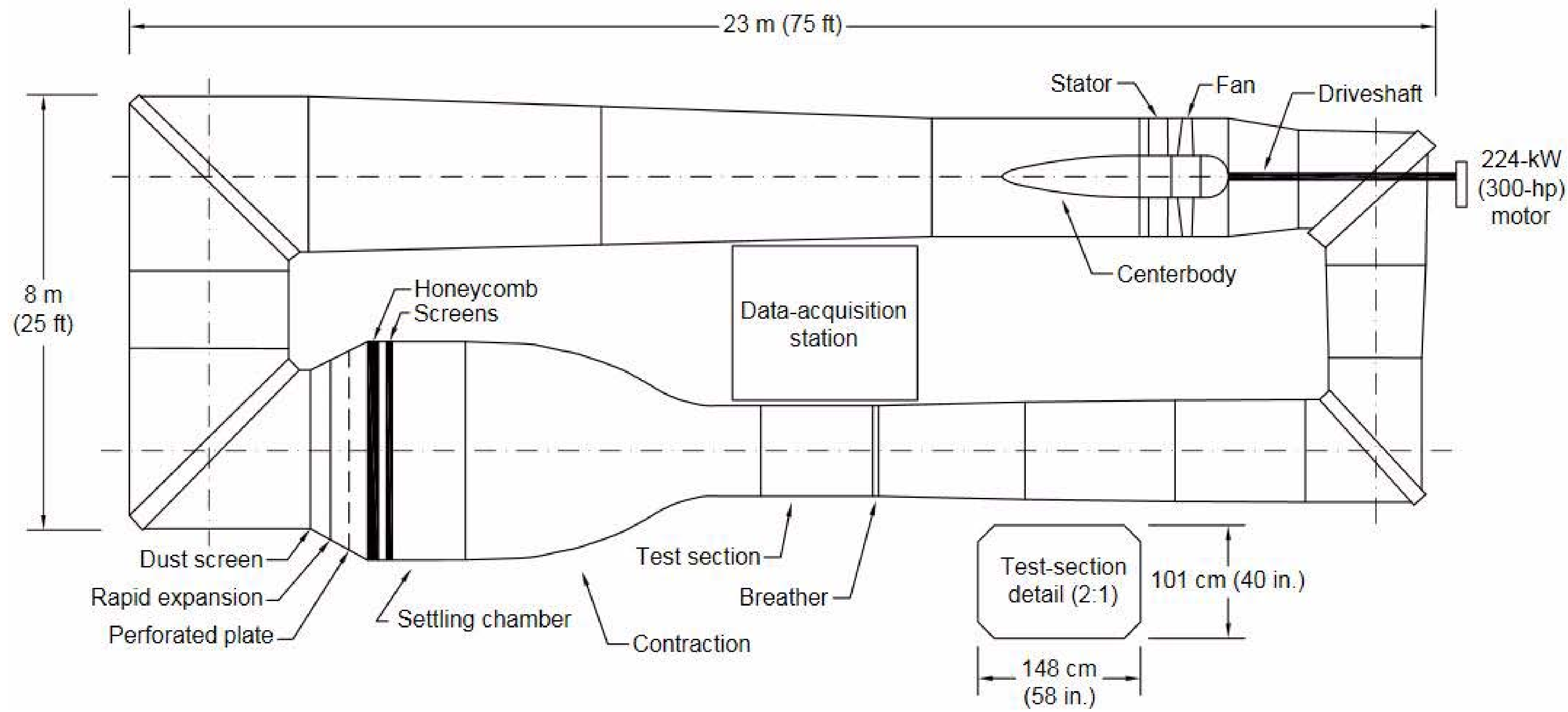

Figure 1.- The Pennsylvania State University Low-Speed, Low-Turbulence Wind Tunnel.

Figure 2.- S407 airfoil model and wake-survey probe mounted in test section.

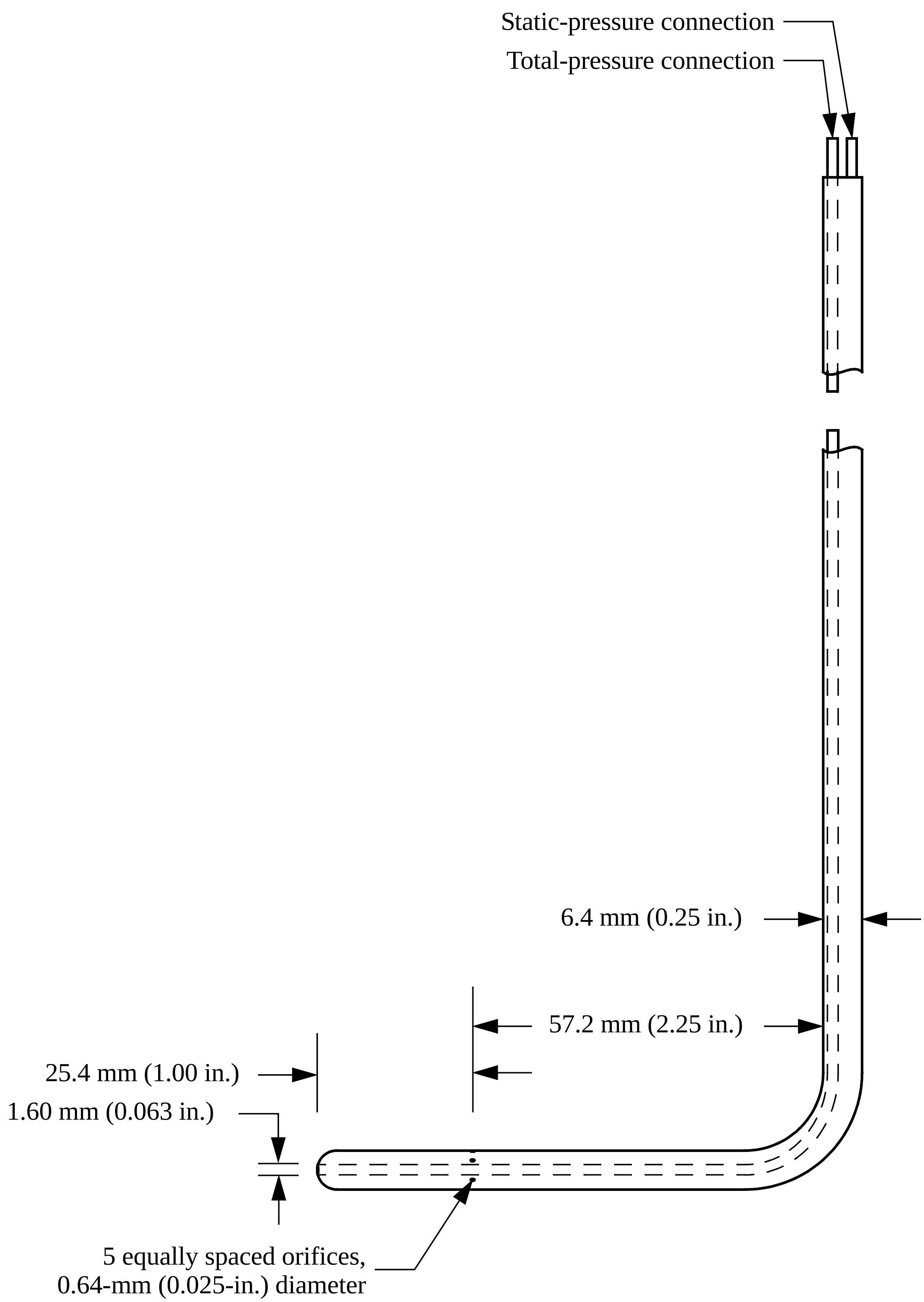

Figure 3.- Wake-survey probe.

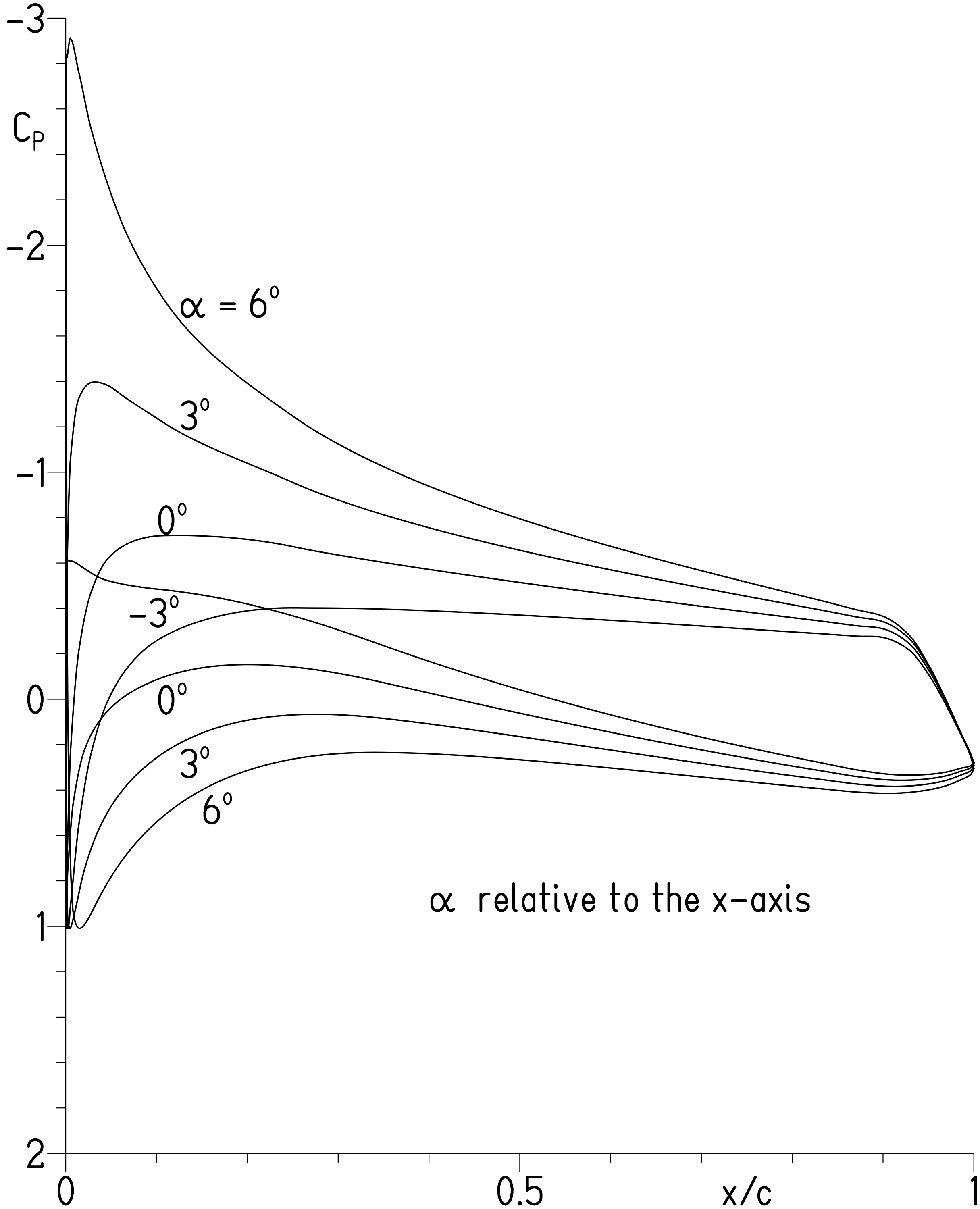

(a) M = 0.20.

Figure 4.- Theoretical (inviscid) pressure distributions.

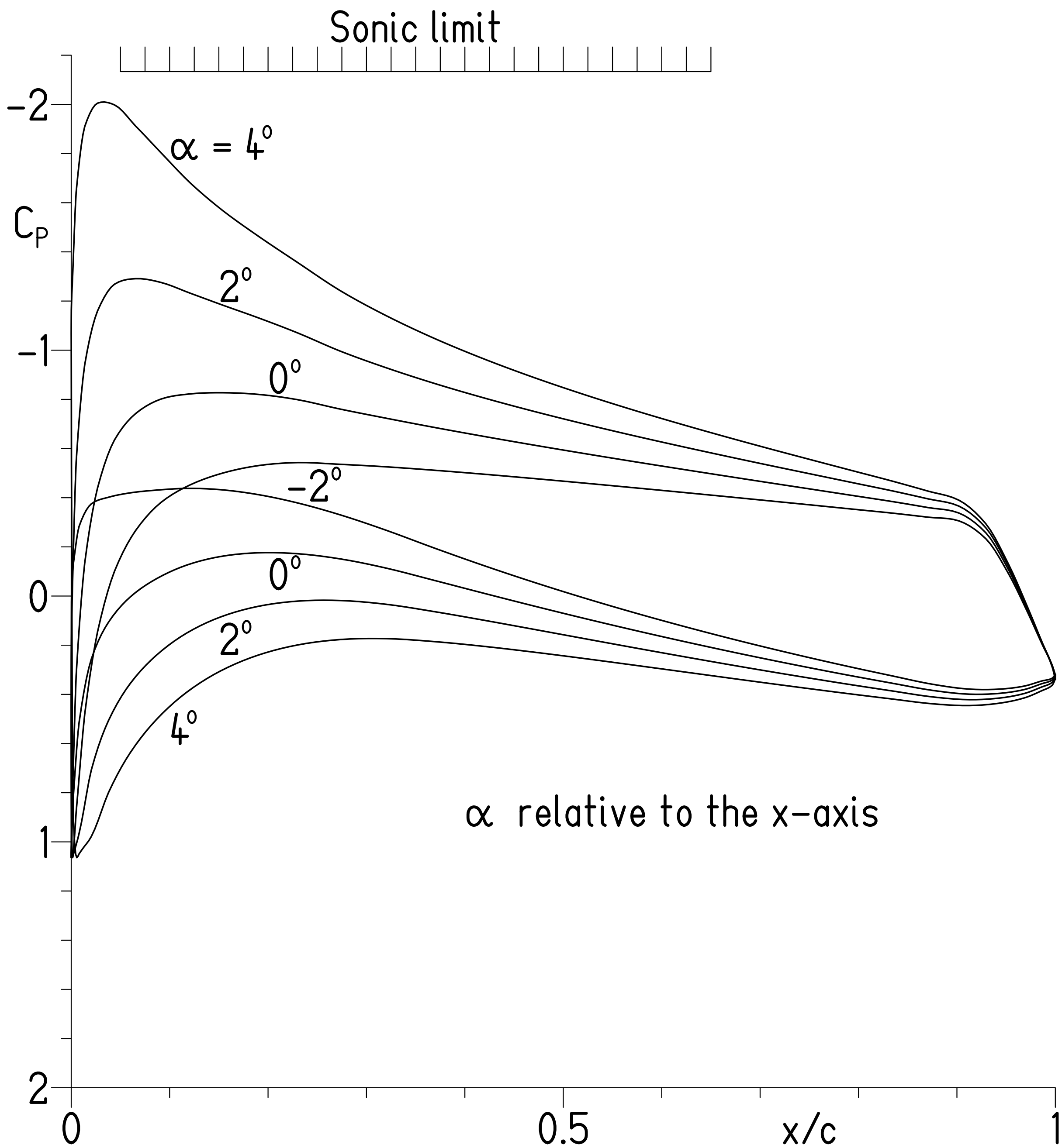

(b) M = 0.50.

Figure 4.- Continued.

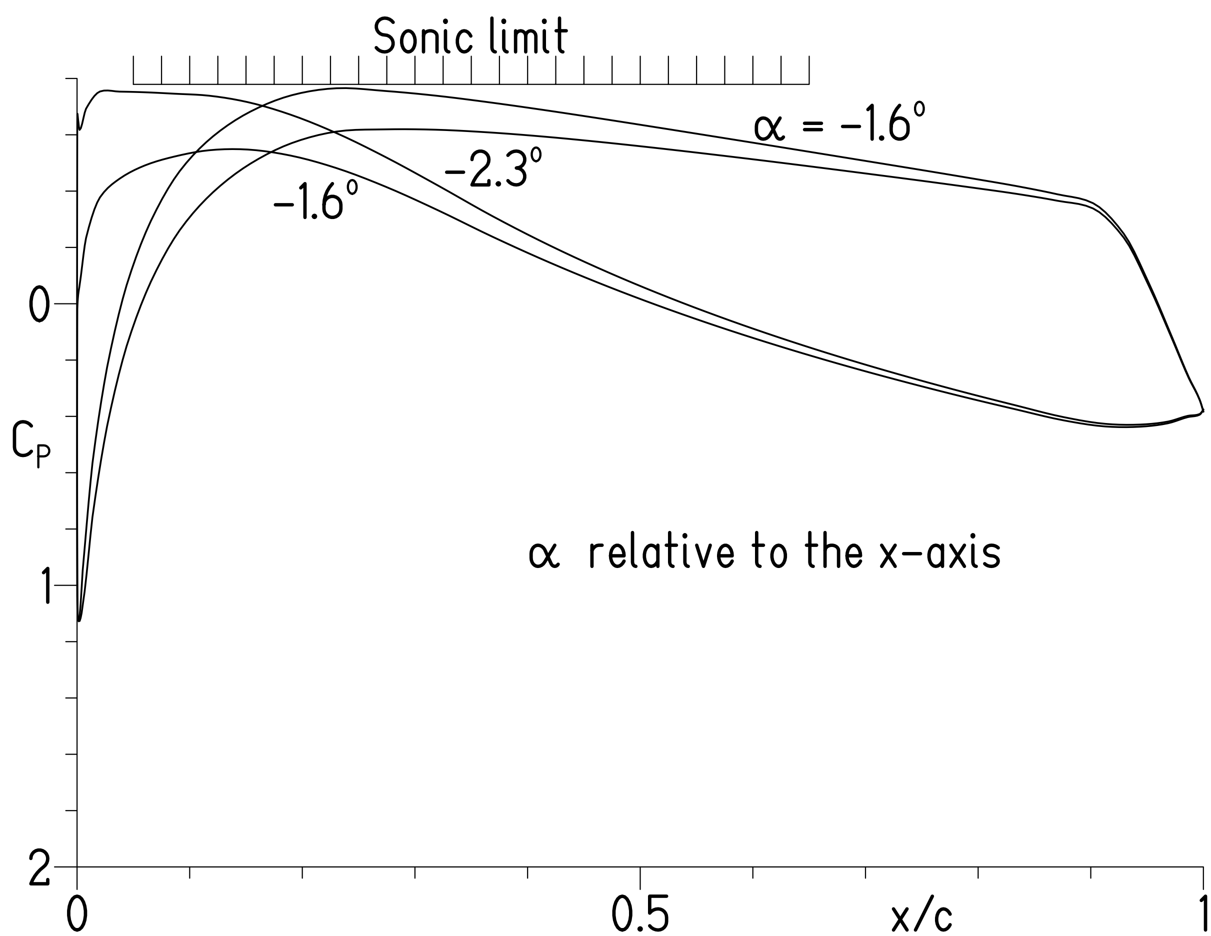

(c) M = 0.70.

Figure 4.- Concluded.

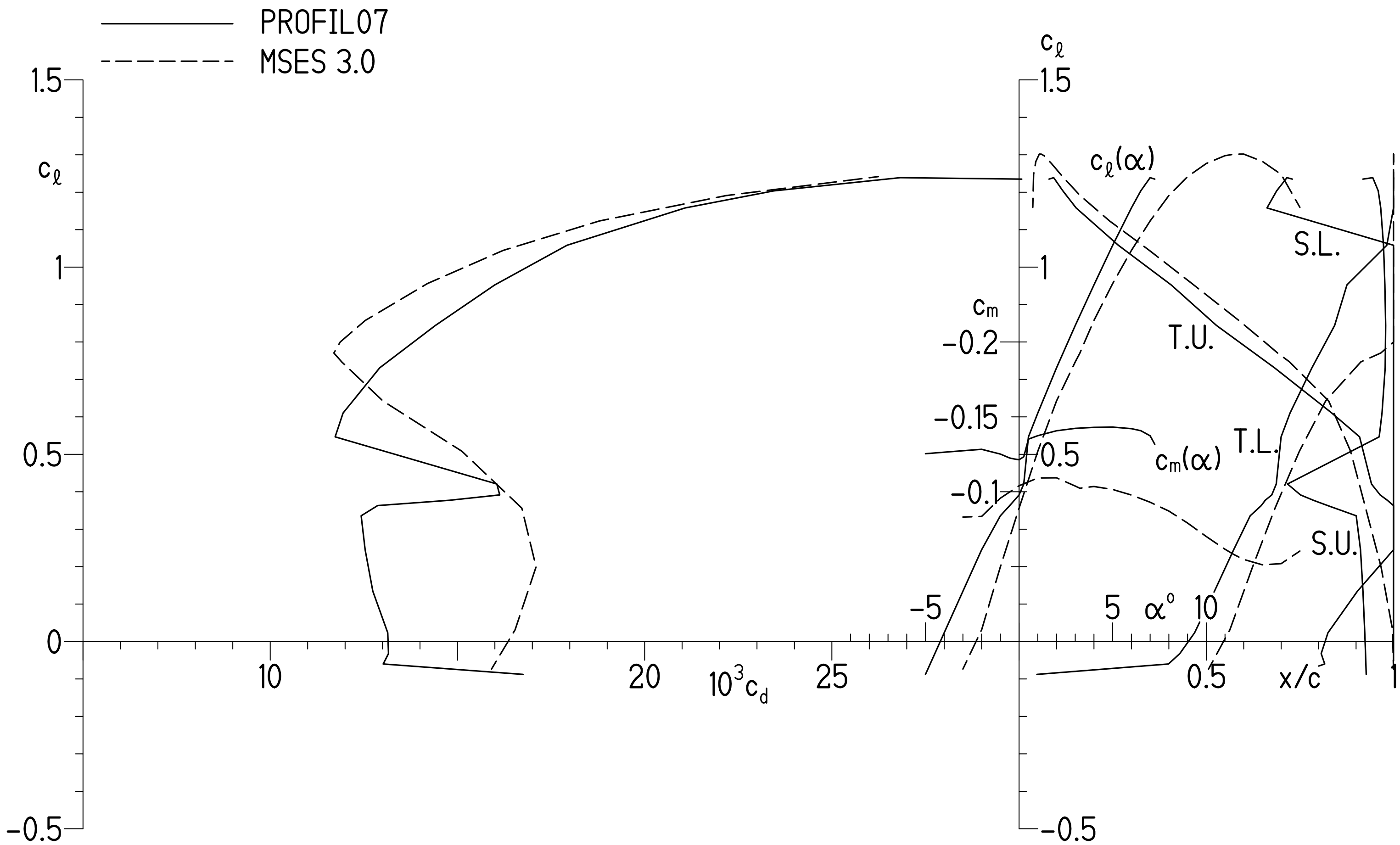

(a) Transition free.

Figure 5.- Theoretical section characteristics at M = 0.20 and R = 147,000.

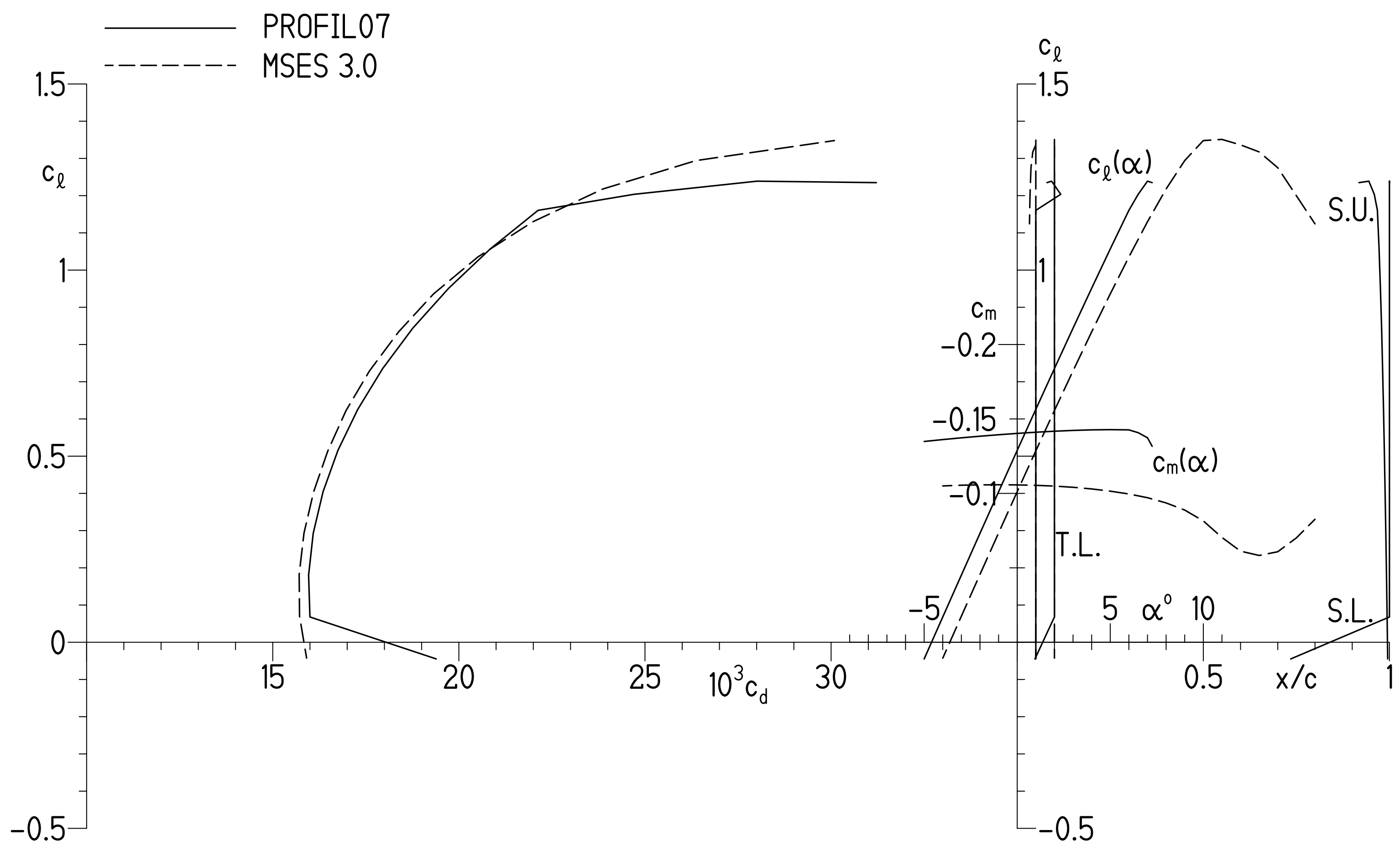

(b) Transition fixed.

Figure 5.- Concluded.

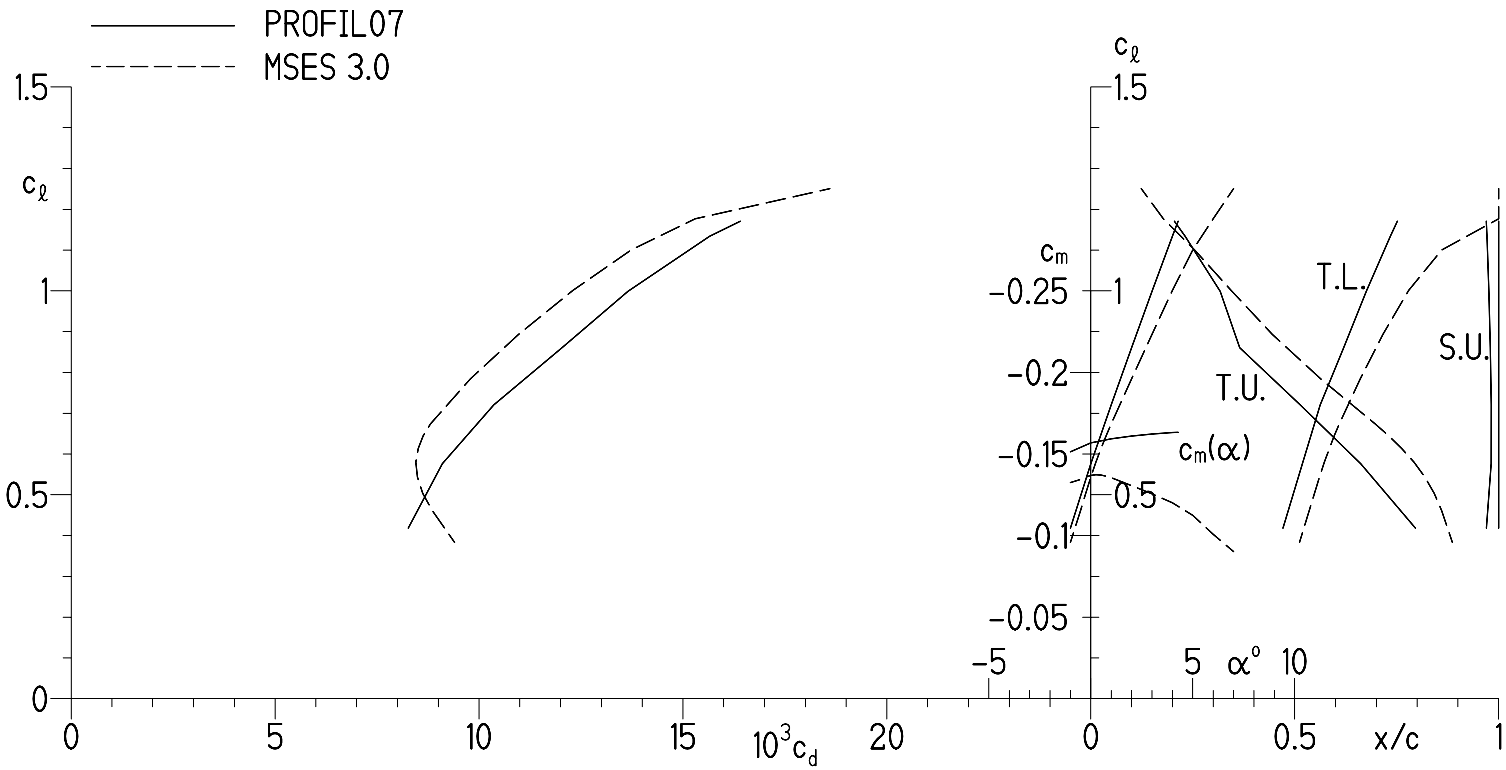

(a) Transition free.

Figure 6.- Theoretical section characteristics at M = 0.50 and R = 368,000.

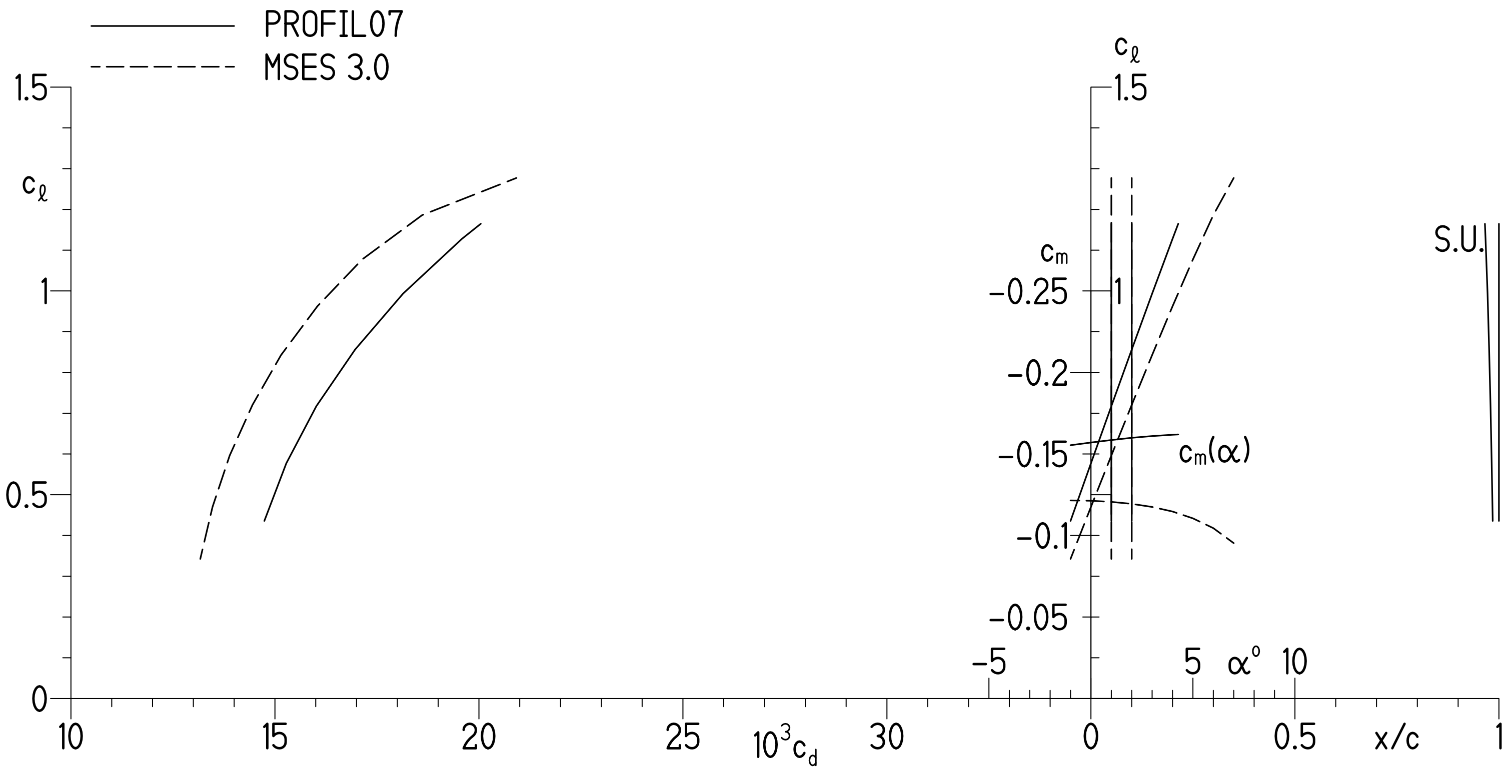

(b) Transition fixed.

Figure 6.- Concluded.

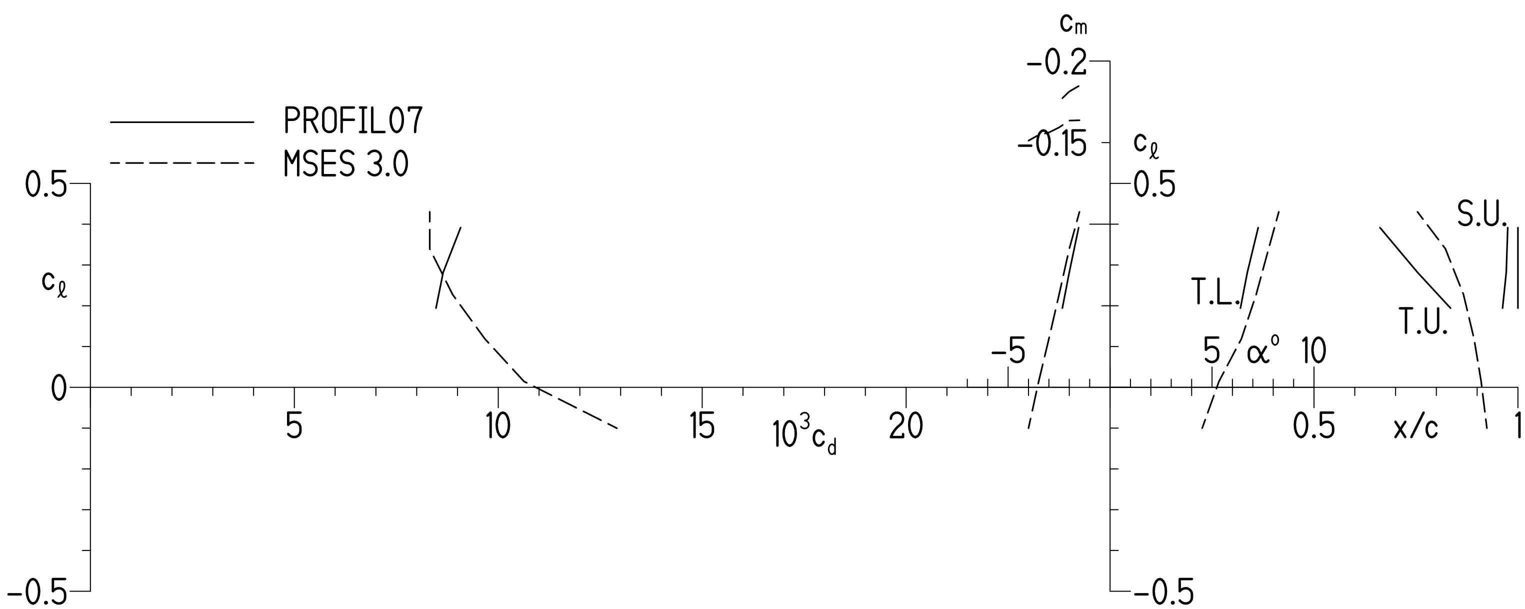

(a) Transition free.

Figure 7.- Theoretical section characteristics at M = 0.70 and R = 552,000.

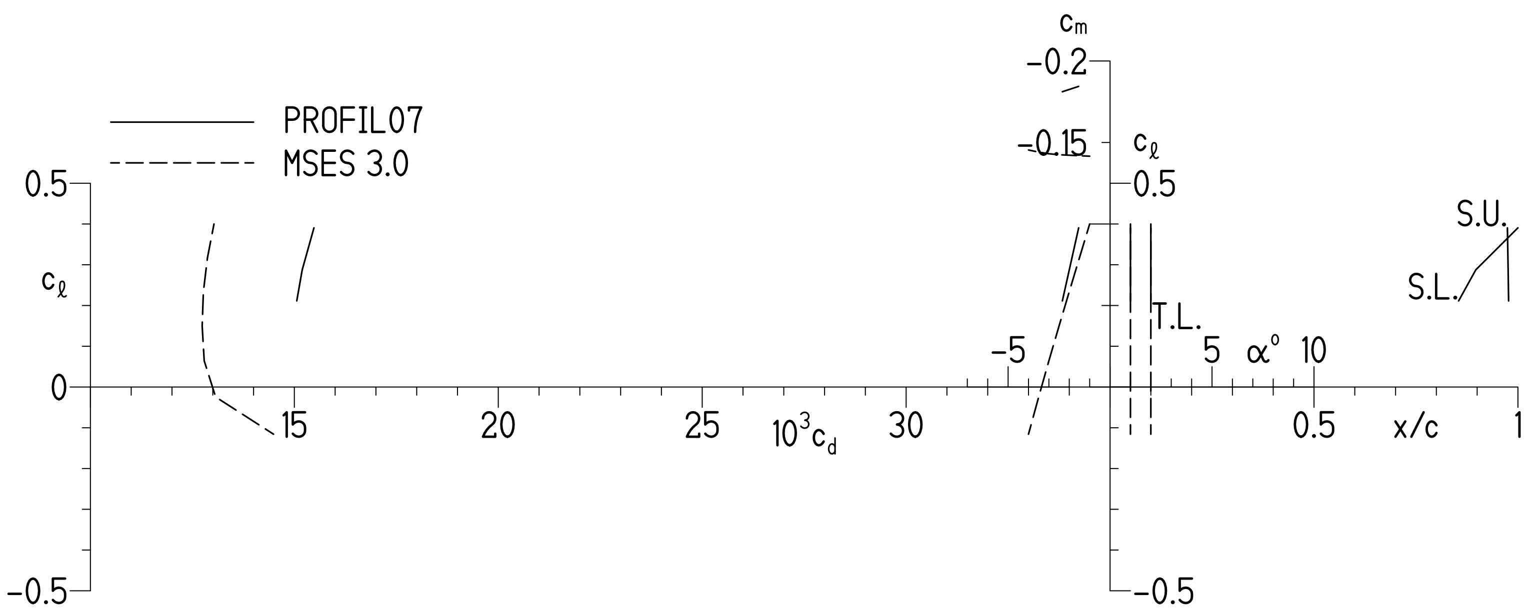

(b) Transition fixed.

Figure 7.- Concluded.

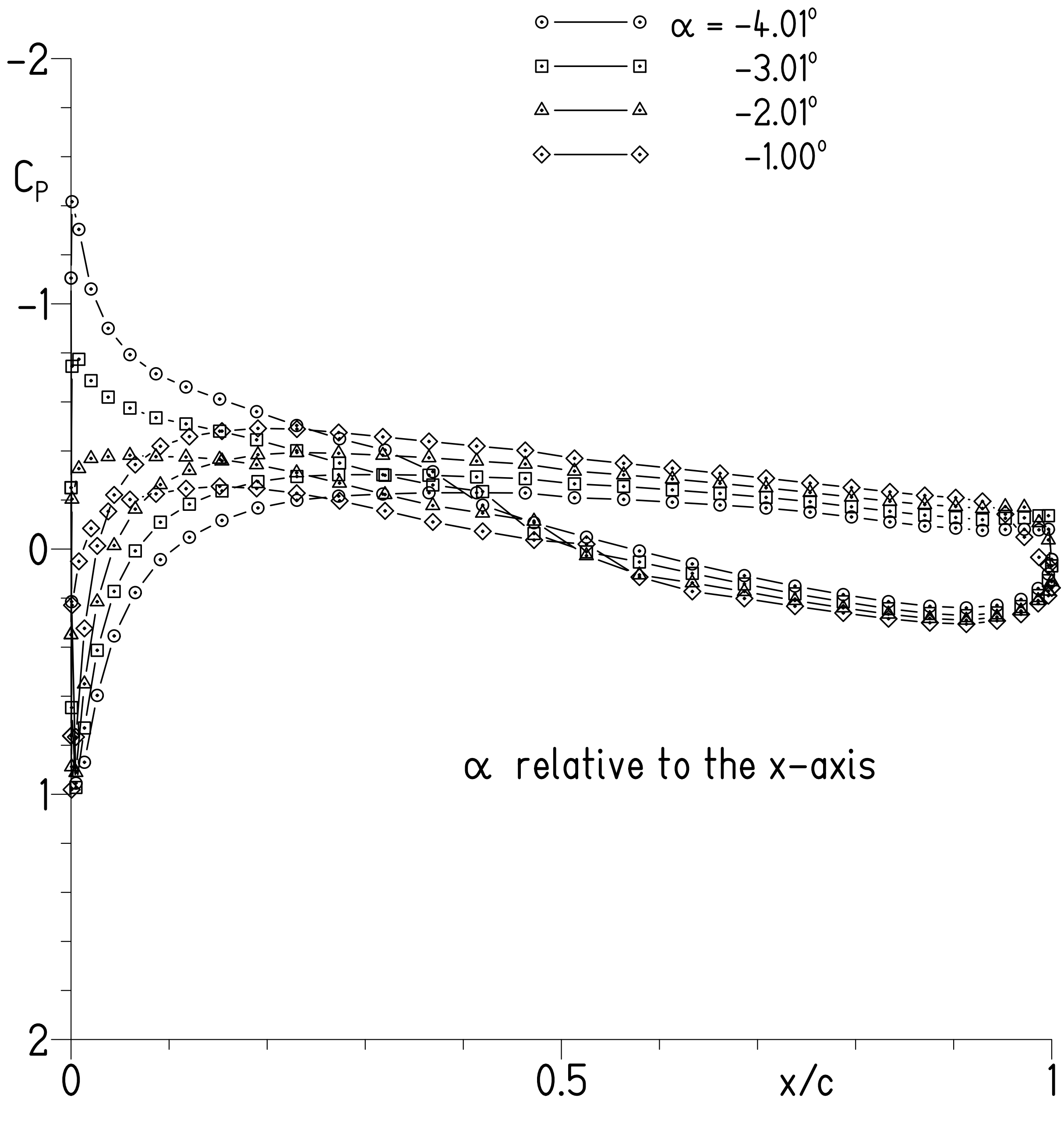

(a) α = −4.01°, −3.01°, −2.01°, and −1.00°.

Figure 8.- Experimental pressure distributions for R = 300,000 and M = 0.09 with transition free.

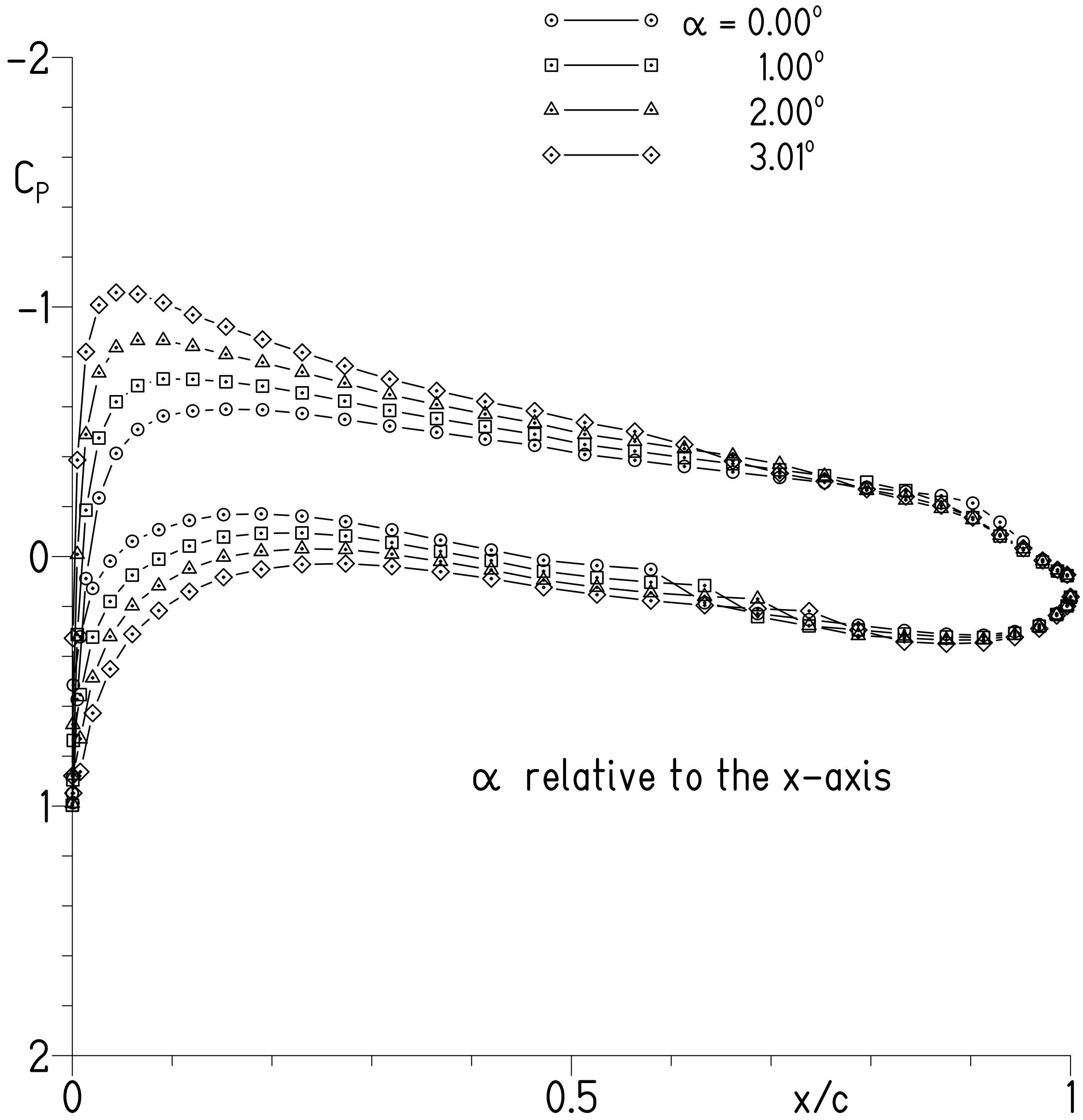

(b) α = 0.00°, 1.00°, 2.00°, and 3.01°.

Figure 8.- Continued.

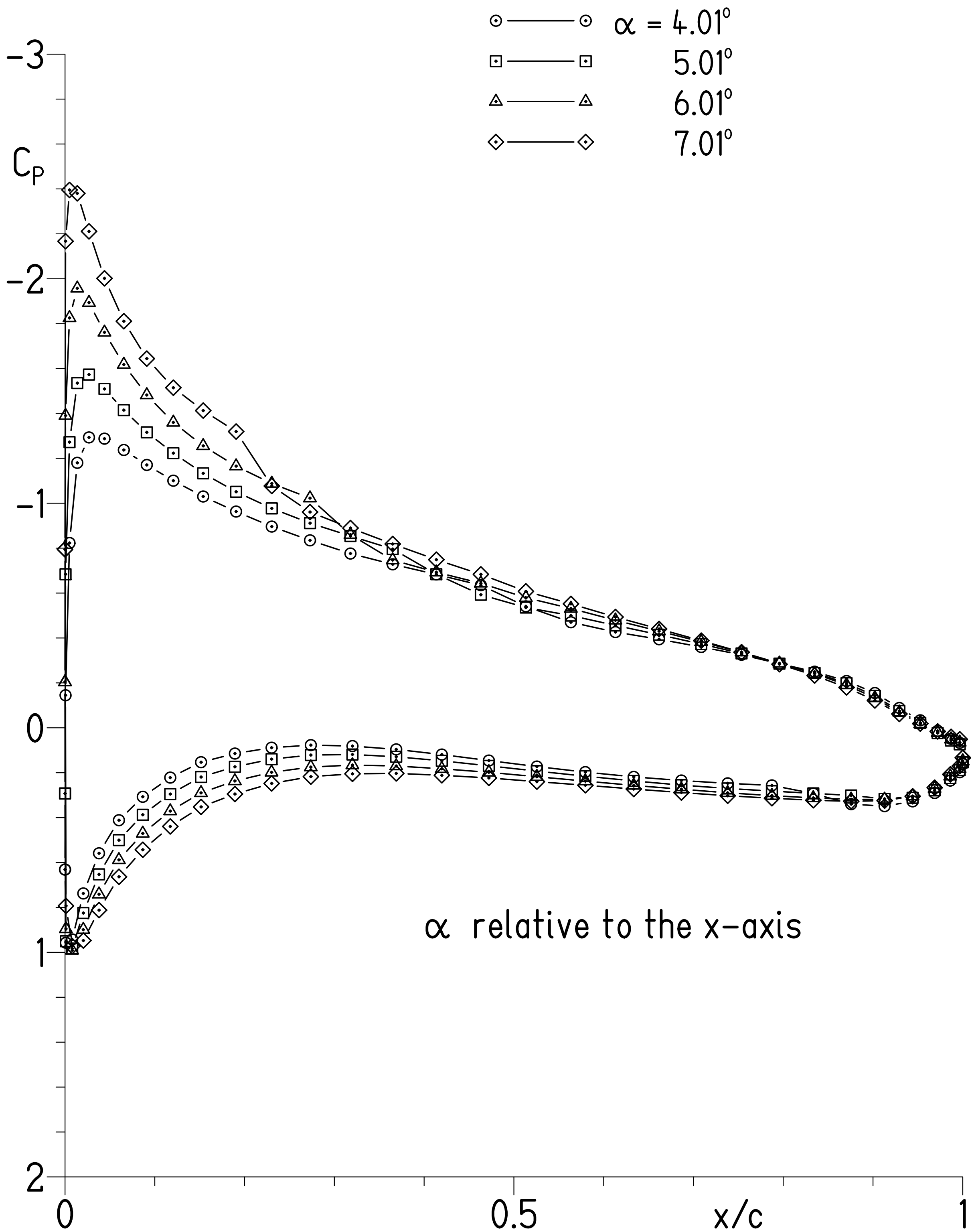

(c) α = 4.01°, 5.01°, 6.01°, and 7.01°.

Figure 8.- Continued.

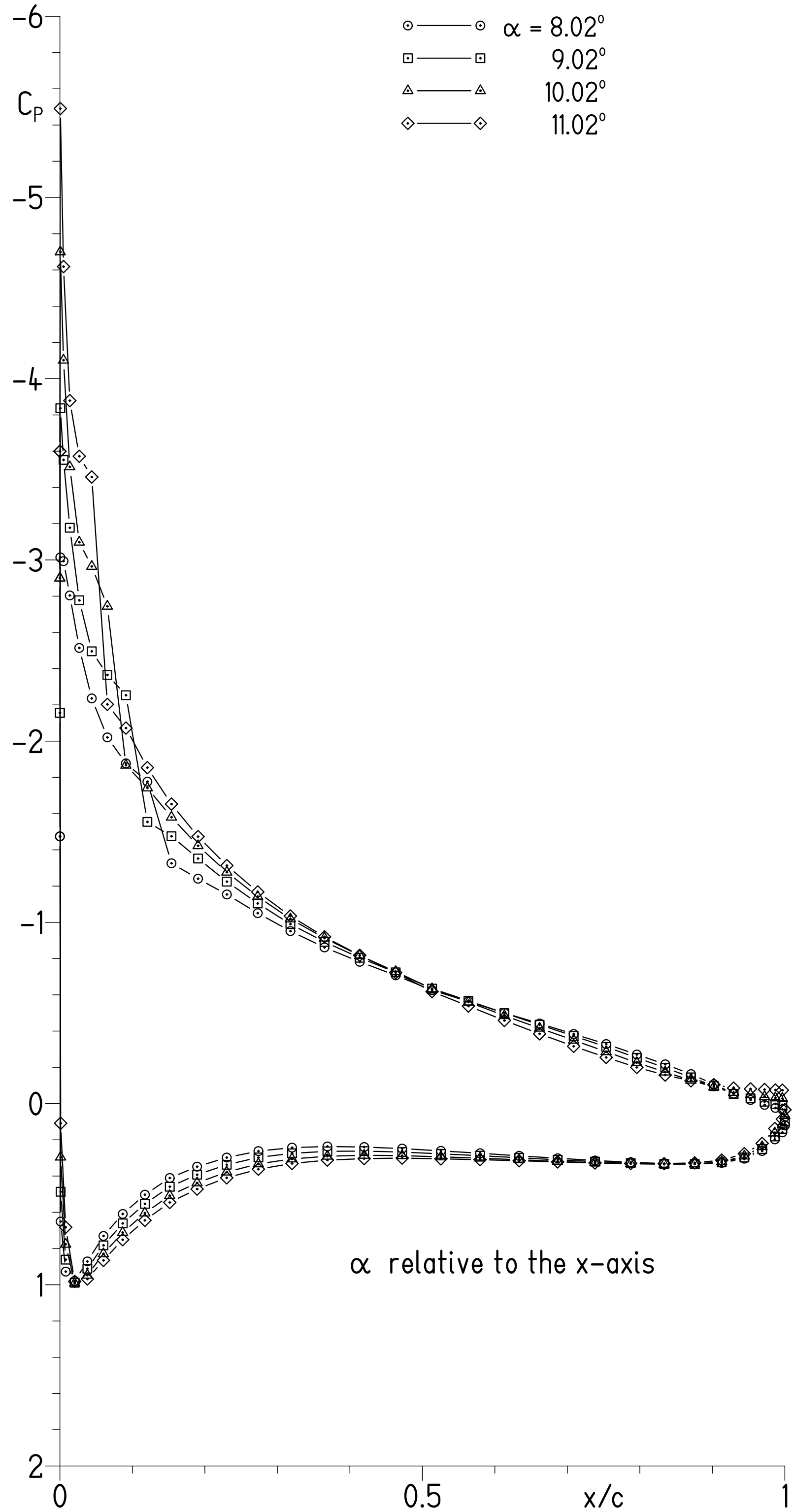

(d) α = 8.02°, 9.02°, 10.02°, and 11.02°.

Figure 8.- Continued.

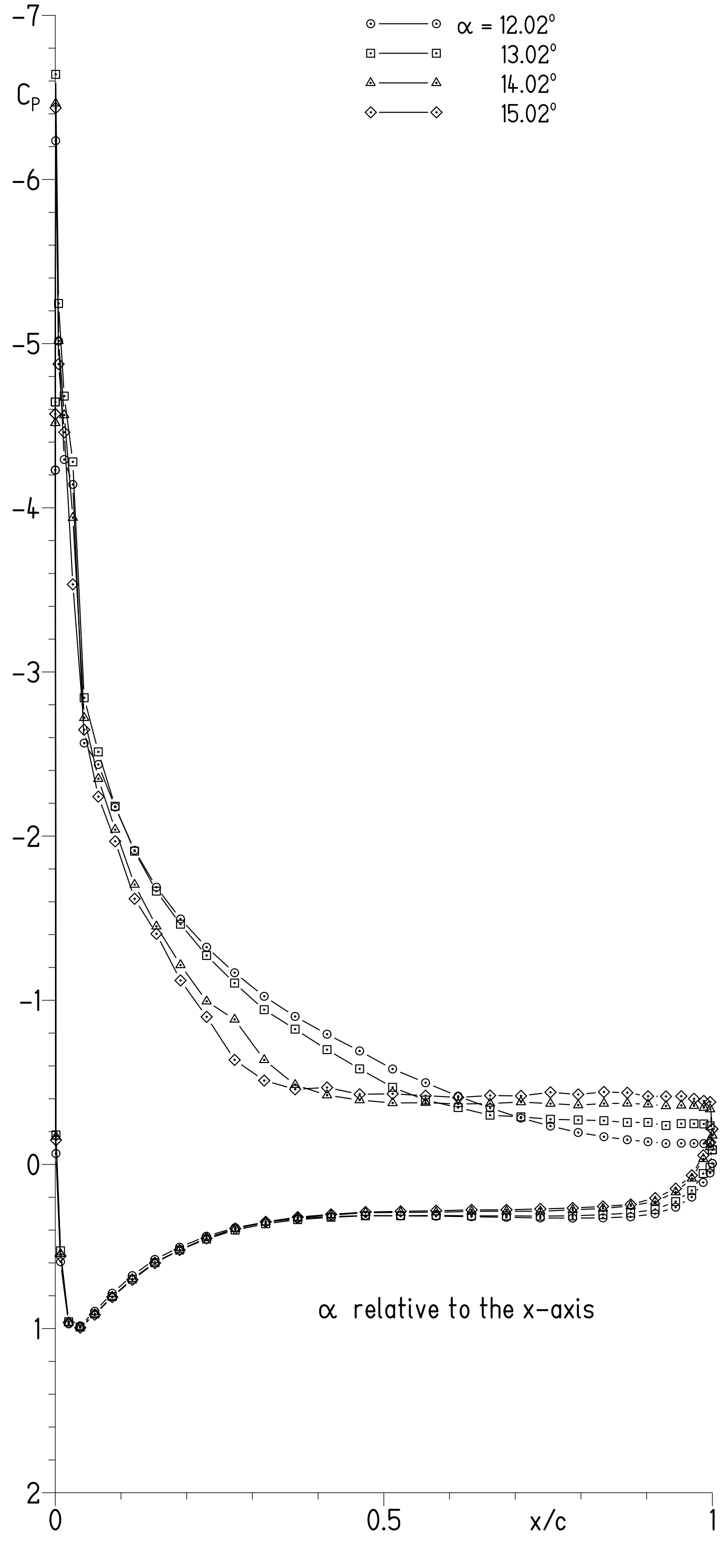

(e) α = 12.02°, 13.02°, 14.02°, and 15.02°.

Figure 8.- Continued.

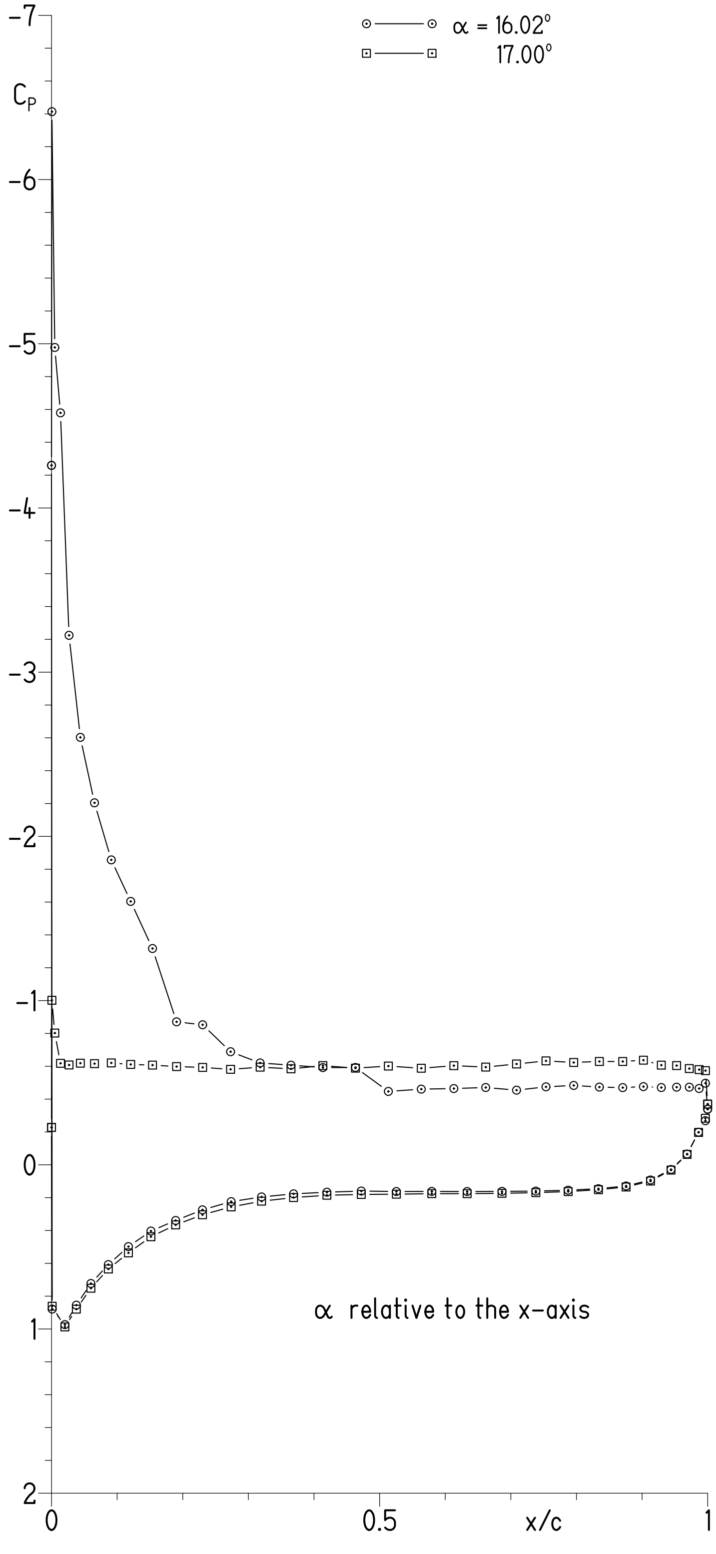

(f) α = 16.02° and 17.00°.

Figure 8.- Concluded.

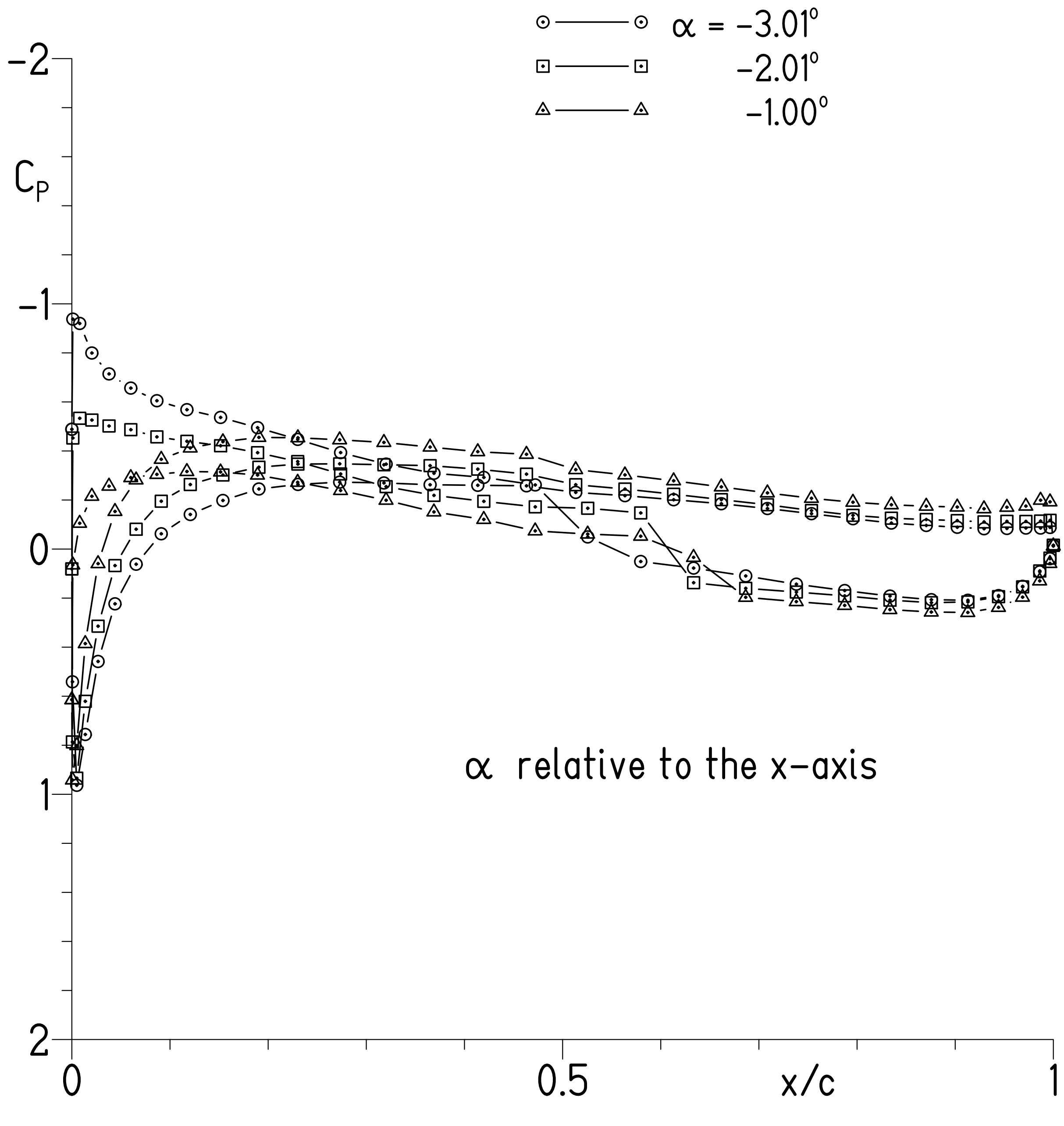

(a) α = −3.01°, −2.01°, and −1.00°.

Figure 9.- Experimental pressure distributions for R = 150,000 and M = 0.04 with transition free.

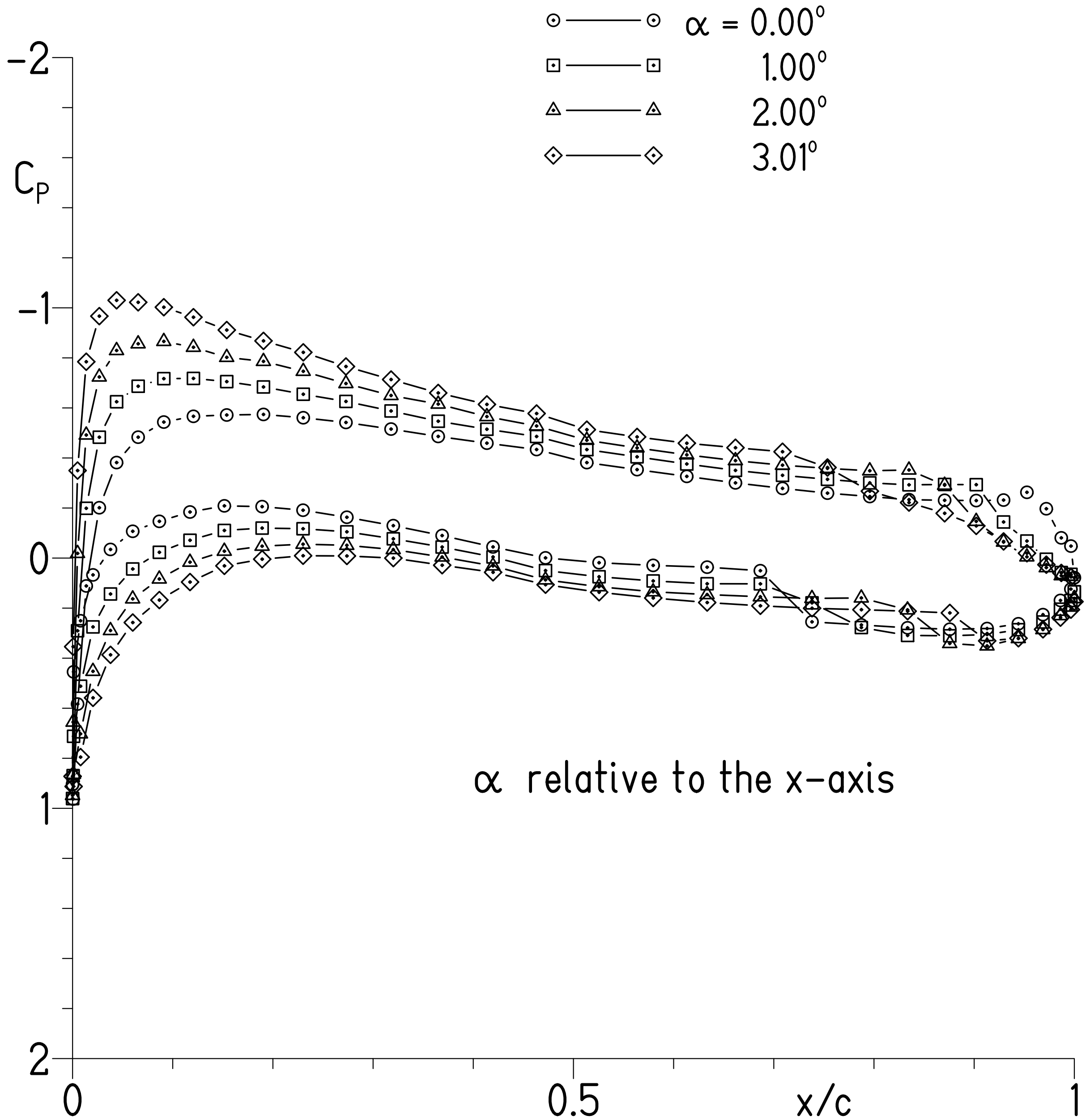

(b) α = 0.00°, 1.00°, 2.00°, and 3.01°.

Figure 9.- Continued.

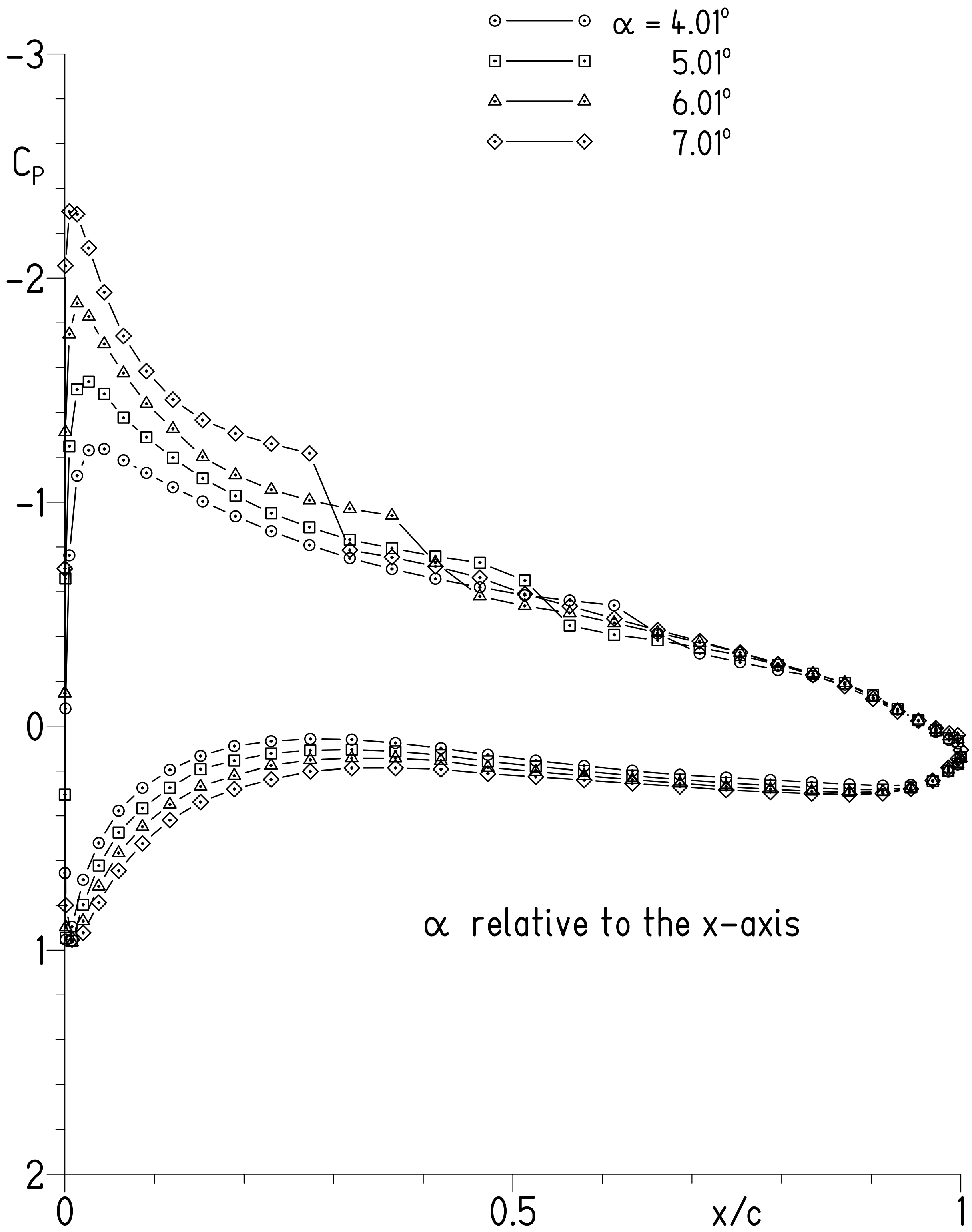

(c) α = 4.01°, 5.01°, 6.01°, and 7.01°.

Figure 9.- Continued.

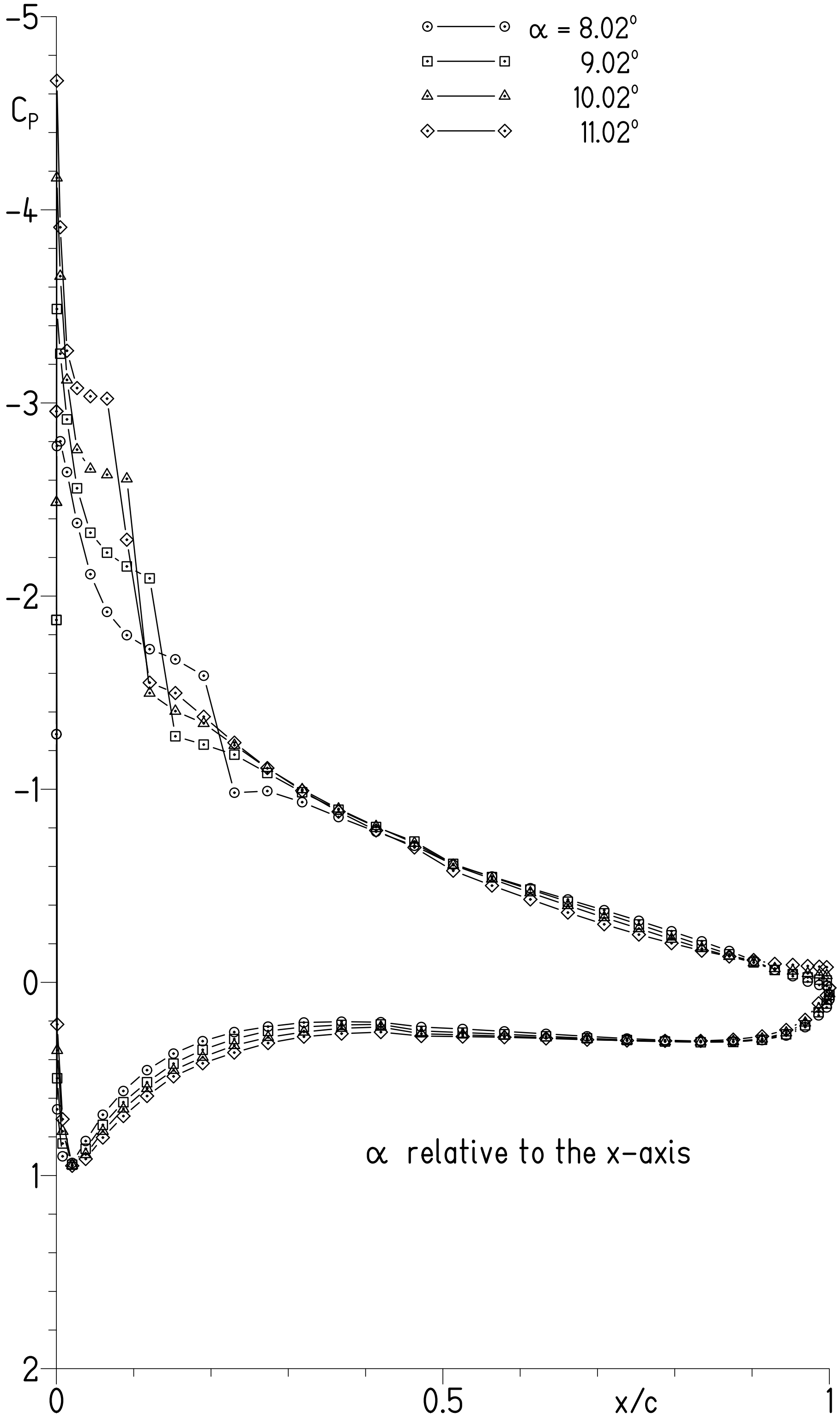

(d) α = 8.02°, 9.02°, 10.02°, and 11.02°.

Figure 9.- Continued.

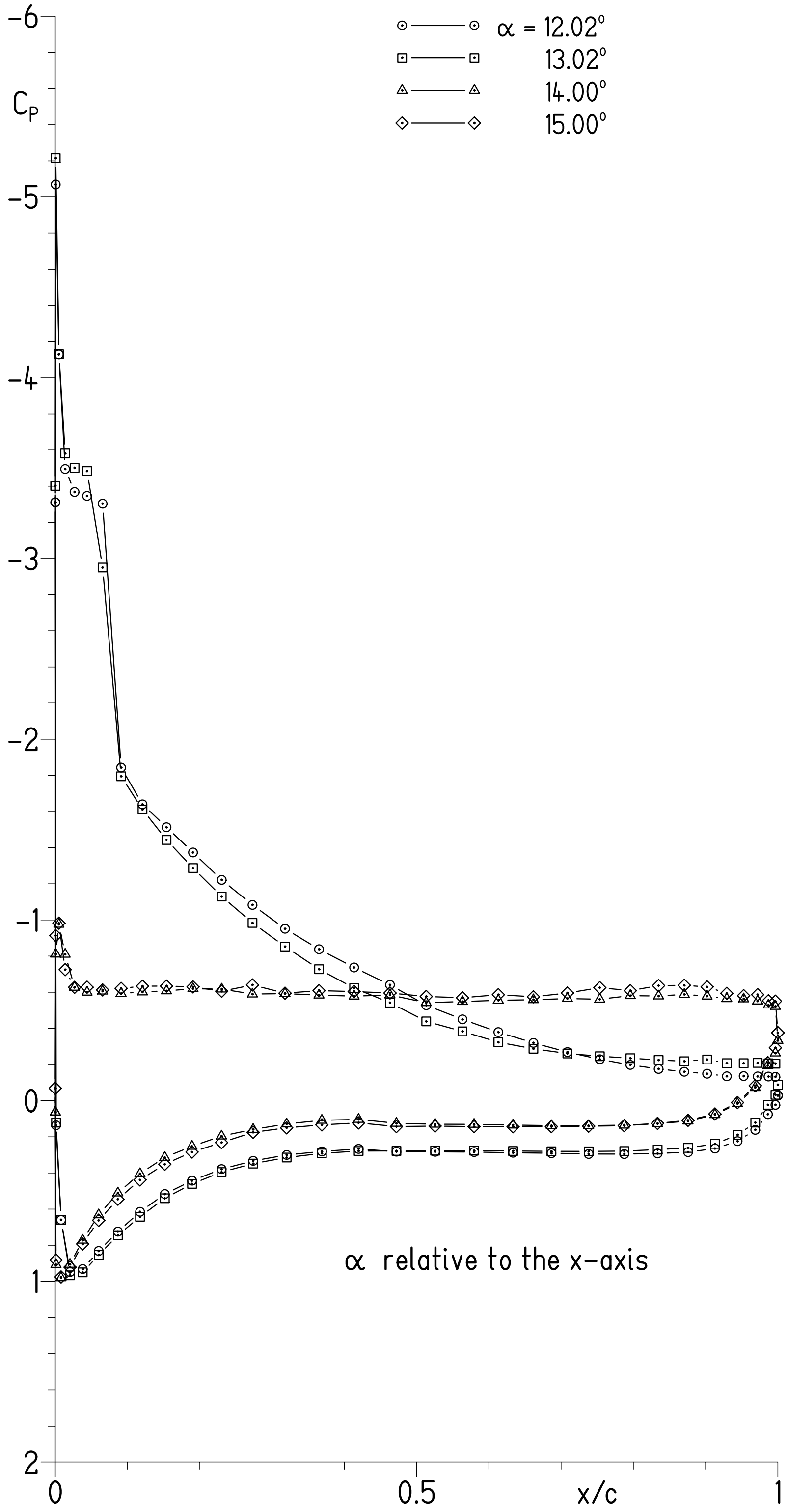

(e) α = 12.02°, 13.02°, 14.00°, and 15.00°.

Figure 9.- Concluded.

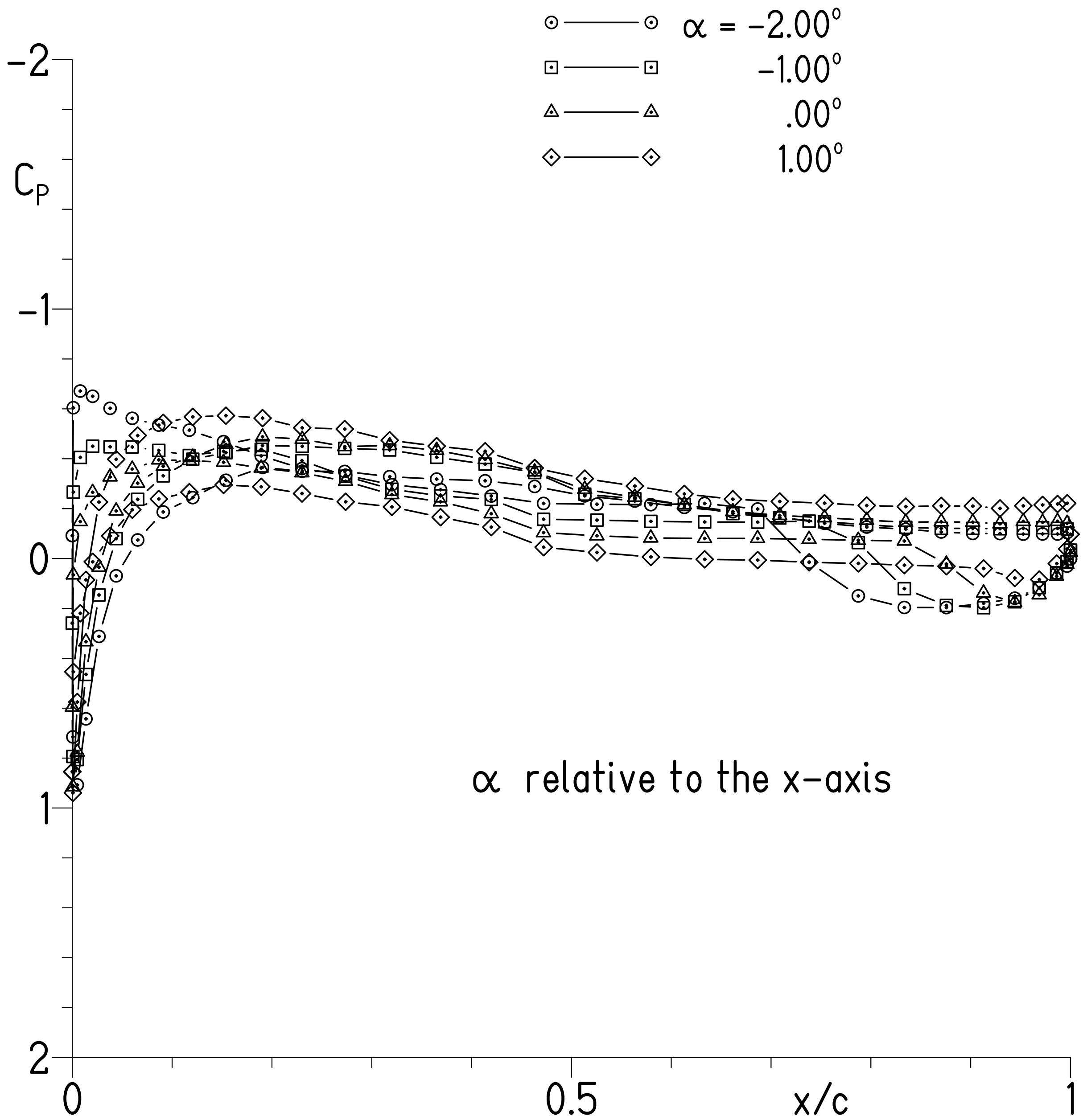

(a) α = −2.00°, −1.00°, 0.00°, and 1.00°.

Figure 10.- Experimental pressure distributions for R = 70,000 and M = 0.02 with transition free.

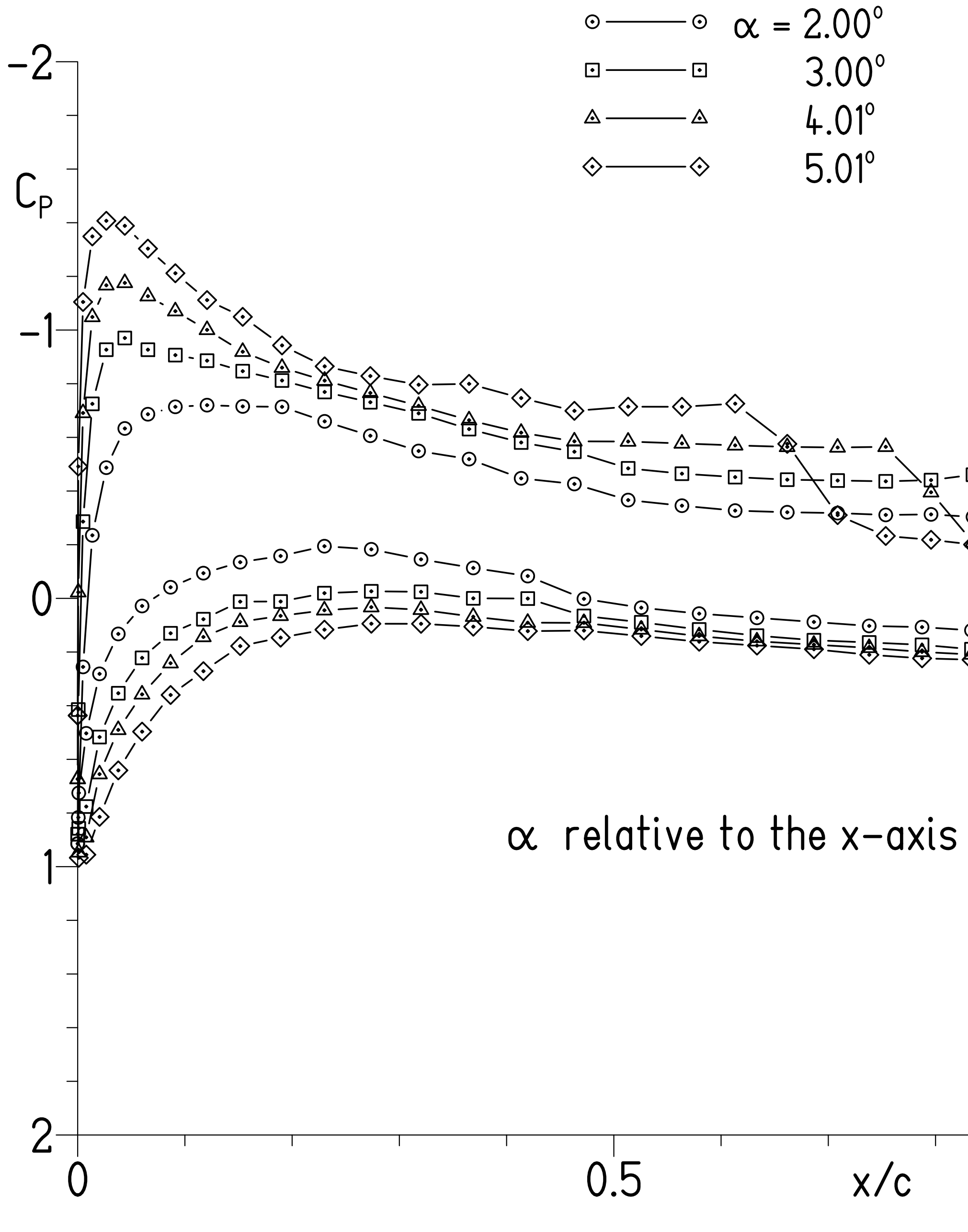

(b) α = 2.00°, 3.00°, 4.01°, and 5.01°.

Figure 10.- Continued.

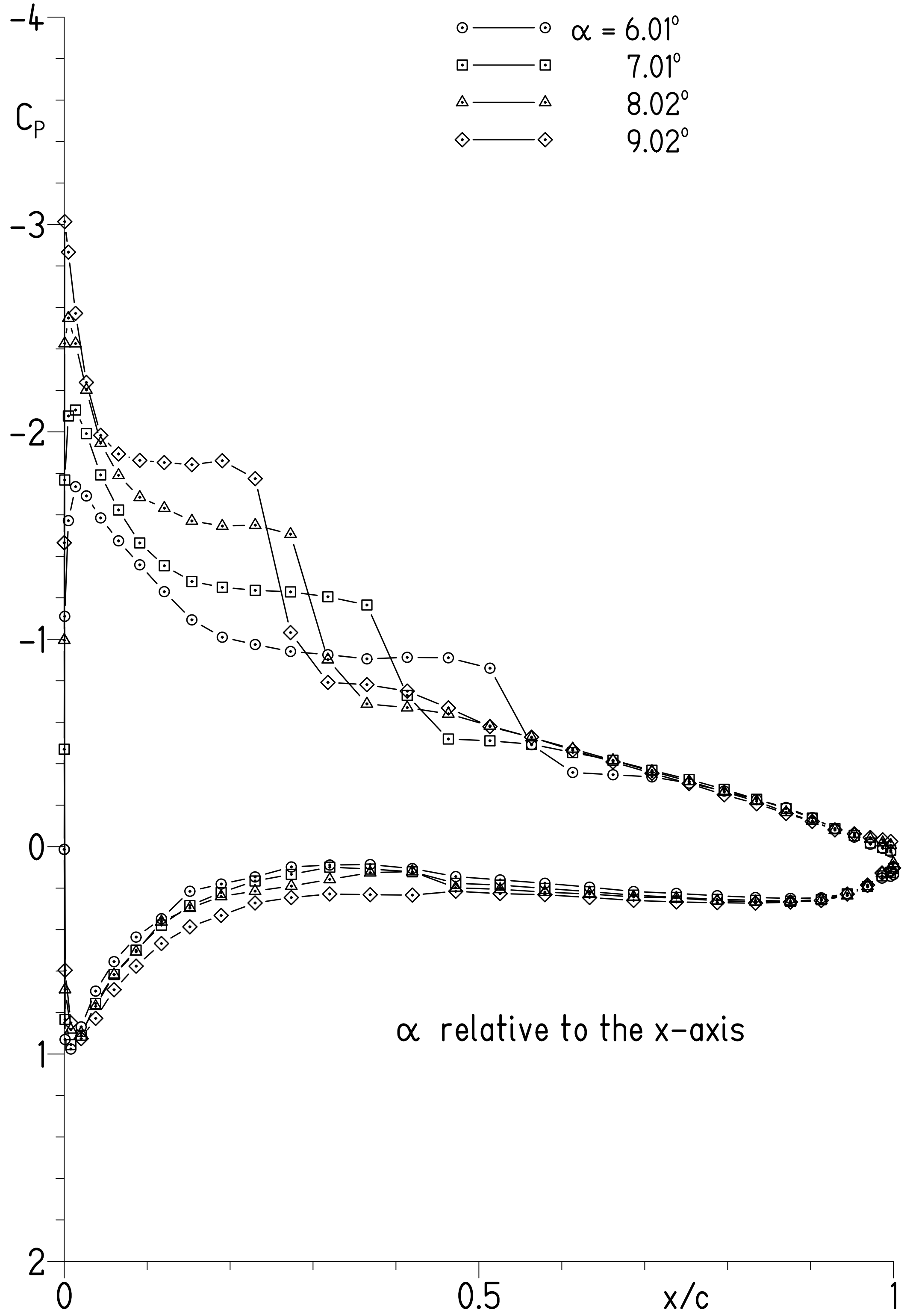

(c) α = 6.01°, 7.01°, 8.02°, and 9.02°.

Figure 10.- Continued.

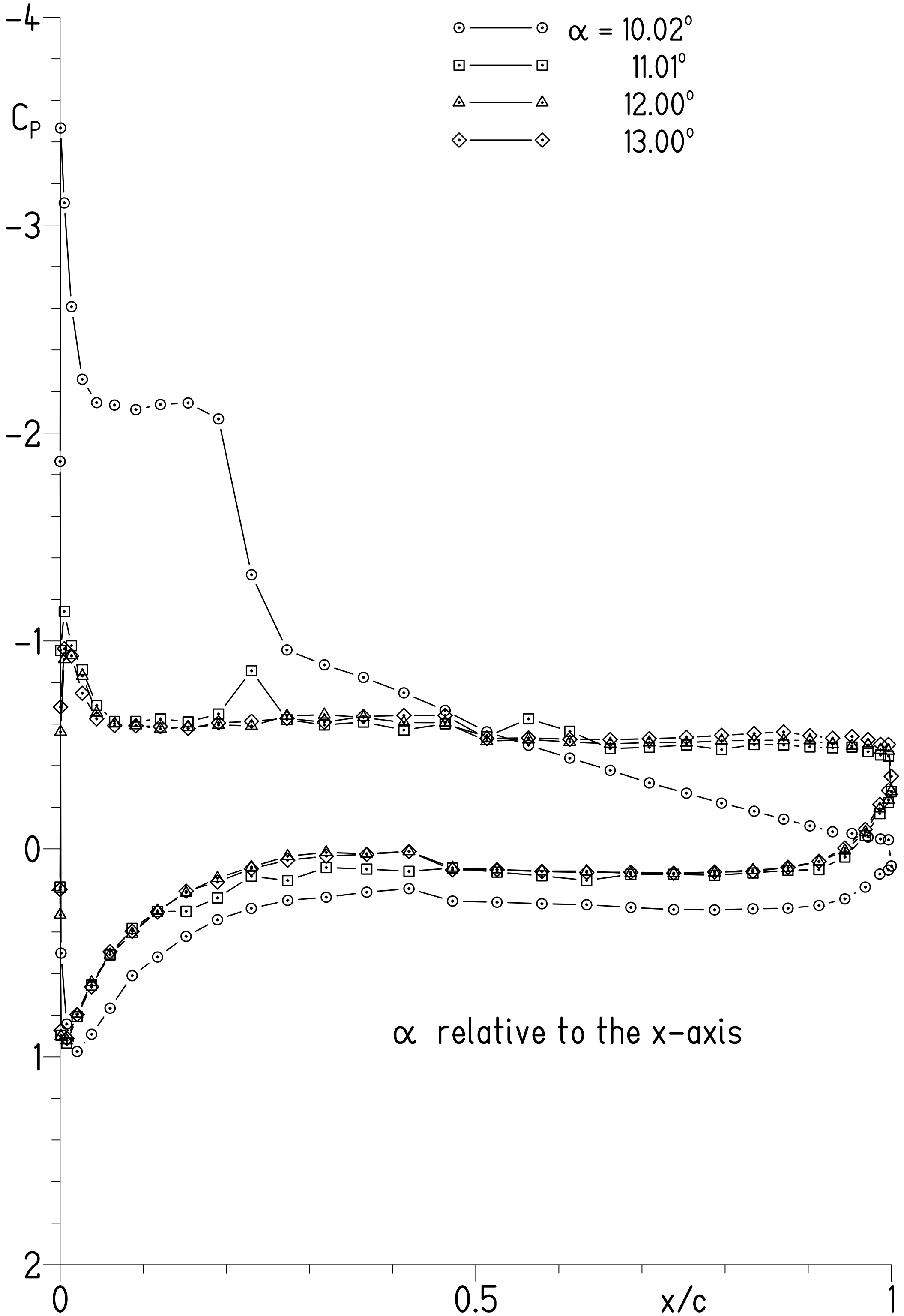

(d) α = 10.02°, 11.01°, 12.00°, and 13.00°.

Figure 10.- Concluded.

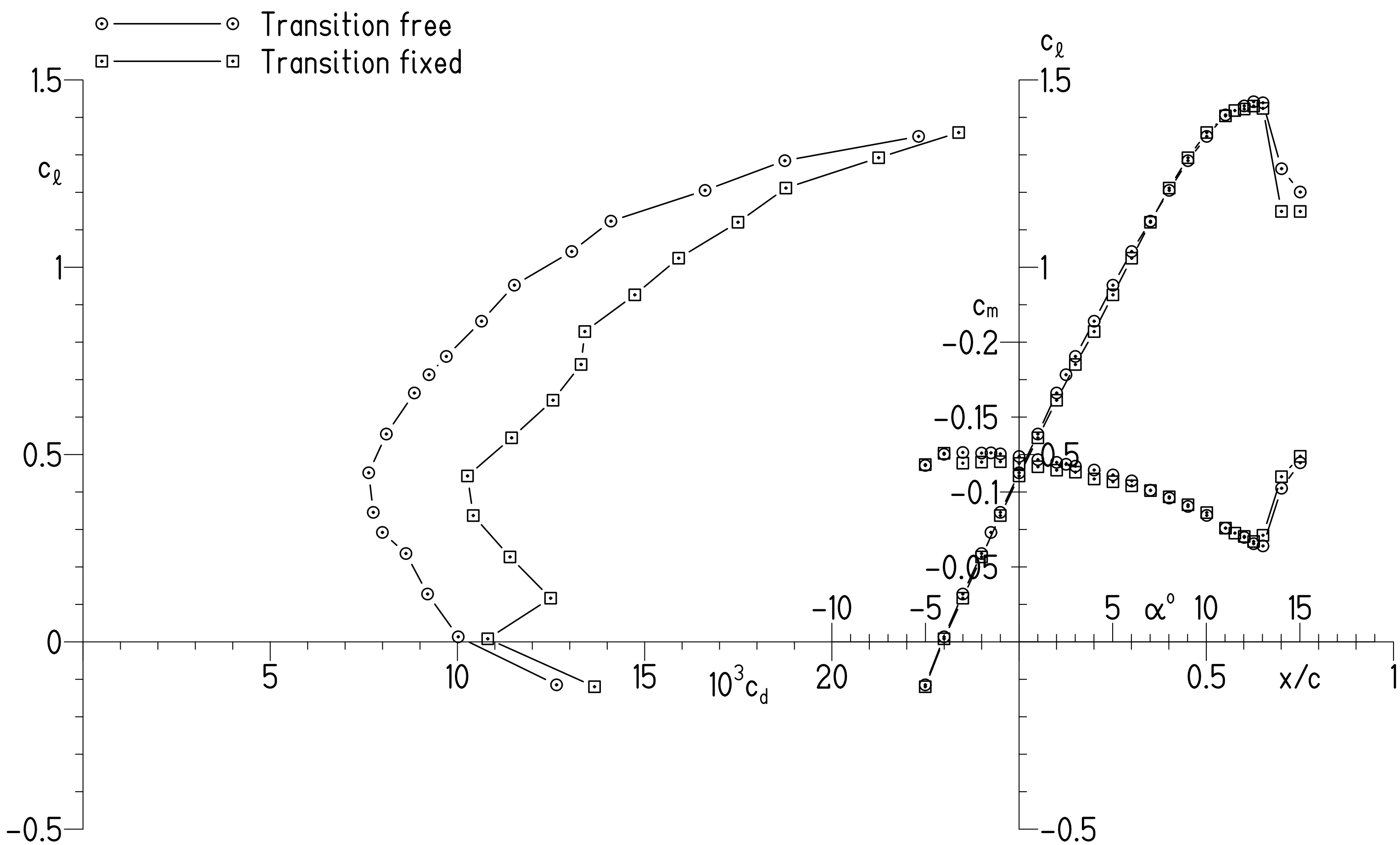

(a) R = 598,000 and M = 0.19.

Figure 11.- Experimental section characteristics with transition free and transition fixed.

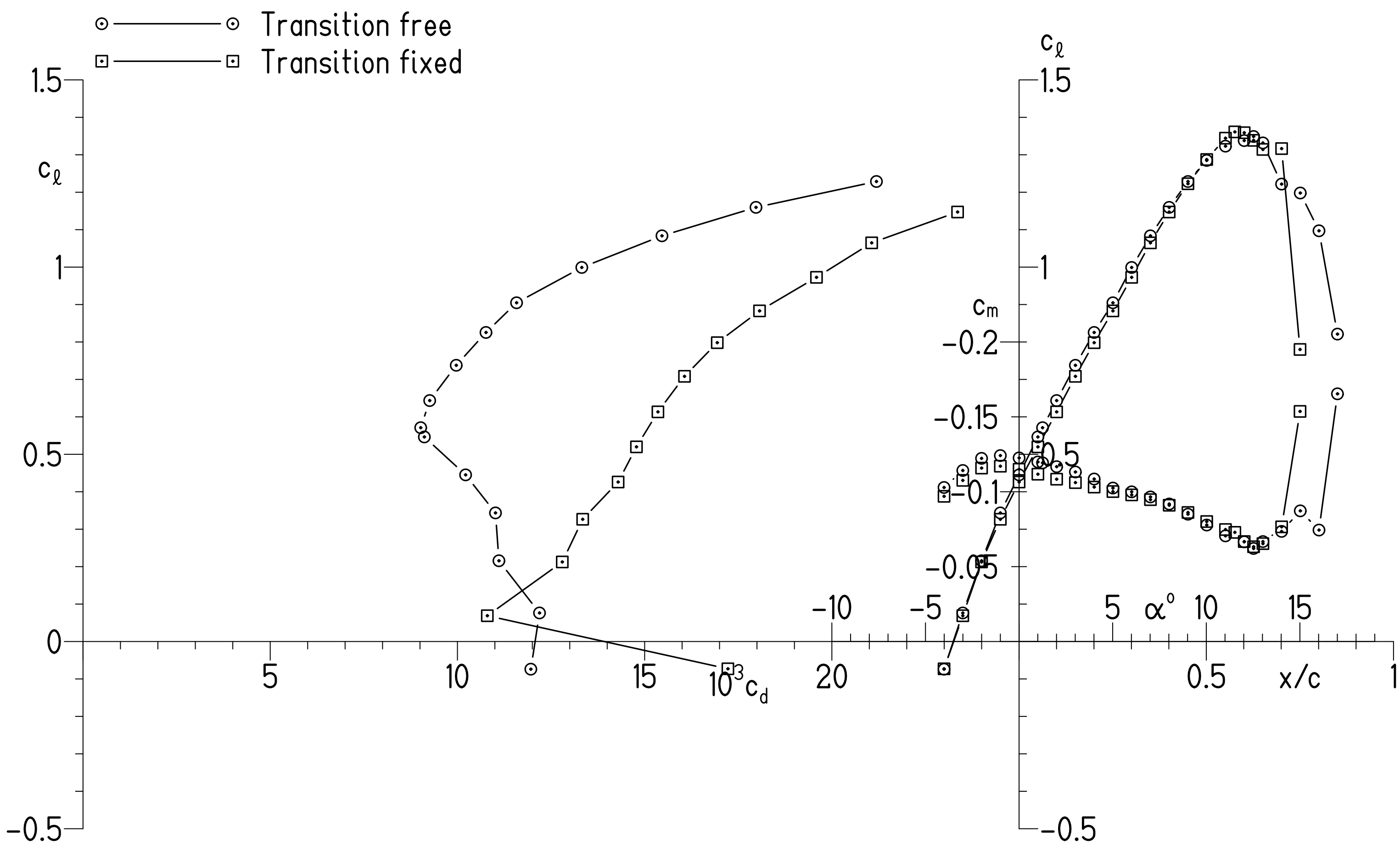

(b) R = 300,000 and M = 0.09.

Figure 11.- Continued.

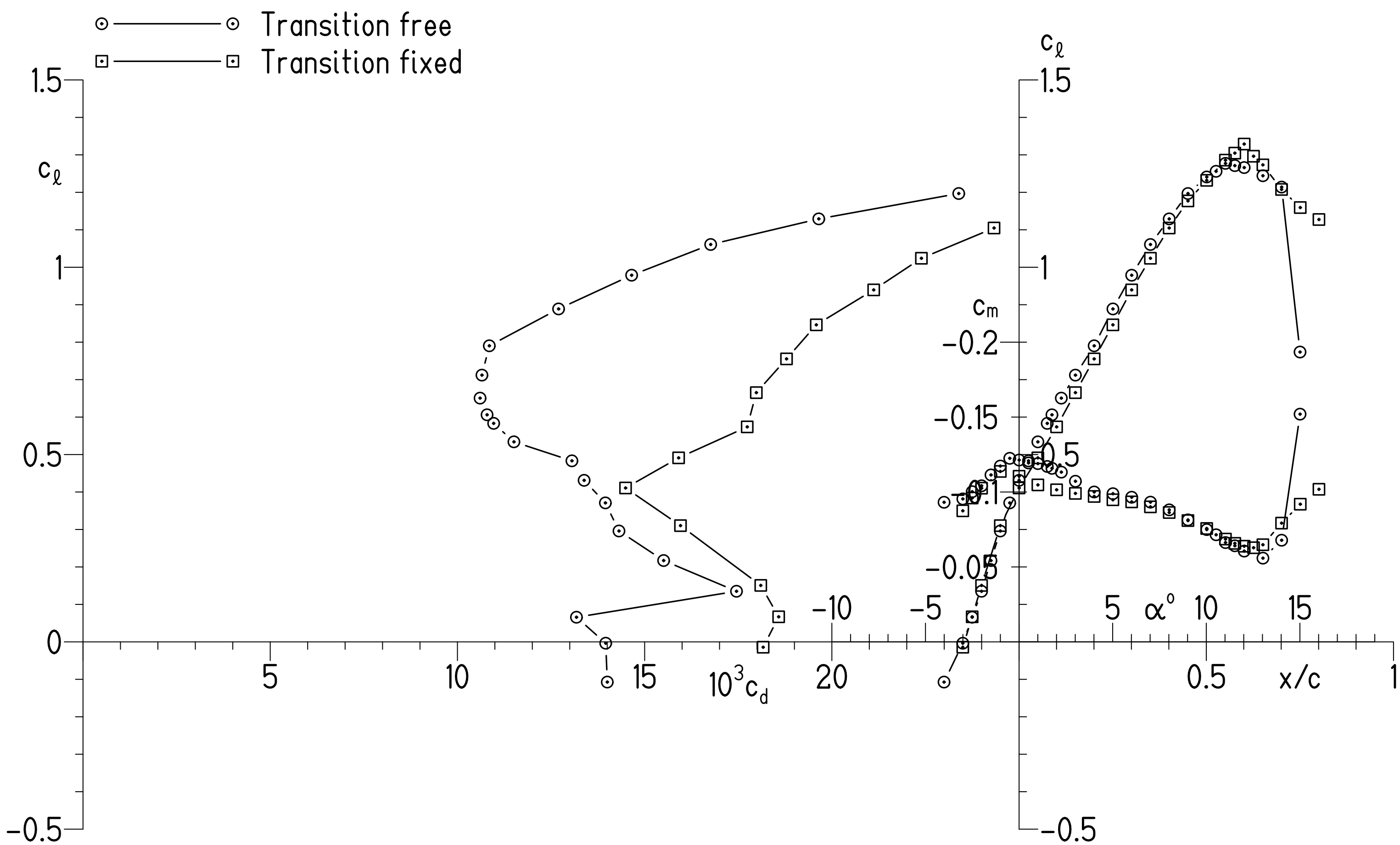

(c) R = 200,000 and M = 0.06.

Figure 11.- Continued.

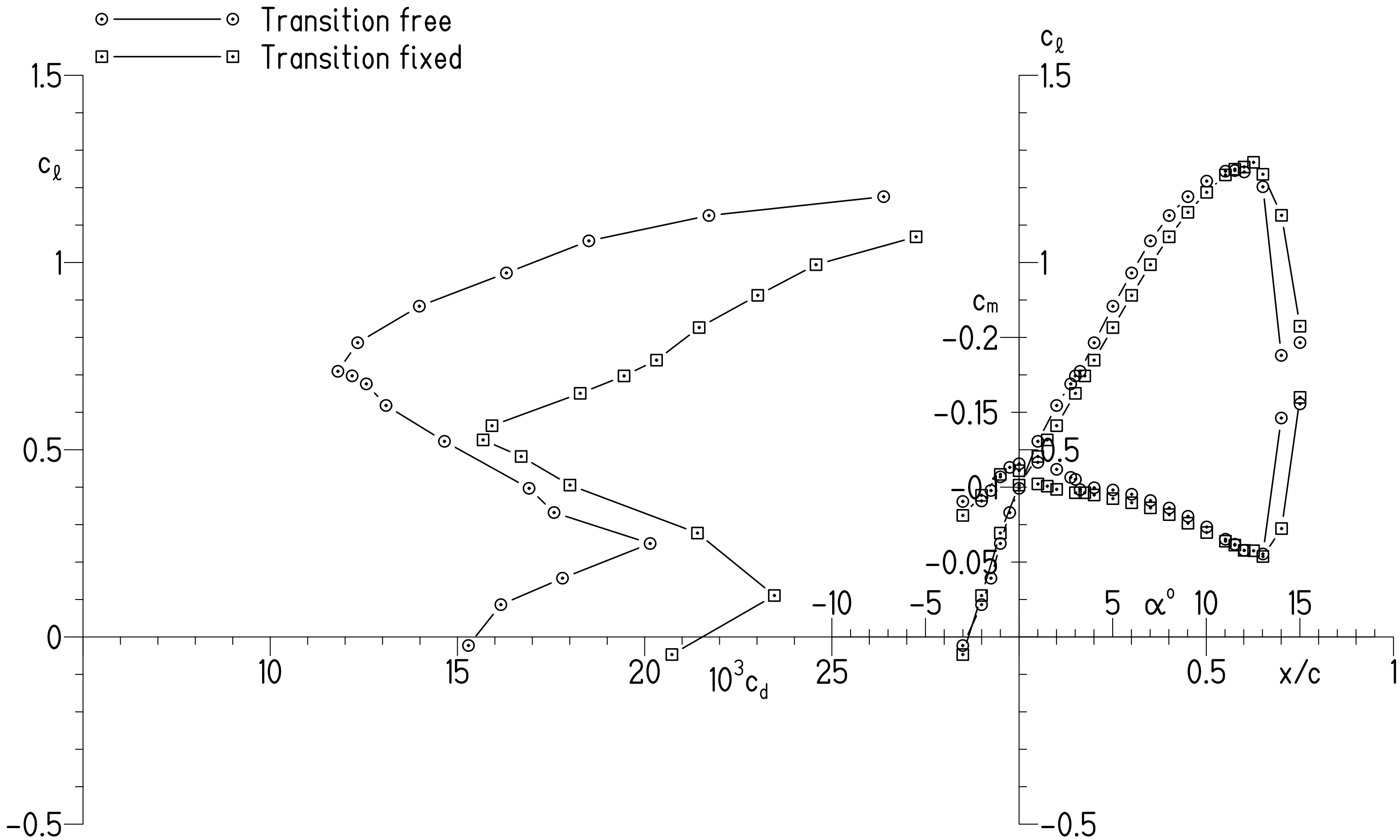

(d) R = 150,000 and M = 0.04.

Figure 11.- Continued.

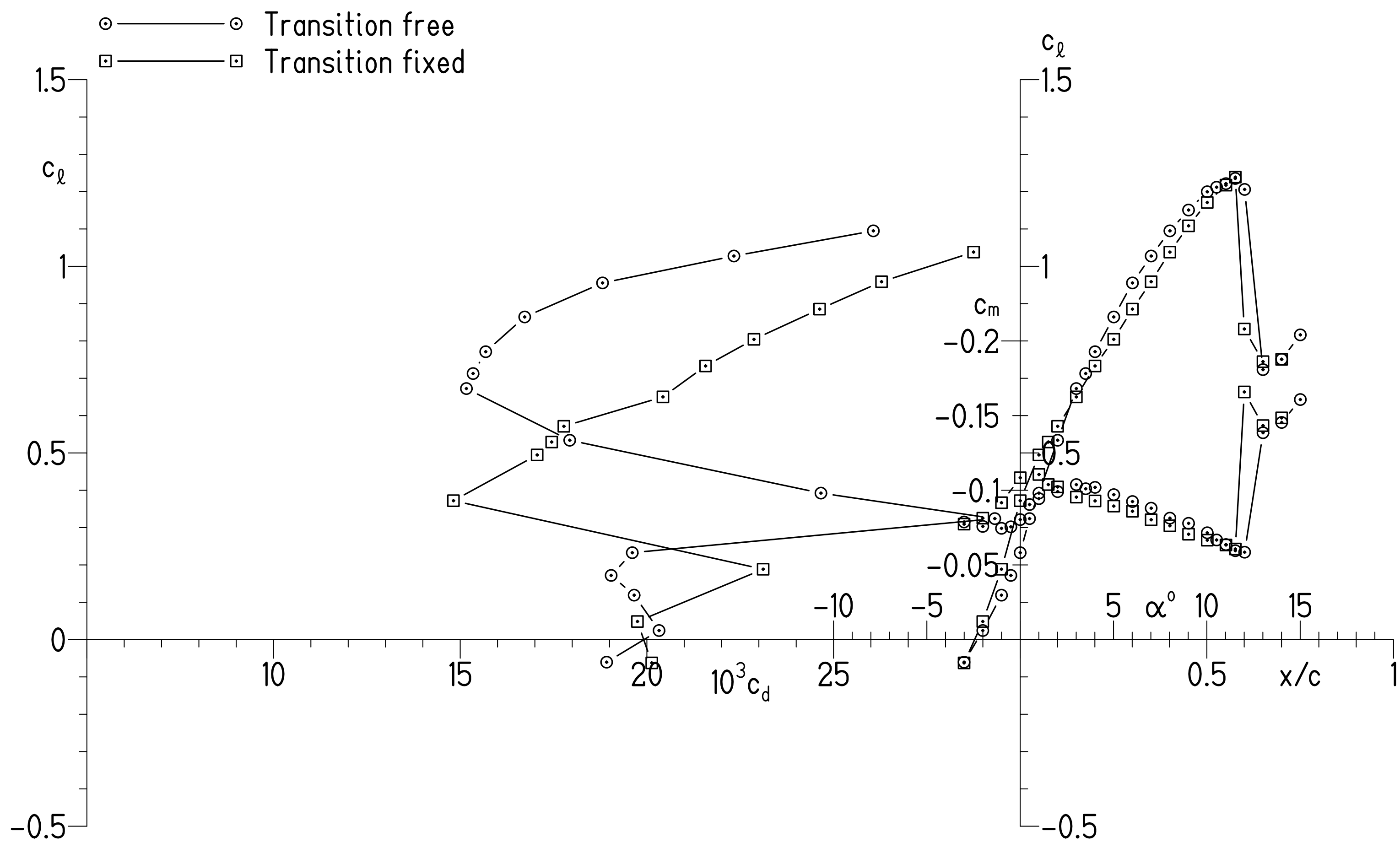

(e) R = 100,000 and M = 0.03.

Figure 11.- Continued.

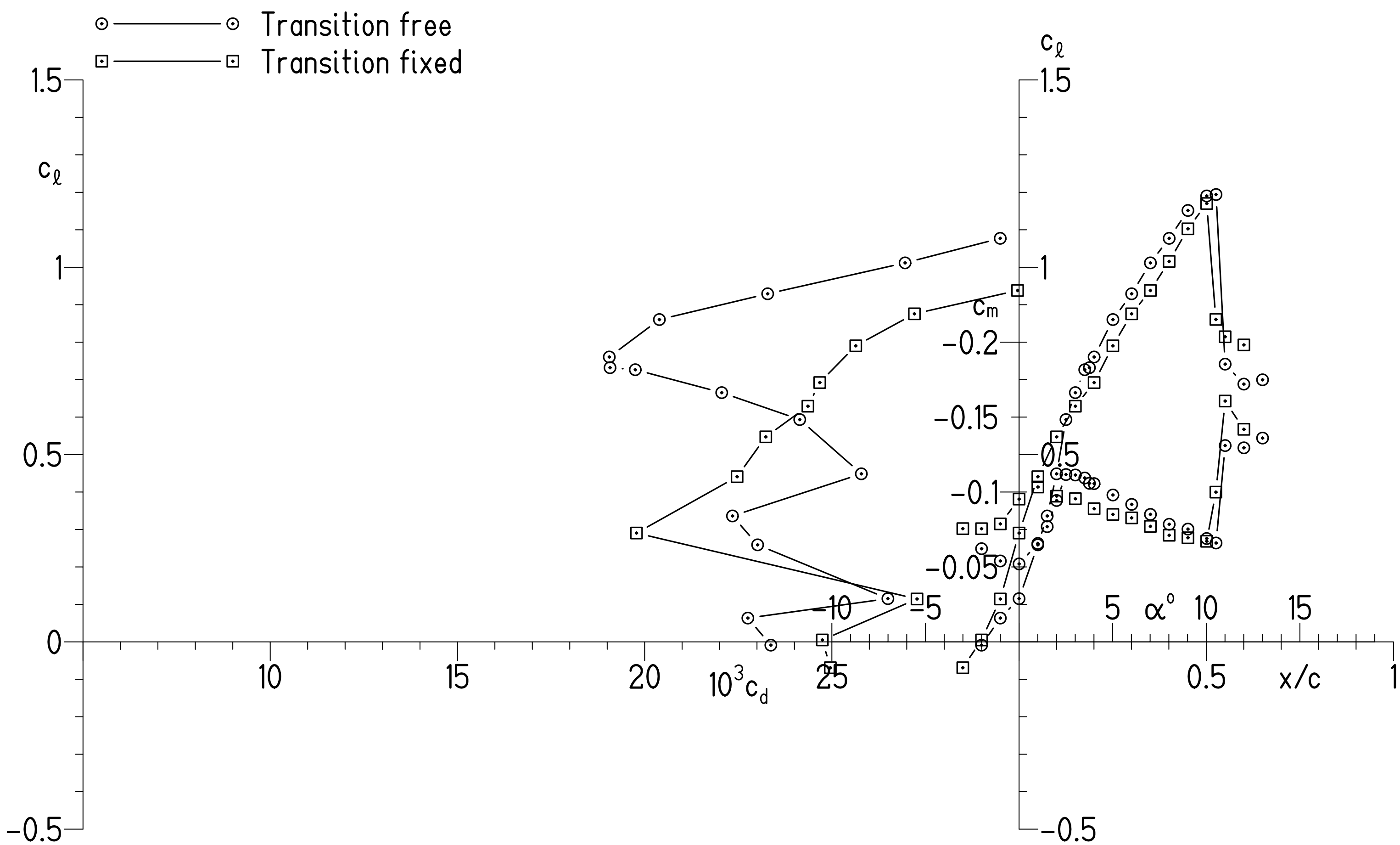

(f) R = 70,000 and M = 0.02.

Figure 11.- Concluded.

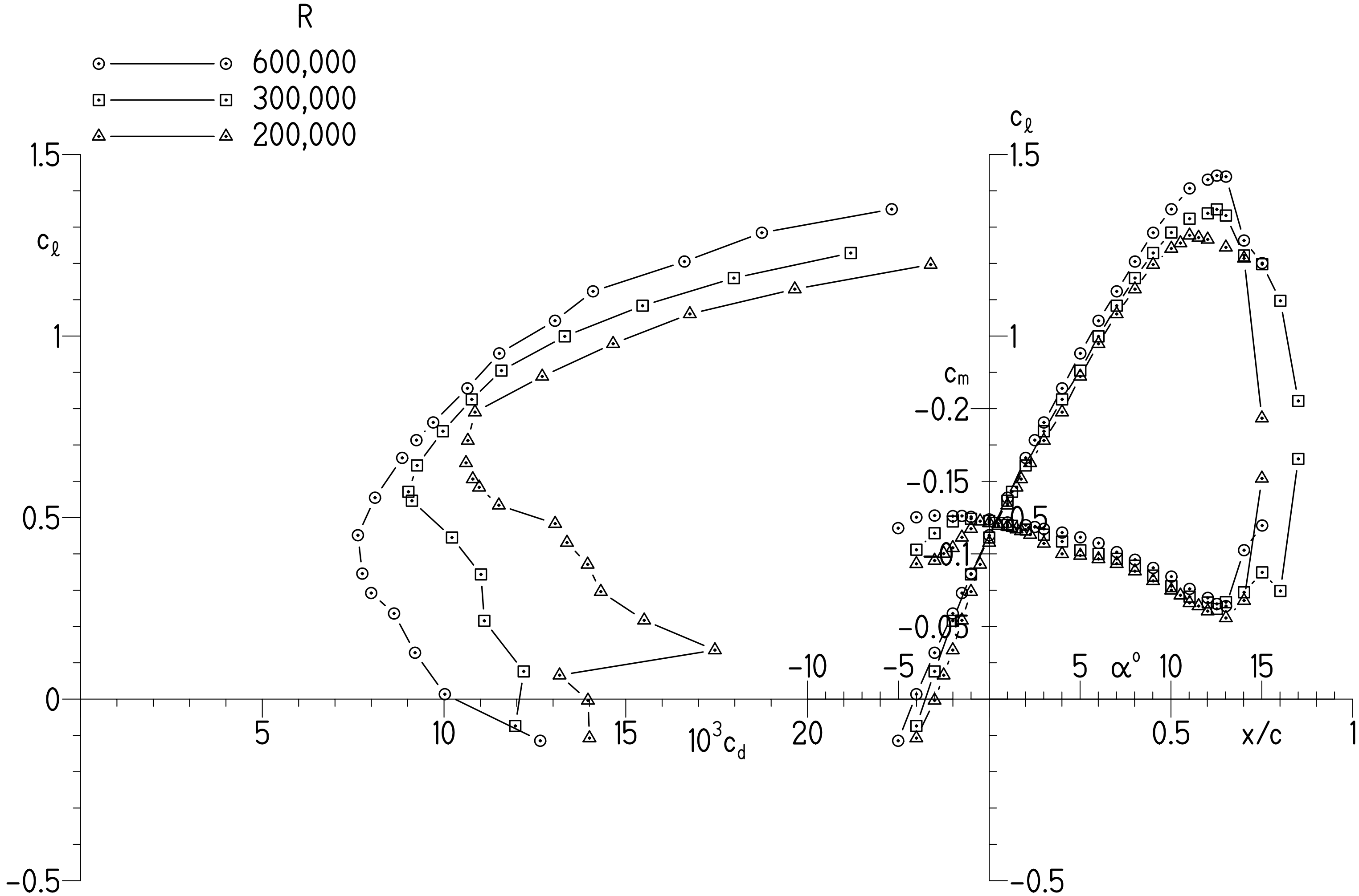

(a) R = 600,000, 300,000, and 200,000.

Figure 12.- Effects of Reynolds number on experimental section characteristics with transition free.

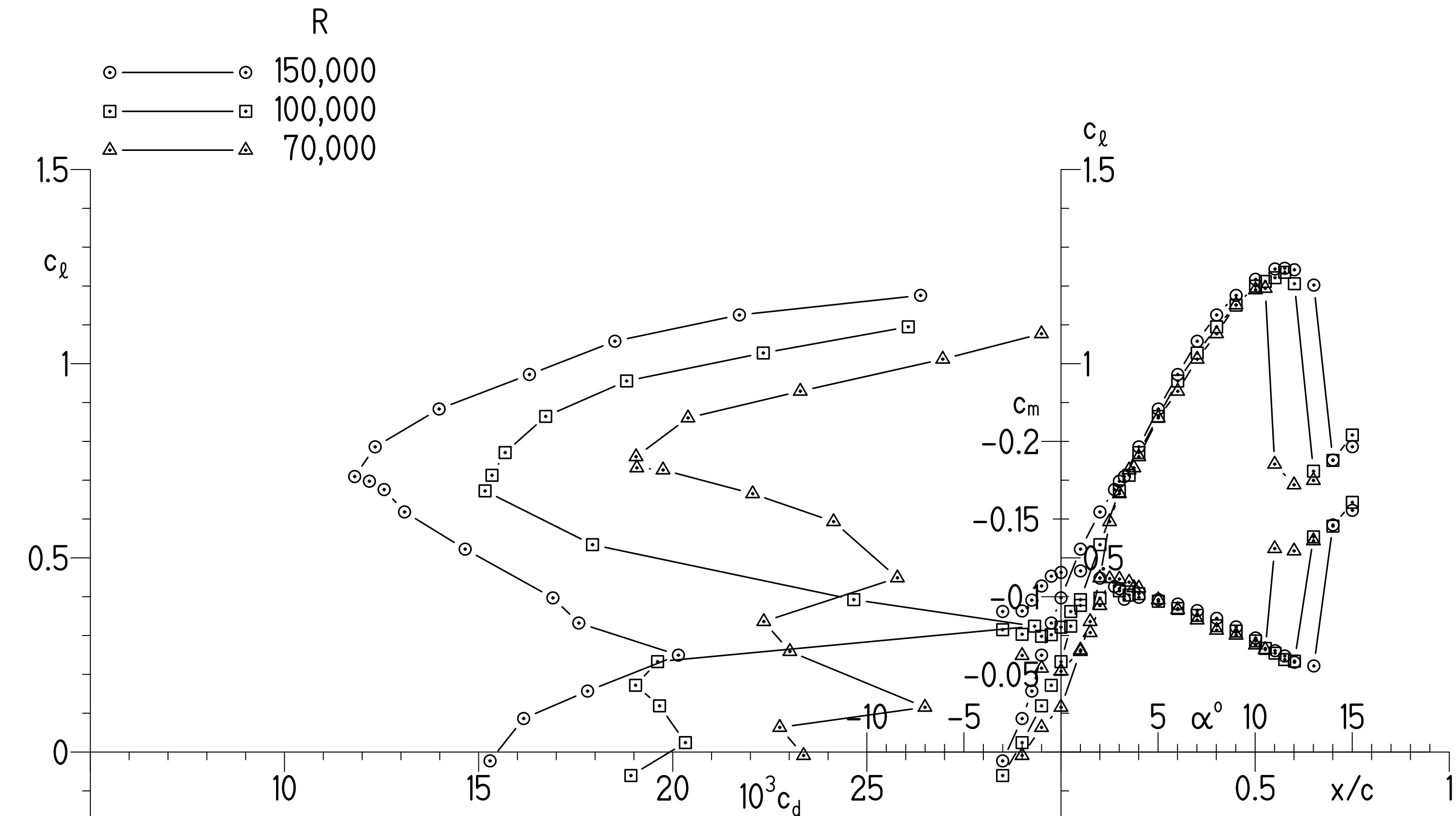

(b) R = 150,000, 100,000, and 70,000.

Figure 12.- Concluded.

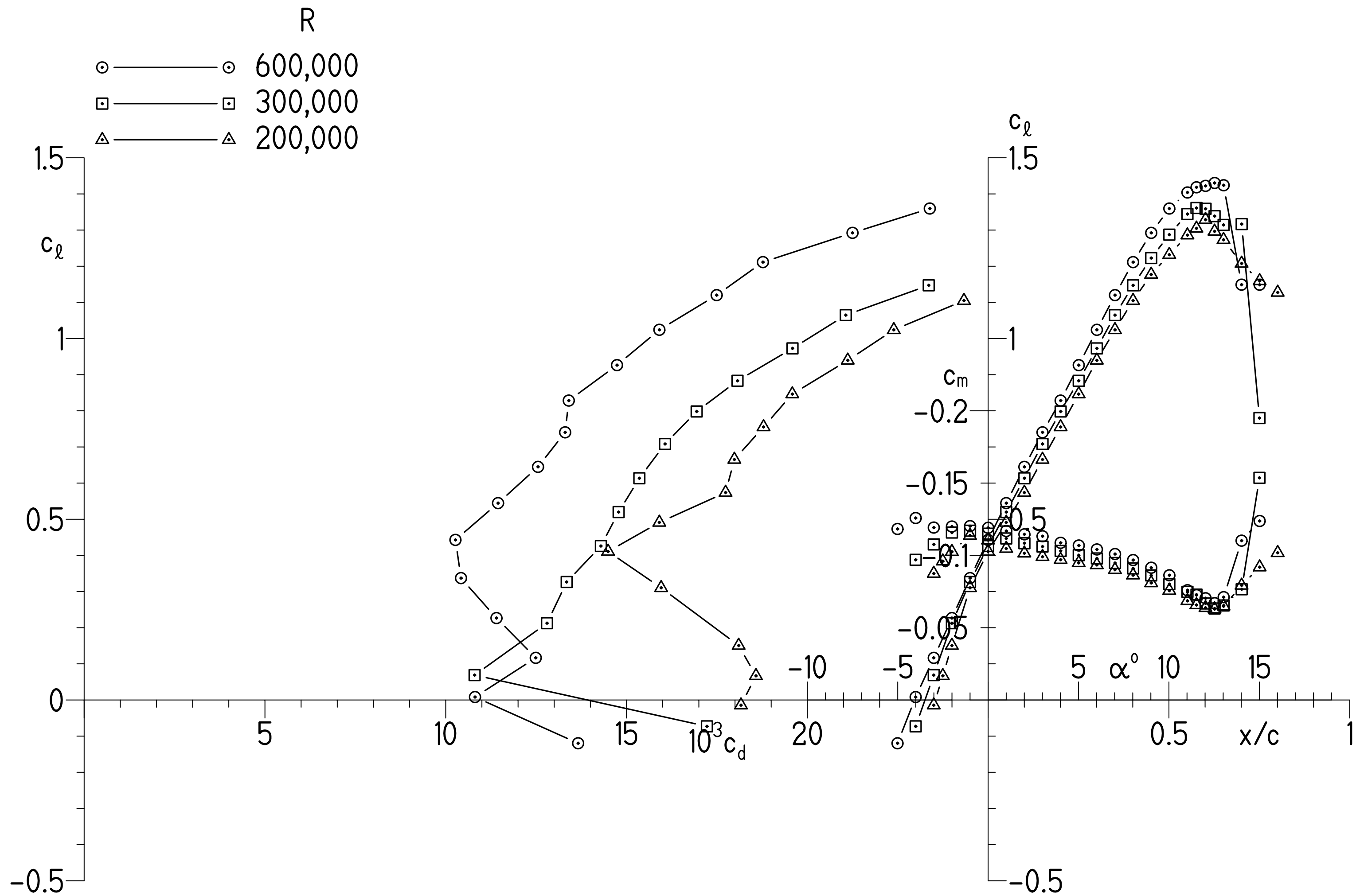

(a) R = 600,000, 300,000, and 200,000.

Figure 13.- Effects of Reynolds number on experimental section characteristics with transition fixed.

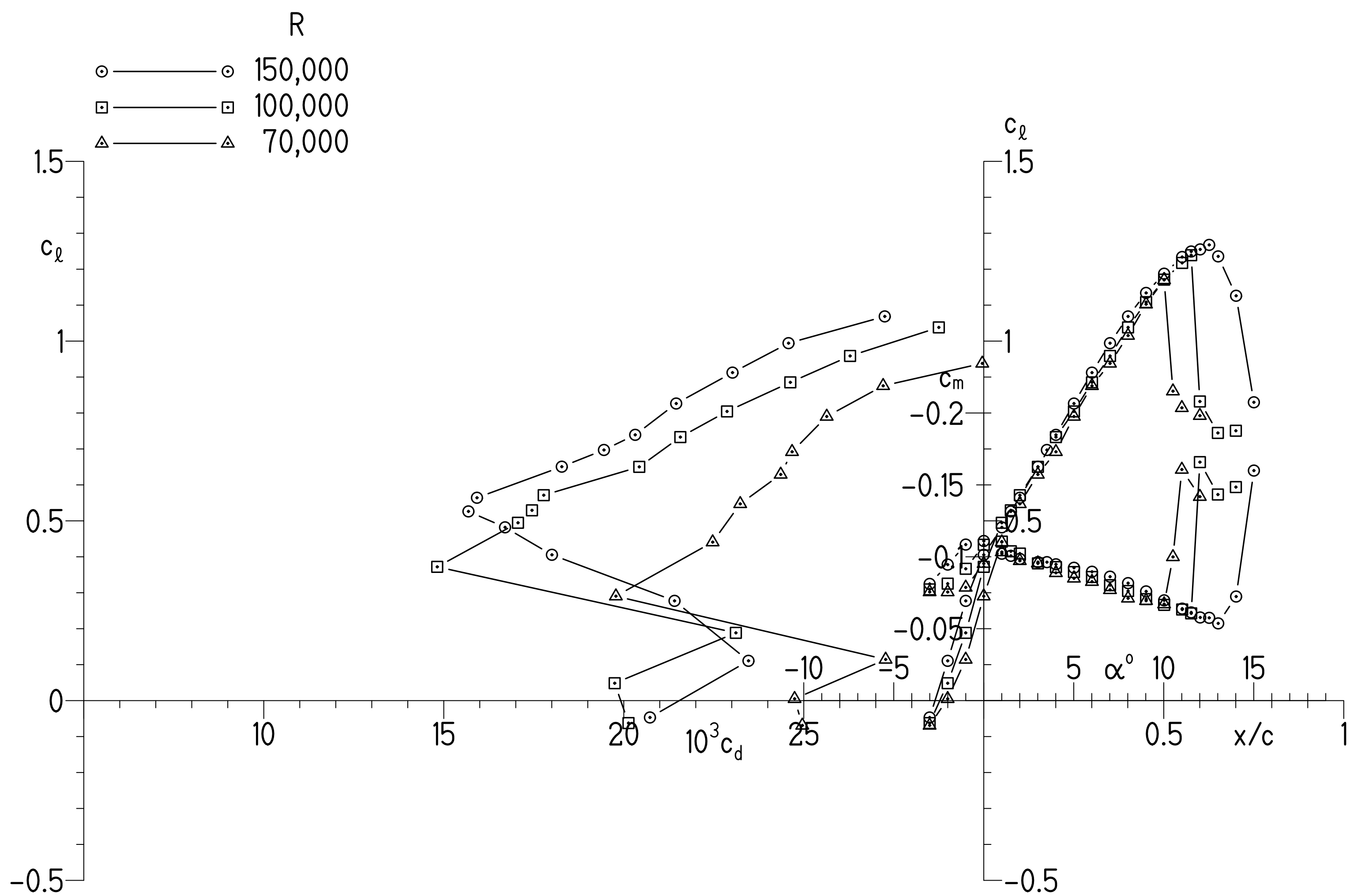

(b) R = 150,000, 100,000, and 70,000.

Figure 13.- Concluded.

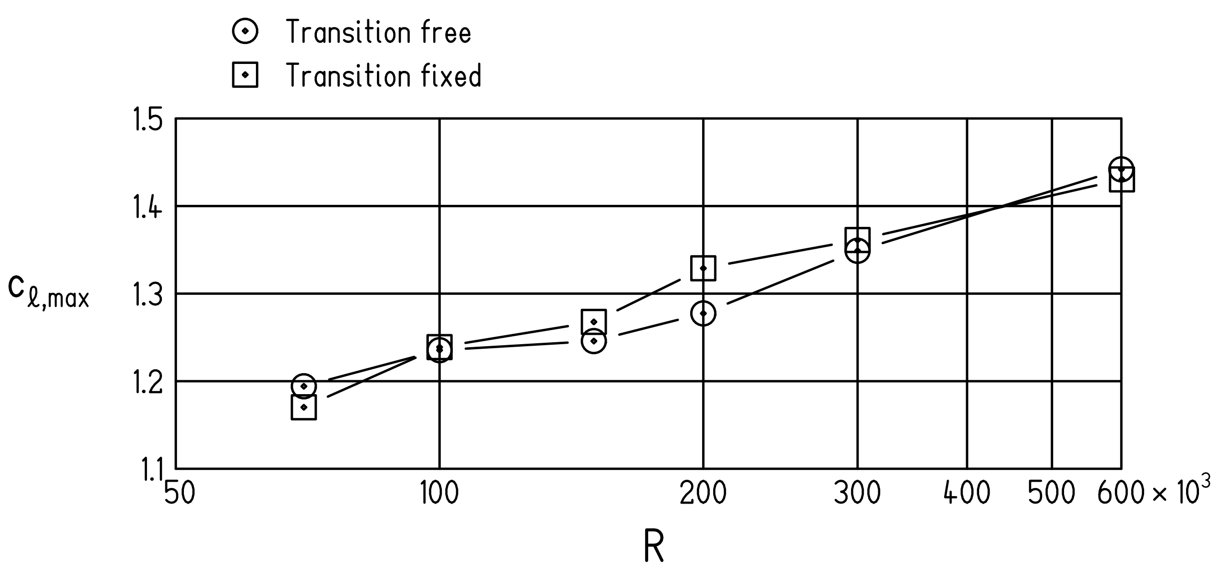

Figure 14.- Variation of experimental maximum lift coefficient with Reynolds number.

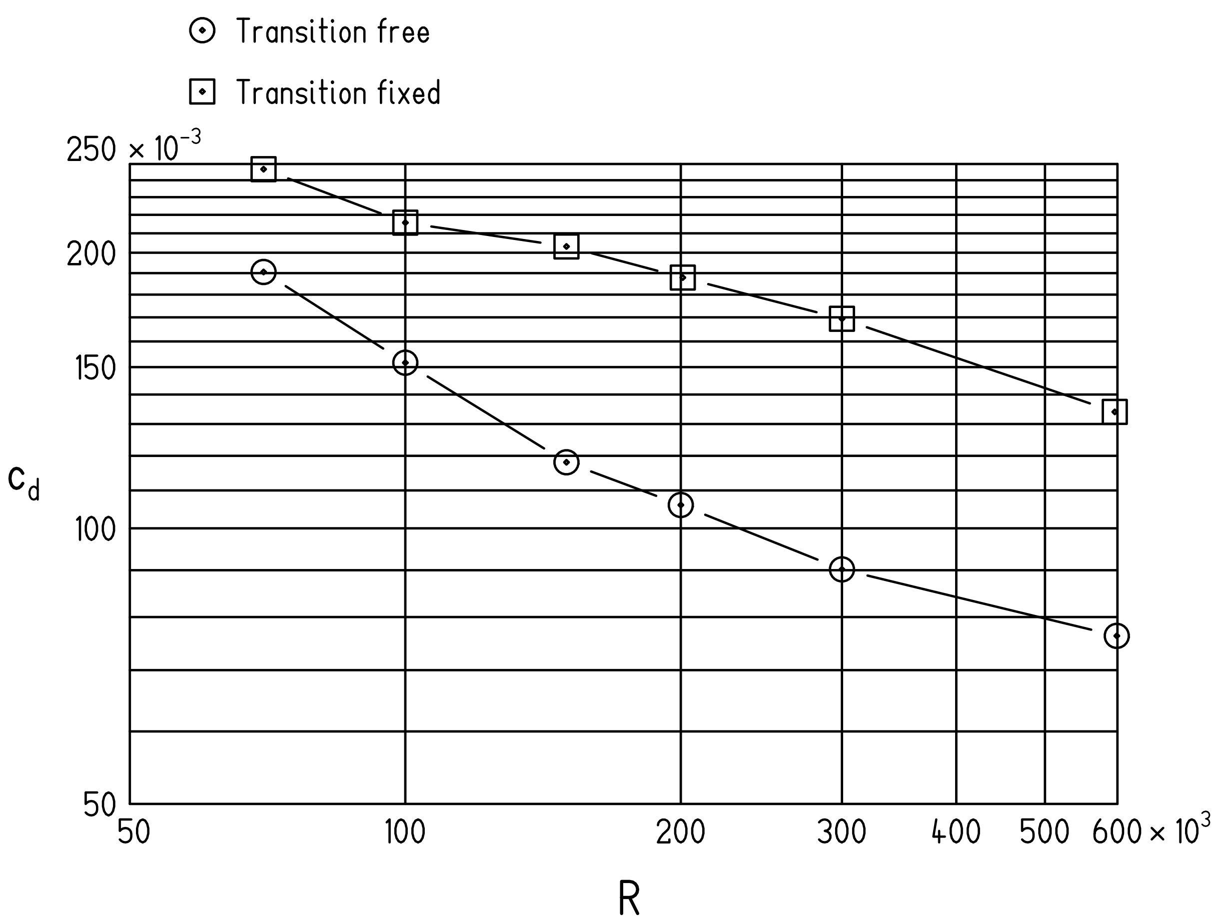

Figure 15.- Variation of experimental profile-drag coefficient with Reynolds number. Data with transition free correspond to $c_{d,min}$; with transition fixed, to c_d at $\alpha = 4°$.

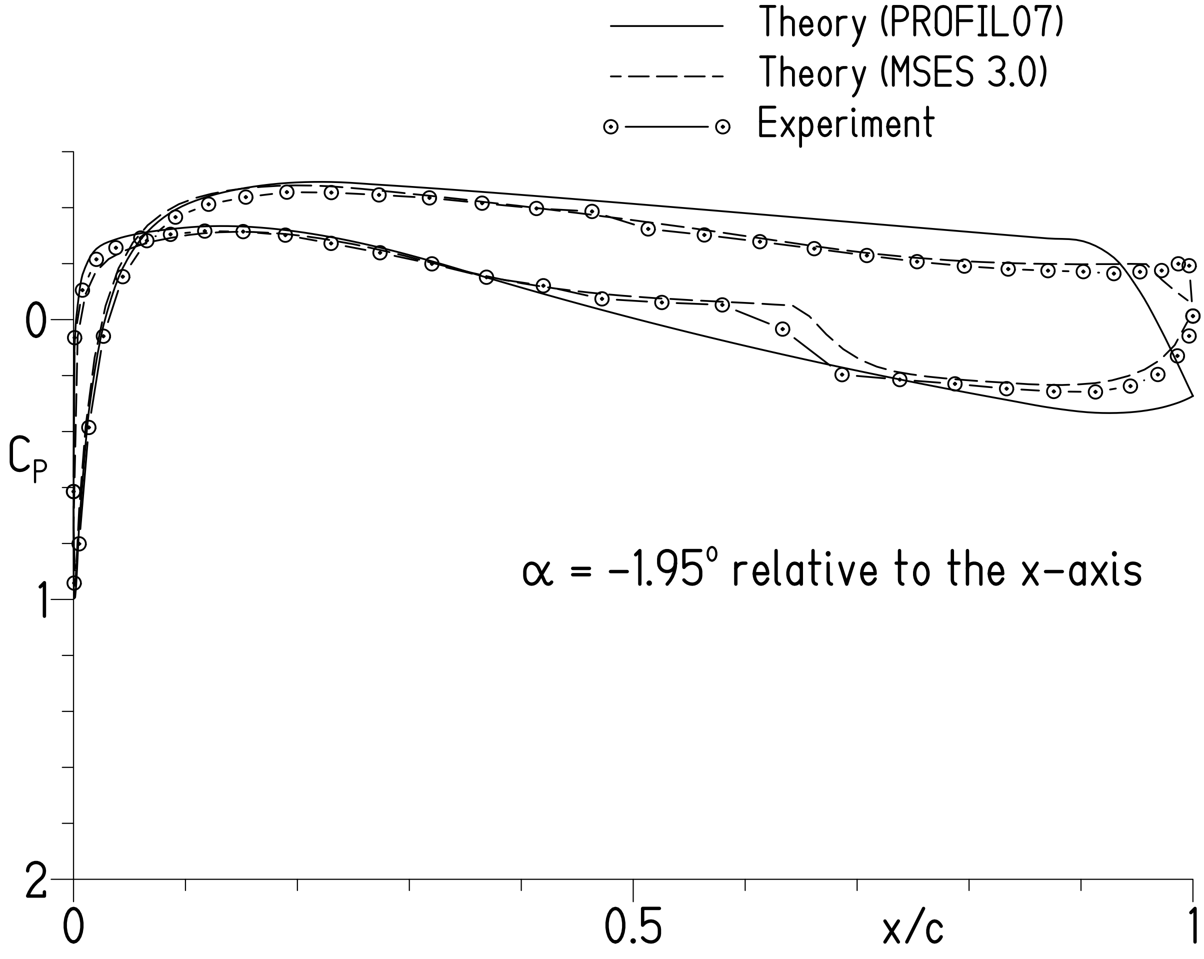

(a) $c_l = 0.25$.

Figure 16.- Comparison of theoretical and experimental pressure distributions for R = 150,000 and M = 0.04.

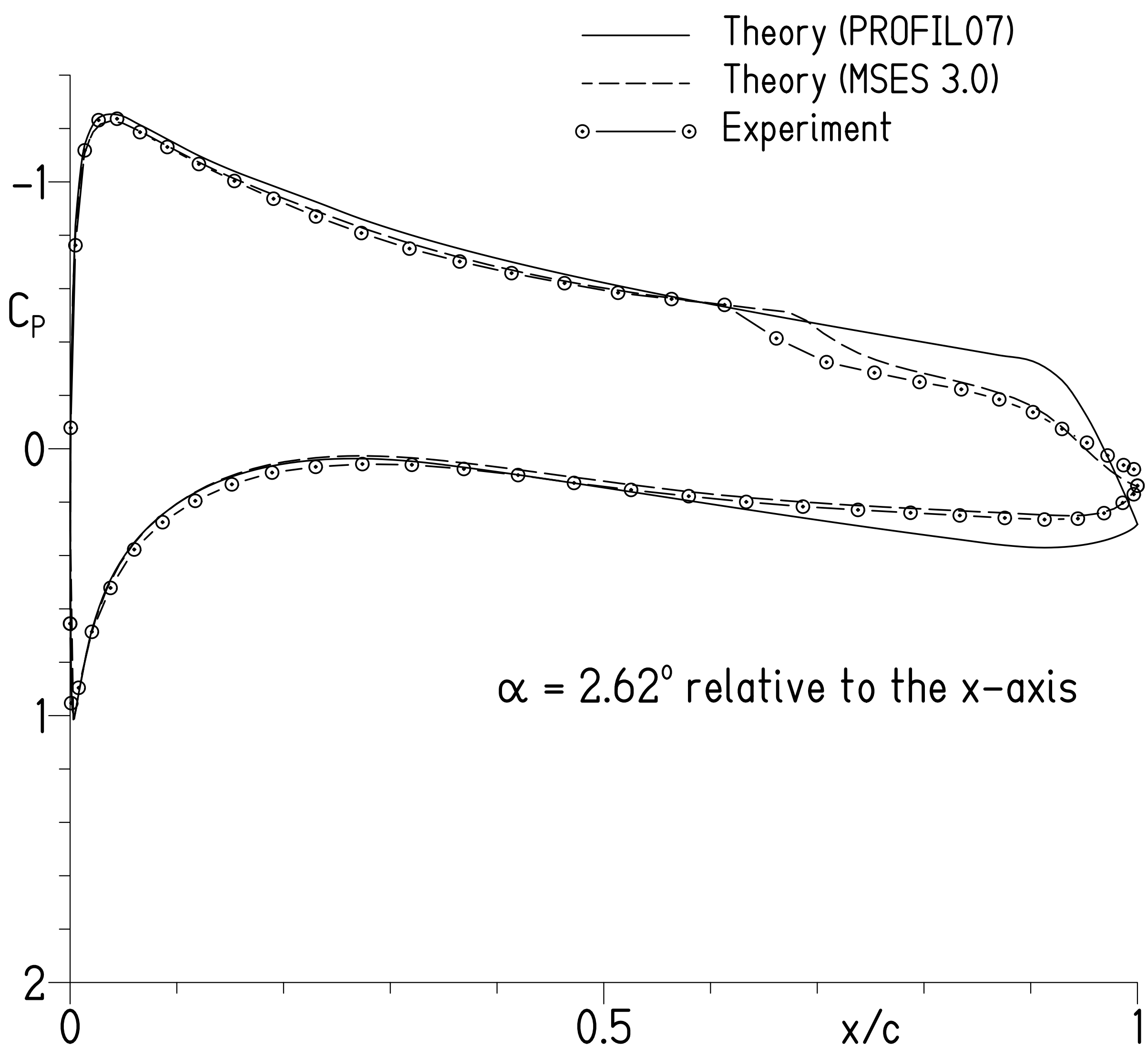

(b) $c_l = 0.79$.

Figure 16.- Continued.

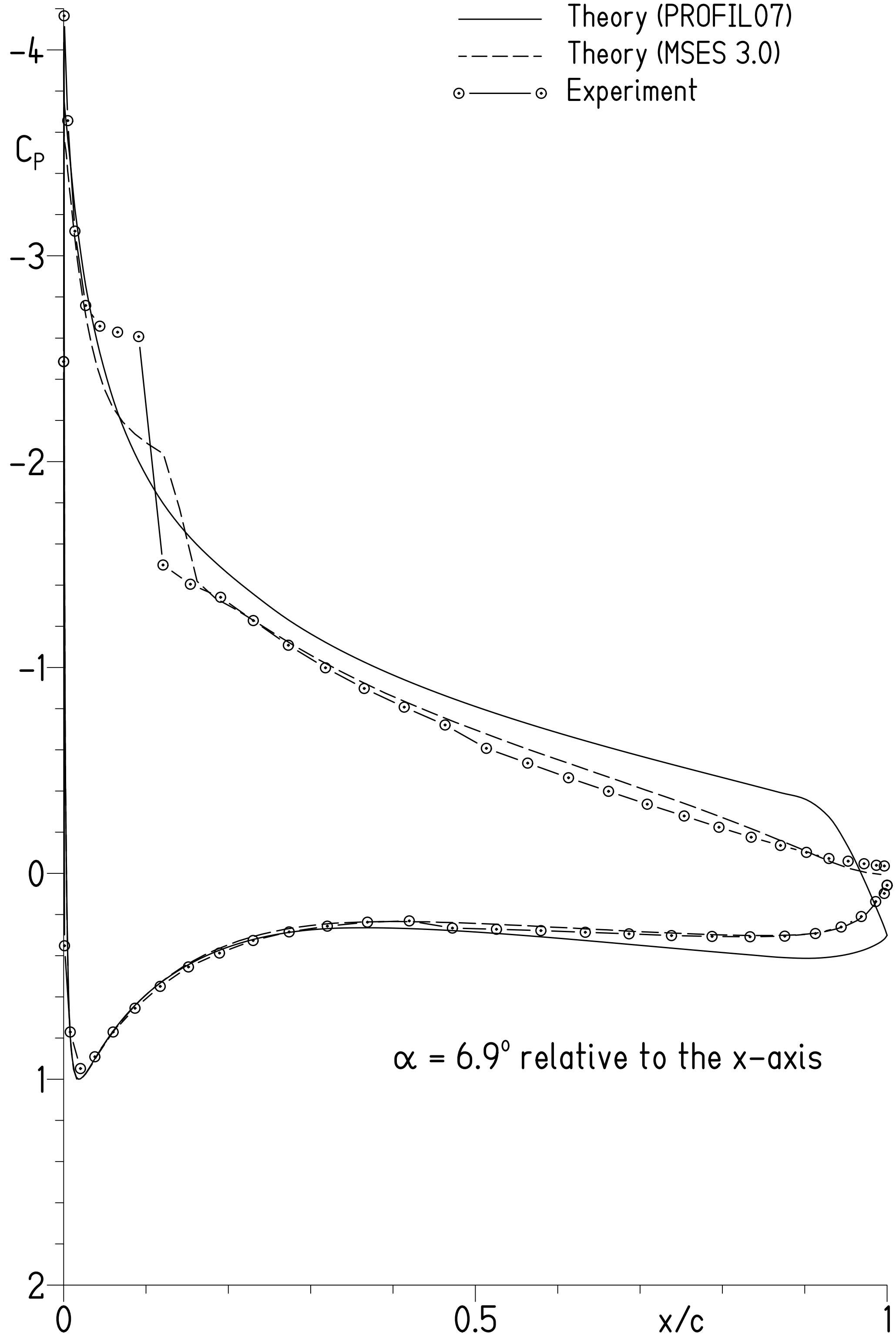

(c) $c_l = 1.22$.

Figure 16.- Concluded.

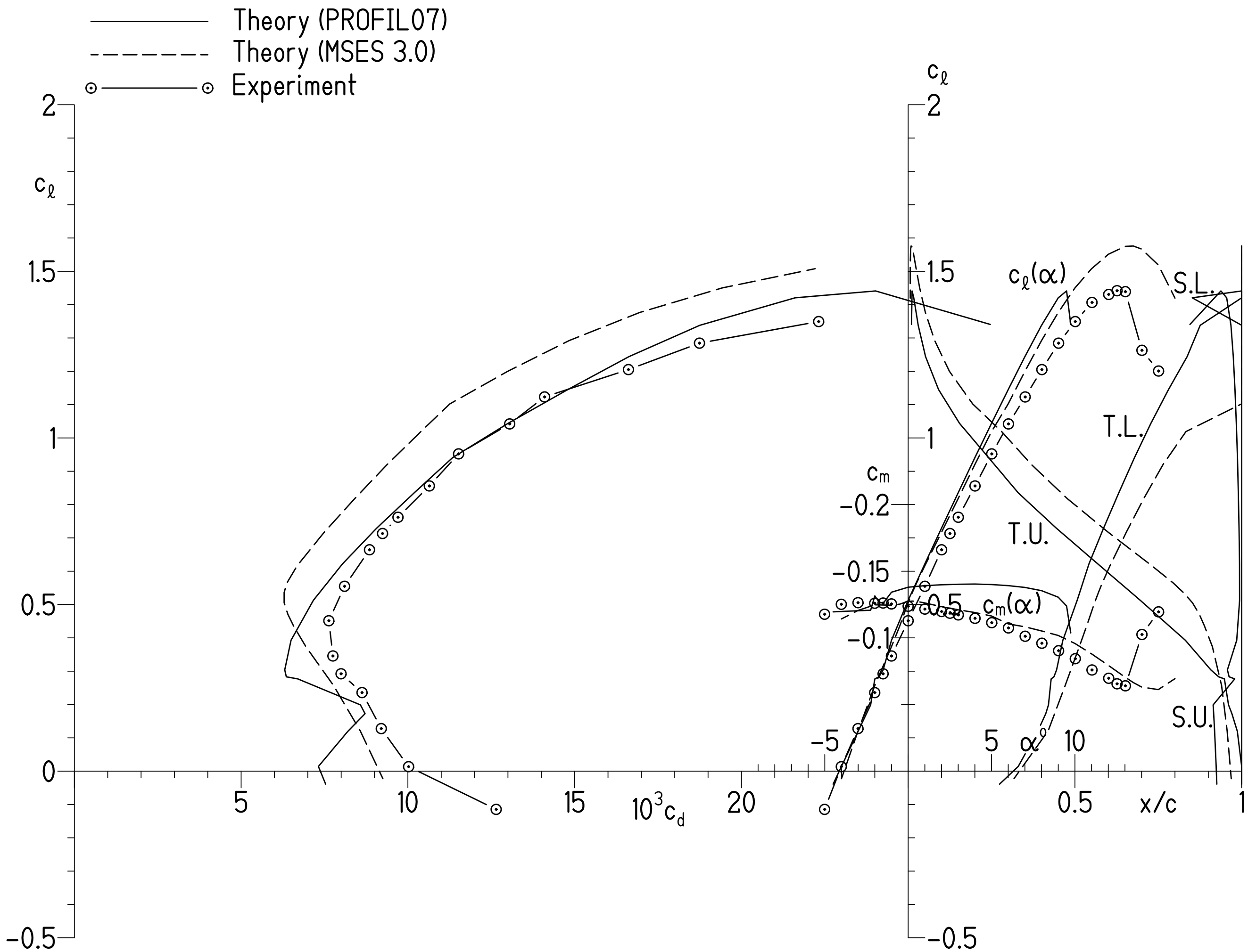

(a) R = 598,000.

Figure 17.- Comparison of theoretical and experimental section characteristics with transition free.

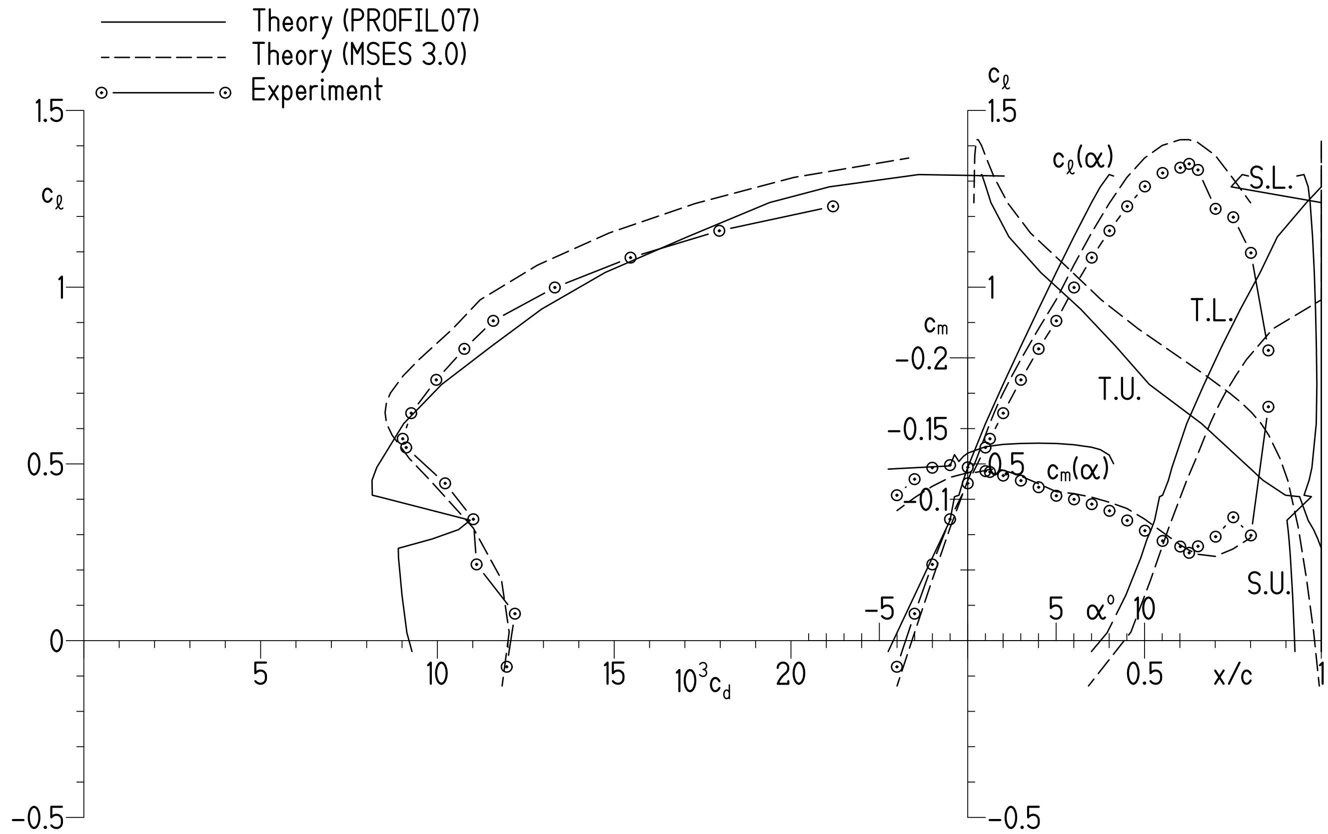

(b) R = 300,000.

Figure 17.- Continued.

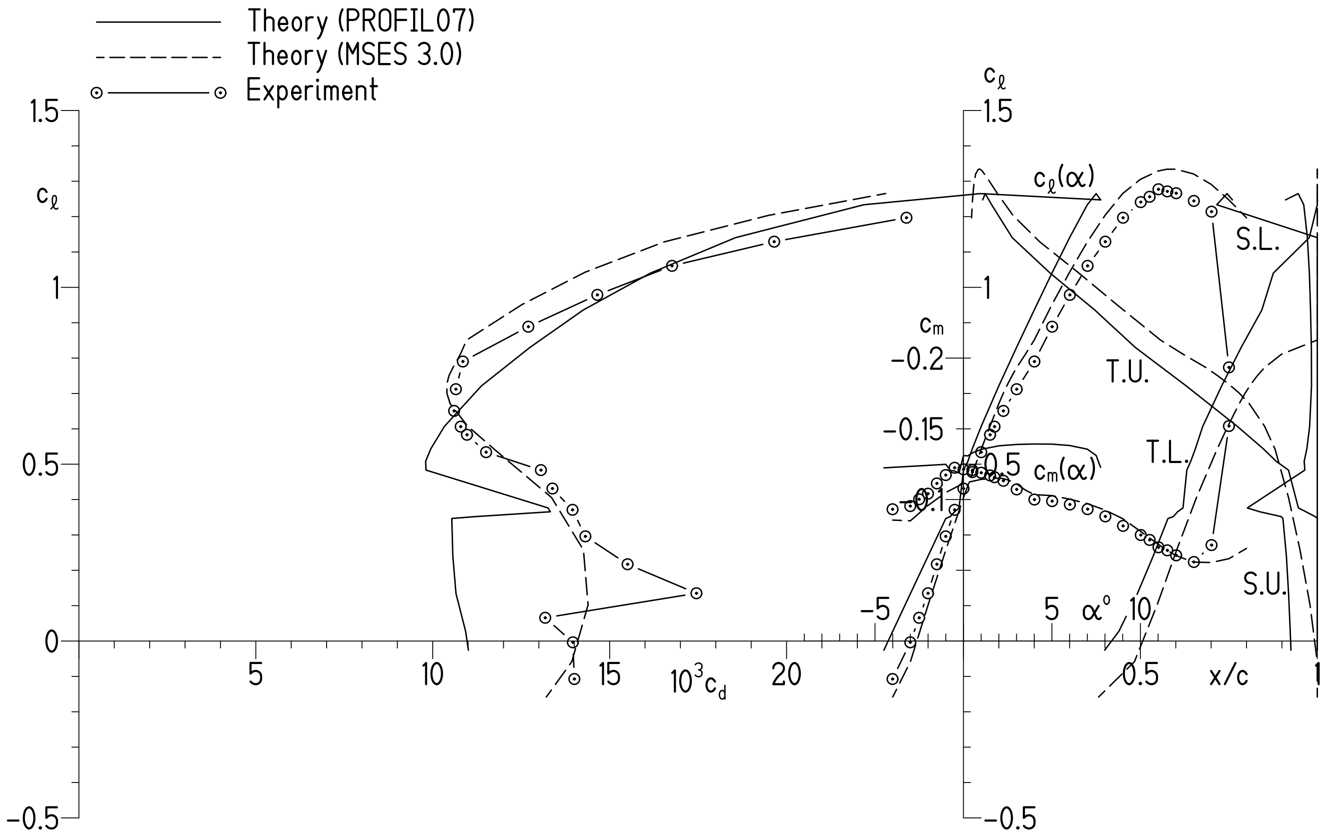

(c) R = 200,000.

Figure 17.- Continued.

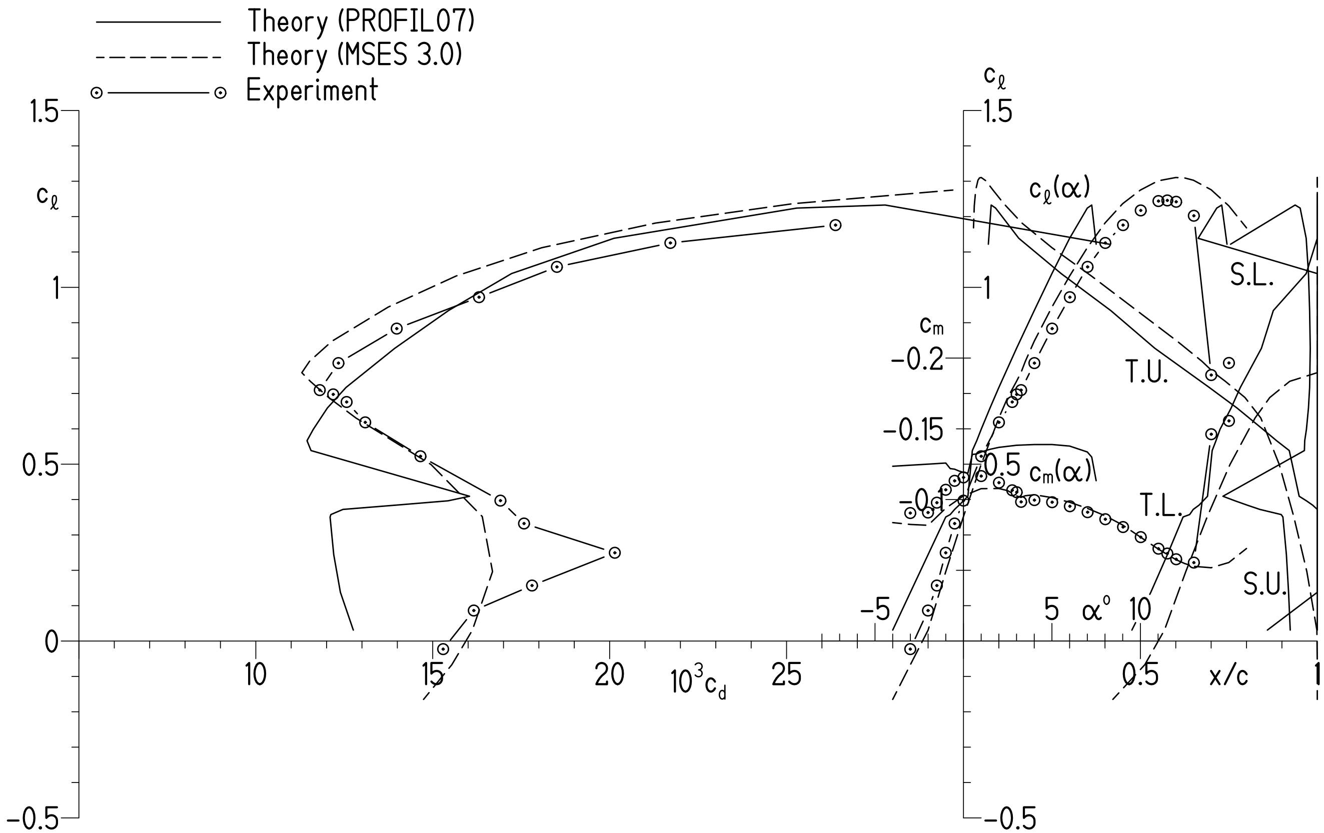

(d) R = 150,000.

Figure 17.- Continued.

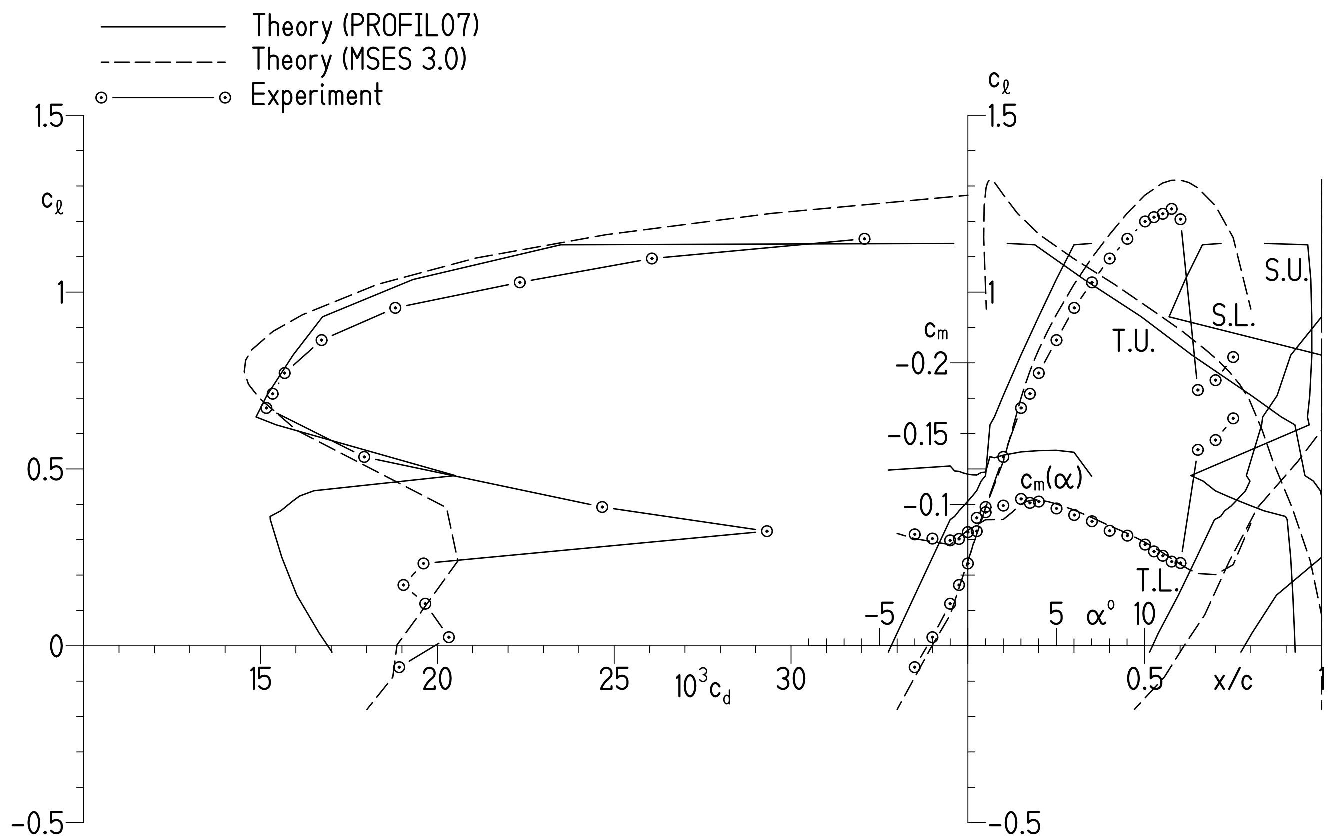

(e) R = 100,000.

Figure 17.- Continued.

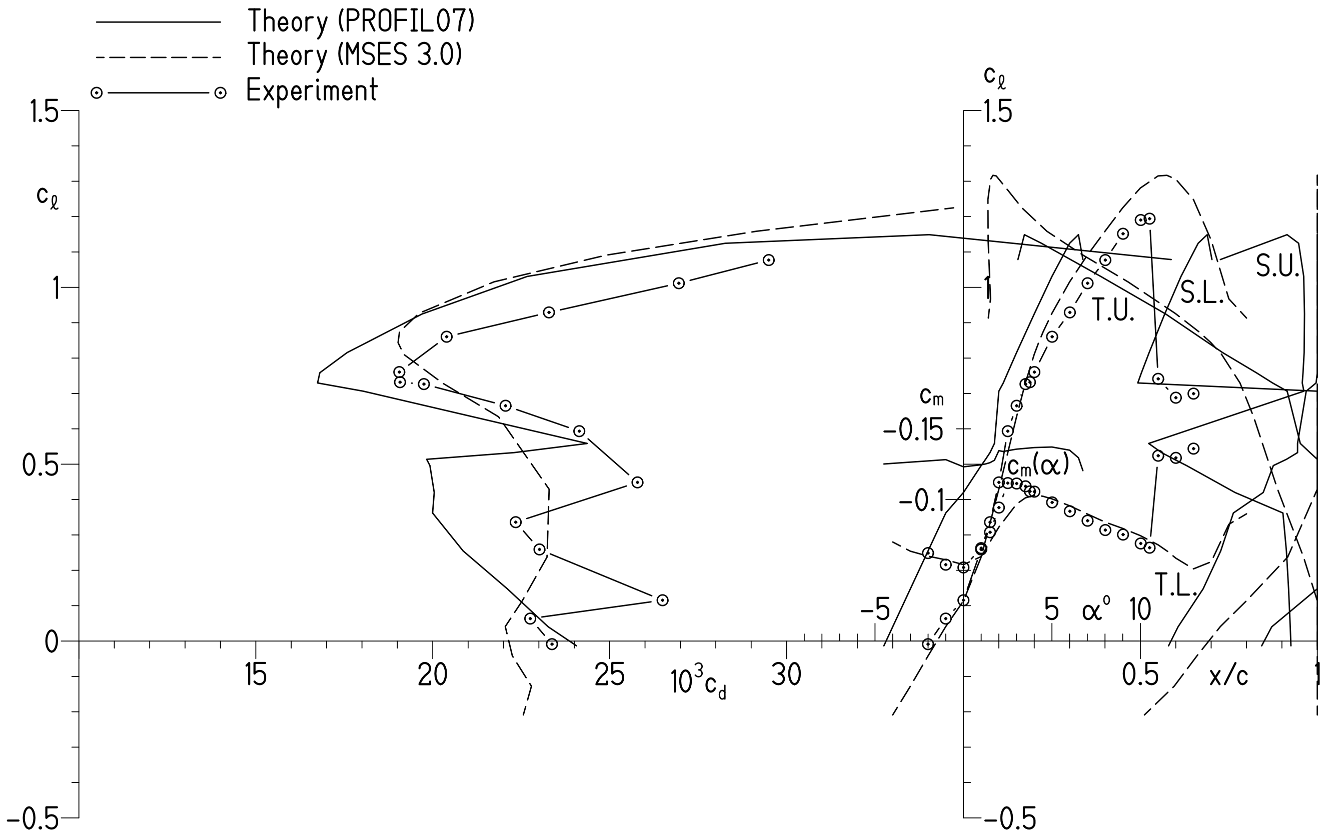

(f) R = 70,000.

Figure 17.- Concluded.

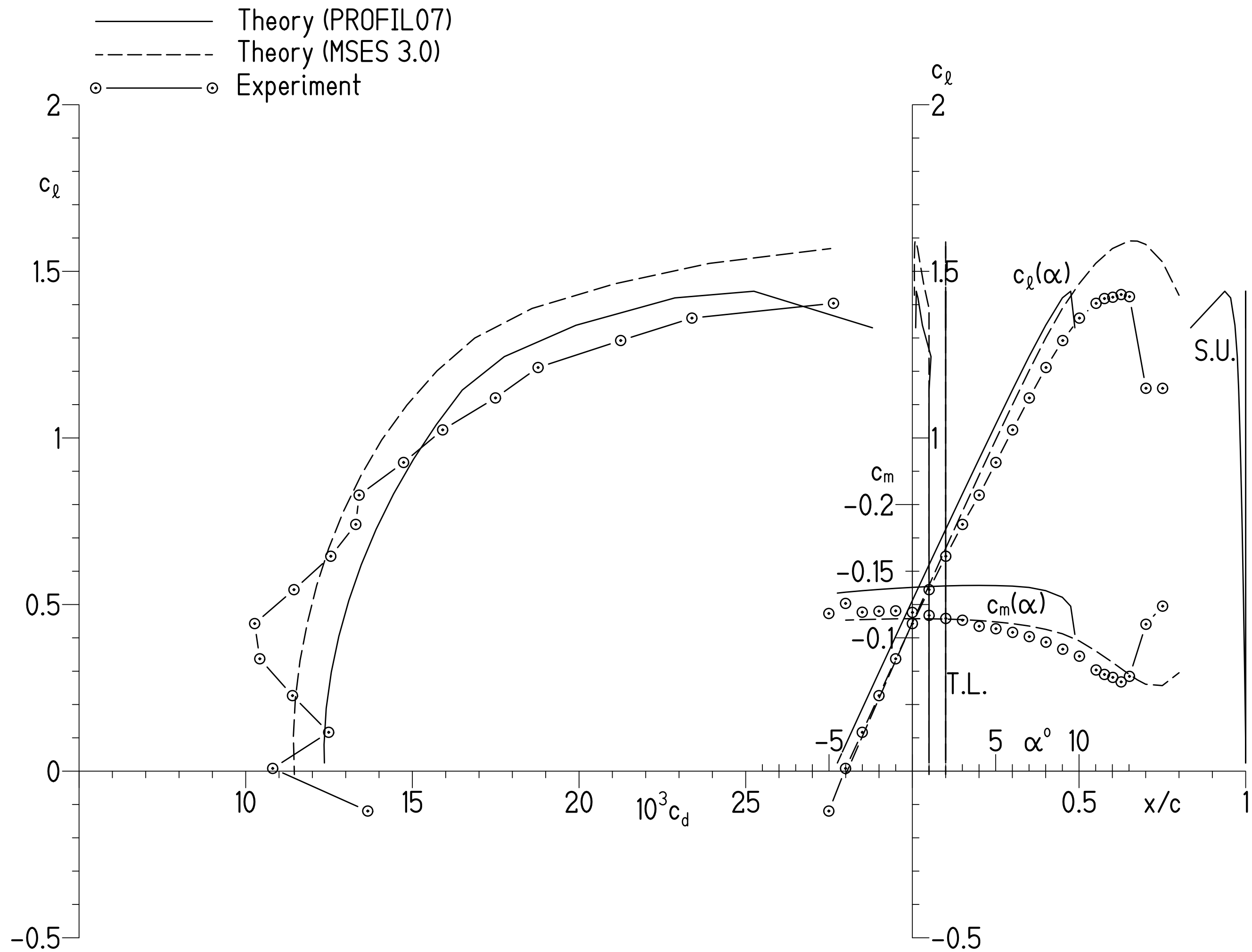

(a) R = 596,000.

Figure 18.- Comparison of theoretical and experimental section characteristics with transition fixed.

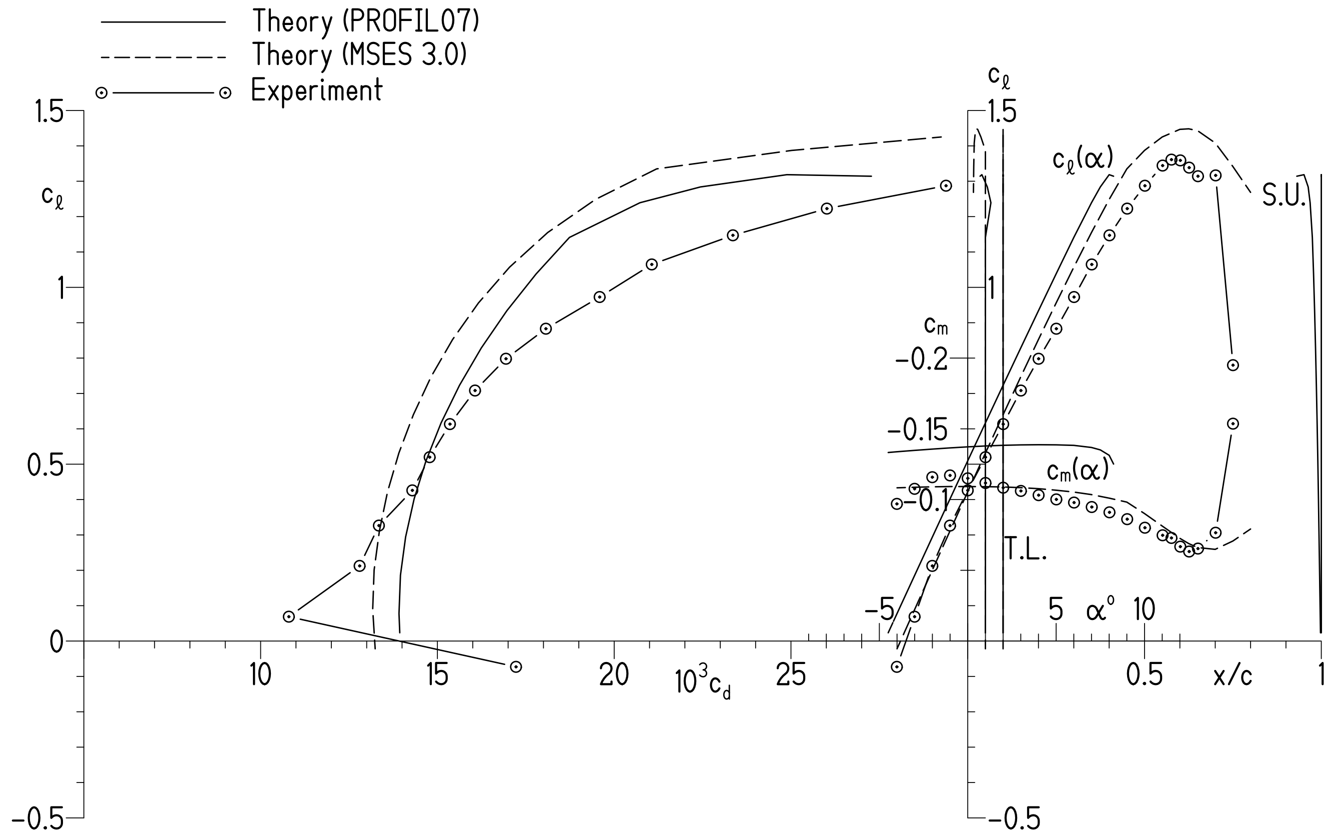

(b) R = 300,000.

Figure 18.- Continued.

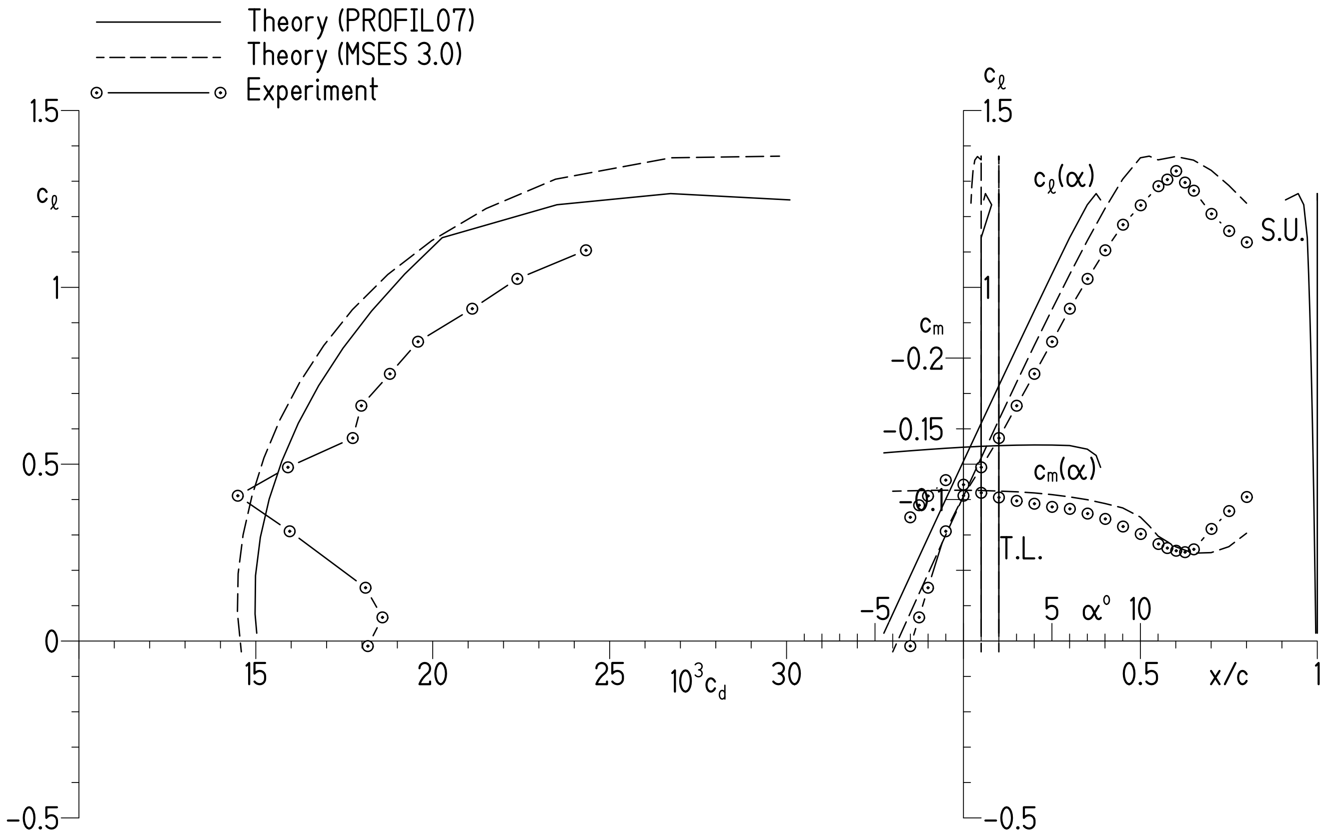

(c) R = 200,000.

Figure 18.- Continued.

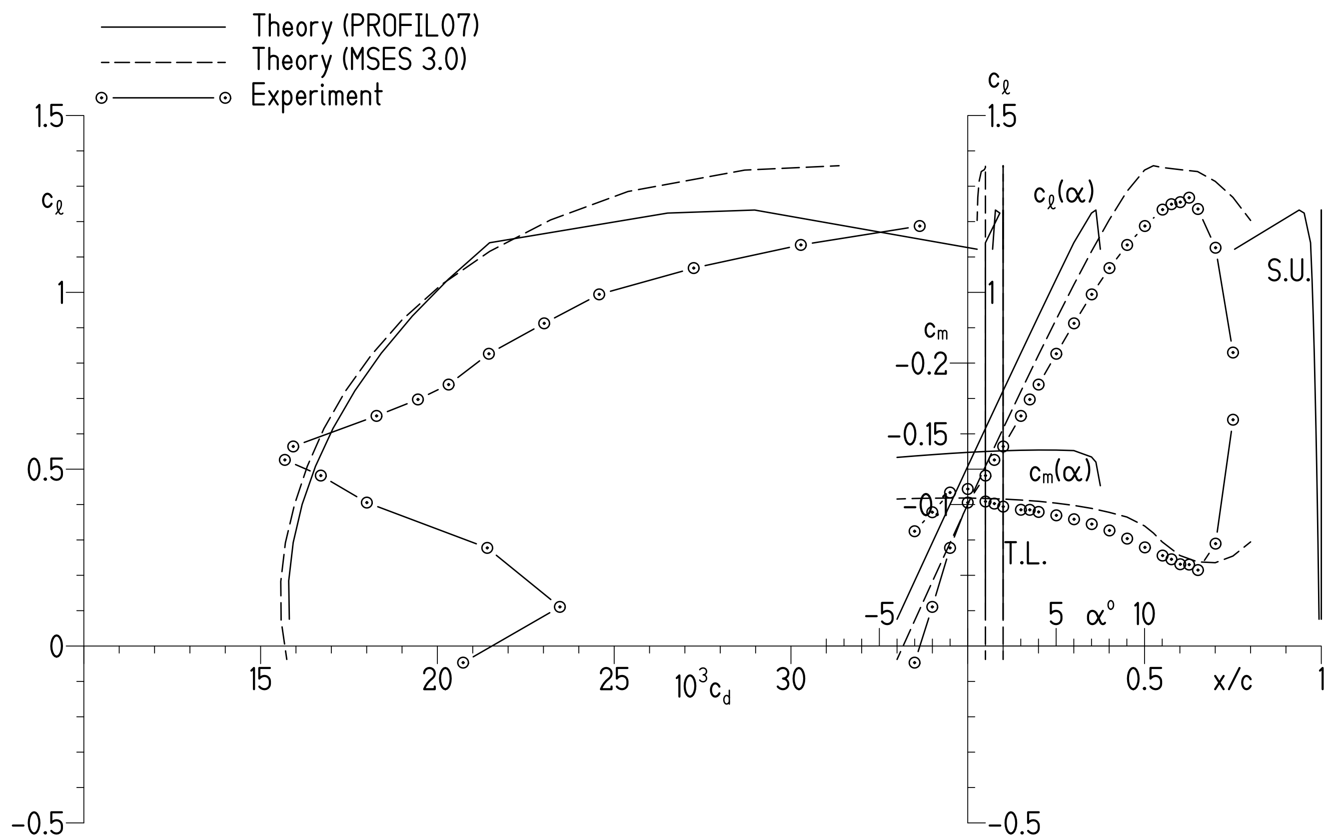

(d) R = 150,000.

Figure 18.- Continued.

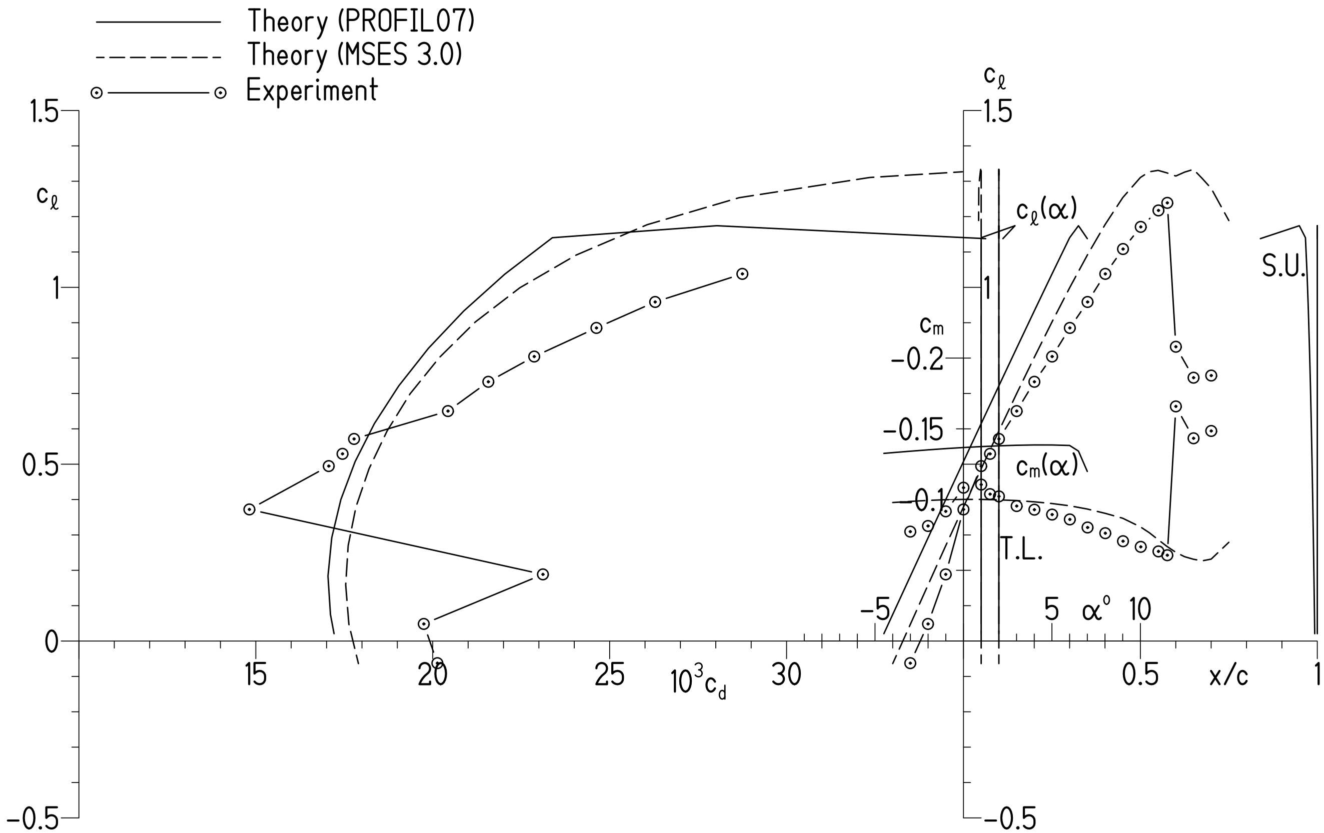

(e) R = 100,000.

Figure 18.- Continued.

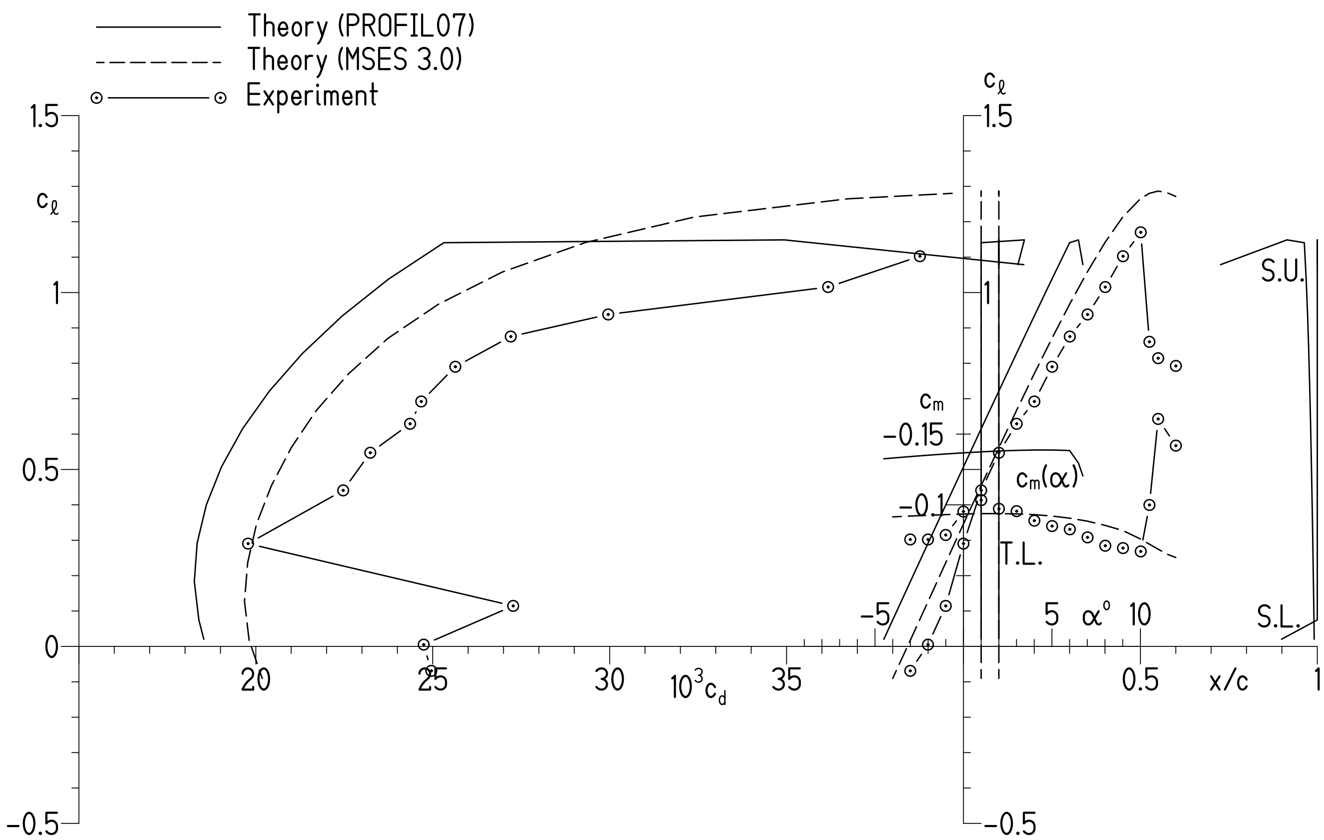

(f) R = 70,000.

Figure 18.- Concluded.

APPENDIX

EXPERIMENTAL SECTION CHARACTERISTICS

R = 598,000, M = 0.19, transition free

α, deg	c_l	c_d	c_m
–5.012	–0.1147	0.012647	–0.11775
–4.010	.0135	.010021	–.12521
–3.008	.1277	.009202	–.12642
–2.006	.2358	.008625	–.12601
–1.504	.2922	.007996	–.12616
–1.003	.3457	.007752	–.12550
–.001	.4514	.007630	–.12374
1.001	.5548	.008101	–.12163
2.004	.6644	.008849	–.11980
2.505	.7132	.009240	–.11853
3.006	.7620	.009703	–.11726
4.008	.8560	.010643	–.11470
5.011	.9522	.011520	–.11143
6.013	1.0421	.013052	–.10748
7.015	1.1231	.014099	–.10124
8.017	1.2052	.016613	–.09600
9.019	1.2845	.018743	–.09040
10.021	1.3493	.022316	–.08441
11.023	1.4067	.026003	–.07594
12.024	1.4307	.031973	–.06973
12.525	1.4419	.033682	–.06556
13.025	1.4391	.061864	–.06406
14.018	1.2631	.118186	–.10256
15.015	1.2009	.160504	–.11957

R = 596,000, M = 0.20, transition fixed

α, deg	c_l	c_d	c_m
–5.013	–0.1197	0.013661	–0.11832
–4.010	.0082	.010809	–.12588
–3.008	.1166	.012489	–.11928
–2.005	.2267	.011403	–.11999
–1.003	.3372	.010422	–.12028
–.001	.4429	.010268	–.11911
1.002	.5447	.011447	–.11689
2.004	.6450	.012552	–.11460
3.006	.7405	.013302	–.11327
4.008	.8284	.013402	–.10873
5.011	.9264	.014736	–.10688
6.013	1.0242	.015908	–.10415
7.015	1.1201	.017492	–.10098
8.017	1.2114	.018771	–.09681
9.020	1.2924	.021249	–.09152
10.021	1.3597	.023386	–.08628
11.023	1.4041	.027633	–.07594
11.524	1.4184	.030342	–.07259
12.024	1.4224	.035191	–.07038
12.525	1.4304	.039325	–.06700
13.024	1.4241	.069726	–.07115
14.015	1.1491	.112291	–.11024
15.014	1.1490	.141475	–.12384

R = 300,000, M = 0.09, transition free

α, deg	c_l	c_d	c_m
–4.010	–0.0739	0.011960	–0.10288
–3.008	.0763	.012192	–.11423
–2.006	.2157	.011108	–.12232
–1.003	.3435	.011016	–.12418
–.001	.4451	.010218	–.12262
1.001	.5464	.009116	–.11992
1.252	.5711	.009019	–.11933
2.004	.6436	.009259	–.11677
3.006	.7378	.009968	–.11323
4.008	.8255	.010762	–.10854
5.010	.9048	.011579	–.10250
6.012	.9991	.013321	–.09997
7.014	1.0836	.015462	–.09657
8.016	1.1596	.017973	–.09186
9.018	1.2287	.021190	–.08504
10.020	1.2850	.025003	–.07781
11.022	1.3231	.030115	–.07057
12.022	1.3380	.036312	–.06658
12.523	1.3489	.035309	–.06215
13.022	1.3318	.032565	–.06676
14.020	1.2218	.087000	–.07357
15.018	1.1980	.117142	–.08728
16.017	1.0971	.127706	–.07446
17.004	.8212	.267439	–.16543

R = 300,000, M = 0.09, transition fixed

α, deg	c_l	c_d	c_m
–4.010	–0.0729	0.017223	–0.09697
–3.008	.0689	.010798	–.10761
–2.005	.2125	.012800	–.11583
–1.003	.3265	.013345	–.11708
–.001	.4260	.014291	–.11503
1.002	.5199	.014781	–.11174
2.004	.6134	.015354	–.10841
3.006	.7083	.016064	–.10613
4.008	.7982	.016939	–.10314
5.010	.8831	.018068	–.10014
6.012	.9727	.019589	–.09791
7.014	1.0648	.021063	–.09475
8.016	1.1472	.023357	–.09101
9.018	1.2227	.026015	–.08617
10.020	1.2874	.029385	–.08013
11.022	1.3444	.033447	–.07479
11.522	1.3612	.037333	–.07290
12.023	1.3590	.041615	–.06676
12.523	1.3386	.047640	–.06330
13.022	1.3143	.067648	–.06539
14.021	1.3166	.107975	–.07659
15.004	.7801	.221866	–.15367

R = 200,000, M = 0.06, transition free

α, deg	c_l	c_d	c_m
–4.010	–0.1073	0.014002	–0.09318
–3.008	–.0036	.013960	–.09543
–2.507	.0658	.013179	–.10024
–2.006	.1351	.017453	–.10419
–1.505	.2171	.015507	–.11143
–1.004	.2960	.014314	–.11736
–.502	.3710	.013951	–.12252
–.001	.4312	.013383	–.12138
.500	.4833	.013057	–.11943
1.001	.5340	.011508	–.11900
1.502	.5833	.010967	–.11709
1.753	.6062	.010791	–.11583
2.254	.6507	.010604	–.11331
3.006	.7121	.010654	–.10722
4.008	.7904	.010851	–.10005
5.010	.8888	.012701	–.09892
6.012	.9788	.014652	–.09656
7.014	1.0608	.016763	–.09327
8.016	1.1292	.019650	–.08813
9.018	1.1969	.023388	–.08144
10.020	1.2411	.028336	–.07497
10.520	1.2562	.030988	–.07151
11.021	1.2774	.033839	–.06631
11.521	1.2714	.037991	–.06416
12.021	1.2662	.058938	–.06062
13.021	1.2444	.070173	–.05591
14.020	1.2141	.096610	–.06787
15.004	.7738	.220786	–.15201

R = 200,000, M = 0.06, transition fixed

α, deg	c_l	c_d	c_m
–3.008	–0.0143	0.018165	–0.08746
–2.507	.0669	.018579	–.09600
–2.005	.1507	.018101	–.10257
–1.003	.3103	.015957	–.11375
–.001	.4108	.014490	–.11053
1.002	.4912	.015907	–.10476
2.003	.5739	.017739	–.10150
3.006	.6653	.017982	–.09910
4.008	.7554	.018789	–.09706
5.010	.8463	.019584	–.09484
6.012	.9396	.021117	–.09343
7.014	1.0240	.022391	–.09011
8.016	1.1048	.024331	–.08634
9.018	1.1771	.026795	–.08096
10.019	1.2320	.029973	–.07568
11.021	1.2860	.033332	–.06862
11.522	1.3047	.033517	–.06575
12.022	1.3289	.036575	–.06384
12.522	1.2964	.039401	–.06283
13.021	1.2733	.078635	–.06484
14.019	1.2077	.105984	–.07927
15.017	1.1594	.129461	–.09189
16.015	1.1275	.152862	–.10184

R = 150,000, M = 0.04, transition free

α, deg	c_l	c_d	c_m
–3.008	–0.0228	0.015294	–0.09049
–2.006	.0863	.016160	–.09085
–1.505	.1570	.017806	–.09782
–1.004	.2496	.020146	–.10693
–.502	.3323	.017580	–.11326
–.001	.3970	.016913	–.11567
1.001	.5225	.014653	–.11663
2.004	.6183	.013092	–.11196
2.755	.6759	.012566	–.10657
3.006	.6974	.012187	–.10523
3.257	.7095	.011807	–.09840
4.008	.7859	.012335	–.09965
5.010	.8834	.013982	–.09815
6.012	.9722	.016308	–.09529
7.014	1.0579	.018509	–.09110
8.016	1.1256	.021716	–.08613
9.018	1.1760	.026383	–.08060
10.019	1.2175	.032419	–.07348
11.020	1.2440	.039717	–.06530
11.521	1.2458	.044862	–.06189
12.021	1.2420	.050794	–.05784
13.020	1.2025	.077509	–.05547
14.004	.7521	.199857	–.14622
15.004	.7863	.224624	–.15566

R = 150,000, M = 0.04, transition fixed

α, deg	c_l	c_d	c_m
–3.008	–0.0469	0.020727	–0.08117
–2.006	.1107	.023464	–.09461
–1.003	.2775	.021410	–.10853
–.001	.4056	.018004	–.11103
1.002	.4820	.016702	–.10218
1.503	.5263	.015685	–.10070
2.004	.5643	.015922	–.09857
3.006	.6507	.018278	–.09634
3.506	.6972	.019449	–.09631
4.007	.7393	.020317	–.09482
5.009	.8264	.021456	–.09242
6.011	.9124	.023020	–.08965
7.013	.9943	.024576	–.08623
8.015	1.0687	.027249	–.08173
9.017	1.1341	.030279	–.07597
10.019	1.1876	.033641	–.06976
11.020	1.2340	.038185	–.06398
11.521	1.2493	.040855	–.06136
12.021	1.2551	.043853	–.05785
12.522	1.2677	.048869	–.05760
13.021	1.2357	.044041	–.05374
14.017	1.1262	.094259	–.07241
15.004	.8299	.199064	–.16000

R = 100,000, M = 0.03, transition free

α, deg	c_l	c_d	c_m
–3.008	–0.0605	0.018922	–0.07879
–2.006	.0243	.020326	–.07581
–1.004	.1190	.019659	–.07453
–.503	.1719	.019043	–.07555
–.002	.2328	.019609	–.08038
.499	.3241	.029319	–.09047
1.000	.3924	.024662	–.09442
2.003	.5340	.017933	–.09913
3.005	.6725	.015166	–.10383
3.506	.7127	.015344	–.10105
4.008	.7712	.015683	–.10197
5.010	.8643	.016727	–.09709
6.012	.9555	.018812	–.09247
7.014	1.0276	.022331	–.08803
8.016	1.0950	.026066	–.08135
9.017	1.1508	.032077	–.07789
10.019	1.1998	.039164	–.07157
10.520	1.2119	.044354	–.06674
11.020	1.2215	.049599	–.06368
11.521	1.2354	.056061	–.05956
12.020	1.2060	.064741	–.05855
13.004	.7233	.177136	–.13856
14.004	.7510	.200184	–.14545
15.004	.8164	.229107	–.16079

R = 100,000, M = 0.03, transition fixed

α, deg	c_l	c_d	c_m
–3.008	–0.0625	0.020131	–0.07735
–2.006	.0484	.019747	–.08134
–1.004	.1885	.023114	–.09168
–.001	.3721	.014818	–.10840
1.001	.4947	.017061	–.11059
1.502	.5293	.017450	–.10385
2.003	.5714	.017776	–.10226
3.006	.6502	.020430	–.09543
4.007	.7330	.021571	–.09287
5.009	.8044	.022868	–.08941
6.011	.8853	.024626	–.08597
7.013	.9587	.026286	–.08028
8.015	1.0381	.028751	–.07625
9.017	1.1084	.032877	–.07058
10.019	1.1710	.038005	–.06659
11.020	1.2175	.046434	–.06337
11.521	1.2389	.048330	–.06068
12.004	.8321	.176726	–.16586
13.004	.7446	.175366	–.14333
14.003	.7507	.201158	–.14850

R = 70,000, M = 0.02, transition free

α, deg	c_l	c_d	c_m
–2.005	–0.0088	0.023370	–0.06219
–1.003	.0635	.022756	–.05400
–.002	.1154	.026496	–.05203
1.000	.2590	.023017	–.06570
1.501	.3361	.022345	–.07692
2.001	.4486	.025787	–.09436
2.503	.5934	.024142	–.11167
3.005	.6653	.022058	–.11137
3.506	.7265	.019750	–.10938
3.756	.7319	.019075	–.10582
4.007	.7605	.019055	–.10562
5.010	.8604	.020393	–.09803
6.012	.9292	.023285	–.09175
7.014	1.0117	.026955	–.08508
8.016	1.0772	.029496	–.07848
9.018	1.1516	.039935	–.07528
10.019	1.1904	.050501	–.06899
10.519	1.1942	.057295	–.06600
11.005	.7414	.149474	–.13102
12.004	.6881	.160762	–.12951
13.003	.6996	.177315	–.13603

R = 70,000, M = 0.02, transition fixed

α, deg	c_l	c_d	c_m
–3.008	–0.0690	0.024960	–0.07557
–2.006	.0051	.024745	–.07553
–1.004	.1145	.027274	–.07874
–.002	.2905	.019781	–.09529
1.001	.4409	.022469	–.10336
2.003	.5473	.023235	–.09724
3.005	.6291	.024359	–.09557
4.007	.6922	.024675	–.08887
5.009	.7903	.025638	–.08505
6.011	.8757	.027205	–.08275
7.013	.9380	.029959	–.07706
8.015	1.0155	.036174	–.07116
9.017	1.1026	.038768	–.06949
10.019	1.1702	.049050	–.06713
10.510	.8608	.054841	–.09995
11.004	.8145	.165448	–.16073
12.005	.7927	.166889	–.14187

REPORT DOCUMENTATION PAGE

Form Approved
OMB No. 0704-0188

1. REPORT DATE *(DD-MM-YYYY)*	2. REPORT TYPE	3. DATES COVERED *(From - To)*
xx-08-2010	FINAL REPORT	Sep 2007 - Jun 2010

4. TITLE AND SUBTITLE

Design and Experimental Results for the S407 Airfoil

5a. CONTRACT NUMBER
W911W6-07-C-0047

5b. GRANT NUMBER

5c. PROGRAM ELEMENT NUMBER

6. AUTHOR(S)

Somers, Dan M. and Maughmer, Mark D.

5d. PROJECT NUMBER

5e. TASK NUMBER

5f. WORK UNIT NUMBER

7. PERFORMING ORGANIZATION NAME(S) AND ADDRESS(ES)

Airfoils, Incorporated
Attn: Dan M. Somers
122 Rose Drive
Port Matilda PA 16870-7535

8. PERFORMING ORGANIZATION REPORT NUMBER

SBIR Topic Number A06-006
Proposal Number A2-2972

9. SPONSORING / MONITORING AGENCY NAME(S) AND ADDRESS(ES)

US Army Aviation Research, Development and Engineering Command (RDECOM)
Aviation Applied Technology Directorate (AATD)
Fort Eustis VA 23604-5577

10. SPONSOR/MONITOR'S ACRONYM(S)

11. SPONSOR/MONITOR'S REPORT NUMBER(S)
RDECOM TR 10-D-109

12. DISTRIBUTION / AVAILABILITY STATEMENT

Approved for public release; distribution is unlimited.

13. SUPPLEMENTARY NOTES

UL Note: No proprietary / limited information may be included in the abstract.

14. ABSTRACT

An 11.43-percent-thick airfoil, the S407, intended for rotorcraft applications has been designed and analyzed theoretically and verified experimentally in The Pennsylvania State University Low-Speed, Low-Turbulence Wind Tunnel. The two primary objectives of high maximum lift and low profile drag have been achieved. The constraints on the pitching moment and the airfoil thickness have been satisfied. The airfoil exhibits a sharp stall, which does not meet the design objective. Comparisons of the theoretical and experimental results generally show good agreement.

15. SUBJECT TERMS

Airfoils, rotorcraft, laminar flow, wind tunnel

16. SECURITY CLASSIFICATION OF: a. REPORT	b. ABSTRACT	c. THIS PAGE	17. LIMITATION OF ABSTRACT	18. NUMBER OF PAGES	19a. NAME OF RESPONSIBLE PERSON
unclassified	unclassified	unclassified	UU	85	Dan M. Somers
					19b. TELEPHONE NUMBER *(include area code)* (814) 357-0500